FINAL Report C

TRyy1110

**Project Title: Design and Evaluation of High-Volume
Fly Ash (HVFA) Concrete Mixes**

Report C: Shear Behavior of HVFA Reinforced Concrete

ABSTRACT

Concrete is the most widely used man-made material on the planet. Unfortunately, producing Portland cement generates carbon dioxide (a greenhouse gas) at roughly a pound for pound ratio. High-volume fly ash (HVFA) concrete – concrete with at least 50% of the cement replaced with fly ash – offers a potential "green" solution. However, because it is still relatively new and has some disadvantages, there are still many questions that need to be answered.

Most research to date has consisted only of the evaluation of the strength and durability of HVFA concrete mixtures, while only a limited number of studies have implemented full-scale testing of specimens constructed with HVFA concrete to determine its potential use in the industry. For this research, a laboratory testing program was developed to investigate the shear performance of reinforced concrete (RC) beams constructed with HVFA concrete. The experimental program consisted of 32 tests performed on full-scale RC beams. The principal parameters investigated were: (1) concrete type (HVFA concrete or conventional concrete (CC)), (2) amount of total cementitious material, (3) amount of shear reinforcement, and (4) amount of longitudinal (flexural) reinforcement. The full-scale test results were compared to the theoretical results using design approaches contained in several codes common to North America. The results indicate that existing design code provisions for conventional concrete are equally applicable to the design of HVFA concrete.

TABLE OF CONTENTS

LIST OF ILLUSTRATIONS

LIST OF TABLES

NOMENCLATURE

Symbol	Description
A	Angular coefficient of linear regression plot (Equation 3-34)
A_c	Area of concrete on flexural tension side
A_p	Area of prestressing steel
A_{ps}	Area of prestressing steel
A_s	Area of longitudinal reinforcement
A'_s	Area of compression reinforcement
A_{sl}	Area of longitudinal reinforcement
A_{sw}	Steel vertical reinforcement area
A_v	Steel vertical reinforcement area
A_{vi}	Cross-sectional area in the ith stirrup crossing the critical crack
$A_{v,min}$	Minimum shear reinforcement area
a	Aggregate size (Equation 3-18)
a	Depth of equivalent rectangular stress block
a	Shear span
$\underline{a}$	Critical crack length
a/d	Shear span-to-depth ratio
a_0	Notch depth
a_0/d	Notch depth-to-depth ratio
a_c	Critical position of diagonal crack
a_g	Aggregate size (AASHTO LRFD, 2004)

a_s Shear span

B Coefficient obtained through linear regression plot (Equation 3-27)

B Width of cross-section

b Width of cross-section

b_v Effective width of cross-section

b_w Width of cross-section

C_i Measured initial compliance

C_u Unloading compliance

c Distance from extreme compression fiber to the neutral axis

c_v Concrete cover for transverse reinforcement

c_x Concrete cover for longitudinal reinforcement

D Diameter of the cylinder

D_{max} Aggregate size

d Characteristic dimension of structure (Equation 3-28)

d Effective depth of cross-section

d' Distance from extreme compression fiber to centroid of

longitudinal compression reinforcement

d_0 Coefficient determined experimentally (Bazant and Pfeiffer, 1987)

d_{agg} Aggregate size

d_{bv} Diameter of transverse steel reinforcement

d_{bx} Diameter of longitudinal steel reinforcement

d_v Effective shear depth (AASHTO LRFD, 2004)

E Modulus of elasticity of the concrete (Equation 3-34)

E_c	Modulus of elasticity of the concrete
E_p	Modulus of elasticity of the prestressing steel
E_s	Modulus of elasticity of the steel
F_c	Concrete compressive force
F_s	Longitudinal reinforcement force
f_1	Principal tensile stress of the concrete
f_2	Principal compressive stress of the concrete
$f_{2,max}$	Maximum principal compressive stress of the concrete
f'_c	Compressive strength of the concrete
f_{ci}	Compressive stress on crack surface
f_{cr}	Concrete stress at cracking
f_{ct}	Tensile strength of the concrete
f_{cx}	Horizontal concrete stress
f_{cy}	Vertical concrete stress
f_{p0}	Parameter to account for level of prestressing (AASHTO LRFD, 2004)
f_t	Splitting tensile strength of the concrete
f'_t	Tensile strength of the concrete
f_v	Tensile stress in the stirrups
f_{vi}	Stress in the ith stirrup crossing the critical crack
f_y	Yield stress of steel
f_{yt}	Yield stress of transverse steel reinforcement
G	Fracture energy consumption (Equation 3-36)

G_F Fracture energy (Work-of-fracture method)

G_f Fracture energy (Size effect method)

G_f Fracture energy (Two parameter method)

G_s Shear modulus of steel

$g_f(\alpha_0)$ Non-dimensional energy release rate (Equation 3-34)

H Height of cross-section

H_0 Thickness of clip gauge holder

h Height of cross-section

jd Distance between resultants of internal compressive and tensile

forces on a cross-section

K_{Ic} Stress intensity factor

k Parameter to reflect size effect (Equation 3-27)

k_1 Coefficient that characterizes bond properties of bars (Equations 3-

20)

k_3 Empirical coefficient (Equation 3-49)

L Length of the beam

M_{exp} Experimentally determined total moment applied to specimen

M_f Factored shear moment

M_n Nominal moment capacity

M_u Factored shear moment

MOR Modulus of rupture of the concrete

N_h Tensile force in longitudinal reinforcement

N_u Factored axial force

n	Curve-fitting factor (Collins and Mitchell, 1997)
n	Number of data points
P	Maximum load at failure (Equation 6-23)
P_{max}	Measured peak load
S	Specimen loading span
s	Center-to-center spacing of steel stirrups
s	Shear crack sliding
s	Standard deviation
s_{mv}	Average spacing of cracks perpendicular to transverse reinforcement
s_{mx}	Average spacing of cracks perpendicular to longitudinal reinforcement
s_x	Crack spacing parameter (AASHTO LRFD, 2004)
s_x	Spacing of longitudinal steel reinforcement
s_{xe}	Effective crack spacing
s_z	Crack spacing parameter (CSA A23.3, 2004)
s_{ze}	Effective crack spacing
s_θ	Crack spacing
$T_{n,1}$	Test criterion (ASTM E178 [2008])
V	External shear force
V_c	Concrete contribution to shear strength
V_{cr}	Ultimate shear force
V_{cz}	Uncracked concrete force

V_d	Longitudinal reinforcement dowel force
V_f	Factored shear force
V_i	Interlock forces
V_n	Nominal shear strength
$V_{n,exp}$	Experimentally determined total resistance
$V_{n,max}$	Maximum nominal shear strength
V_p	Vertical component of prestressing force
V_r	Nominal shear resistance
V_s	Steel contribution to shear strength
V_{test}	Experimentally determined total shear resistance
V_u	Factored shear force
v	Shear stress
v_{ci}	Shear transferred by aggregate interlock
$v_{ci,max}$	Maximum shear transferred by aggregate interlock
v_{cxy}	Shear stress on concrete layer face
W	Depth of cross-section (Equation 6-10)
W	Total energy dissipated (Equation 3-26)
W_{ext}	Work of external force (Equation 3-36)
w	Average crack width (Equation 3-18)
w	Crack opening (Einsfeld and Velasco, 2006)
w	Unit weight of the concrete (Equation 6-28)
w	Width of idealized prismatic strut
w/c	Water-to-cement ratio

w/cm	Water-to-cementitious material ratio
$\bar{x}$	Arithmetic average
y	Diagonal crack extent (Equation 3-38)
z	Inner level arm
α_0	Aggregate shape factor (Equation 3-51)
α_0	Relative notch length (Equation 3-35)
α_1	Coefficient for bond characteristics of reinforcement (Vecchio and Collins, 1993)
α_2	Coefficient for type of loading (Vecchio and Collins, 1993)
β	Brittleness number (Equation 3-27)
β	Concrete softening coefficient (Equation 3-14)
β	Deviation angle (Equation 7-32)
β	Shear retention factor (AASHTO LRFD, 2004)
γ_{xy}	Shear strain
δ_e	Variation of unbounded length
δ_s	Unbounded length of reinforcement
ε_0	Concrete strain at peak stress
ε_1	Principal tensile strain in concrete
$\bar{\varepsilon}_1$	Uniaxial tensile strain in the perpendicular direction
ε_2	Principal compressive strain in concrete
ε_c	Compressive strain in the concrete
ε'_c	Compressive strain in the concrete
ε_{cr}	Crack strain in concrete

ε_s Measured longitudinal strain at the center of gravity at the bottom steel reinforcement

ε_s Strain in the tension reinforcement

ε'_s Measured longitudinal strain at the top steel reinforcement

ε'_s Strain in the compression reinforcement

ε_{sm} Measured longitudinal strain at the bottom steel reinforcement

ε_{td} Transverse strain

ε_x Longitudinal strain (AASHTO LRFD, 2004)

ε_x Strain in the x-direction

ε_{xx} Horizontal strain

ε_{xy} Shear strain

ε_y Strain in the y-direction

ε_{yield} Yield strain of steel

ε_{yy} Vertical strain

$\boldsymbol{\theta}$ Shear crack angle

$\boldsymbol{\theta_c}$ Shear crack angle

ξ Concrete softening coefficient

$\xi f'_c$ Concrete peak softened stress

$\xi \varepsilon_0$ Concrete softened compressive strain

$\boldsymbol{\rho_L}$ Longitudinal reinforcement ratio

$\boldsymbol{\rho_s}$ Longitudinal reinforcement ratio

$\boldsymbol{\rho_v}$ Transverse reinforcement ratio

$\boldsymbol{\rho_w}$ Longitudinal reinforcement ratio

$\boldsymbol{\rho_x}$	Longitudinal reinforcement ratio
σ_N	Nominal stress at failure (Equation 3-27)
Σ_s	Reduced cross section of rebar (Equation 3-38)
$\emptyset$	Capacity reduction factor
$\emptyset_c$	Capacity reduction factor
$\emptyset_s$	Capacity reduction factor
Γ	Fracture energy per unit length of splitting crack extension

1. INTRODUCTION

1.1. BACKGROUND

Fly ash is one of the by-products of the combustion of coal in electric power generating plants. For over 75 years, fly ash has been widely used as a supplementary cementitious material for the production of concrete in the United States and other countries. Typically, fly ash replacement levels for the production of concrete have been limited to roughly 35% by weight of the total cementitious materials due to concerns about in-place performance and constructability.

Concrete, which is the most widely used construction material on the planet, is a composite of coarse and fine aggregates, Portland cement, and potable water. However, Portland cement production poses challenges of excessive energy usage and depletion of natural resources. Additional to this, there is an abundance of coal combustion products (CCPs), such as fly ash, that are disposed of in landfills that could instead be utilized positively in the production of concrete. Portland cement is chemically manufactured from calcium, silicates, and aluminates in a process that releases carbon dioxide as a by-product into the atmosphere and reduces the mineral resources of our planet. In 2007, the world production of cement was approximately 2.6 billion metric tons, with 127 million produced and consumed within the United States. However, when a ton of fly ash is used in place of Portland cement, 55 gallons of oil required to produce the Portland cement is saved and an equal amount of carbon dioxide that would be produced by the manufacturing process is prevented from entering the Earth's atmosphere, hence making a significant positive impact on the environment and preservation of natural resources (ACAA, 2009).

Portland cement is the most expensive material used in the production of concrete. The cost of one ton of fly ash is typically half the price of one ton of Portland cement. Therefore, the production cost for concrete can also be reduced by replacing a portion of the cement with less expensive cementitious materials. High-volume fly ash (HVFA) concrete may be produced with significant cost savings when compared to conventional Portland-cement concrete.

In an attempt to improve the environment and enhance the concrete industry, it is essential to provide more sustainable and green options as solutions and better alternatives to existing products. Extensive research has been done in an attempt to make concrete products more sustainable and cost effective, and HVFA concrete is one potential option.

In addition to the economic and environmental advantages presented above, HVFA concrete has shown better performance characteristics when compared to conventional Portland-cement concrete. Fly ash is now used in concrete for many reasons, including: improvements in workability of fresh concrete, reduction in temperature rise during initial hydration, improved resistance to sulfates, reduced expansion due to alkali-silica reaction, and increased durability and strength of hardened concrete (ACI 232.2R, 2003).

The two most common classes of fly ash used in concrete are Class C and Class F as defined by ASTM C618 [2008] "Standard Specification for Coal Fly Ash and Raw or Calcined Natural Pozzolan for Use in Concrete". Both classes are pozzolanic, meaning they react with excess calcium hydroxide (CH) in concrete, formed from cement hydration, to form calcium silicate hydrate (CSH), but Class C fly ash also contains

higher levels of calcium which makes it more desirable for higher replacement percentages.

In conclusion, HVFA concrete could offer a solution to the problem of meeting the increasing demands for concrete in the future in a sustainable manner and at reduced or no additional cost, and at the same time reducing the environmental impact of two industries that are essential to economic development, the Portland cement industry and the coal-fired power industry. The use of high volumes of fly ash in concrete generates a direct link between durability and resource productivity, thus increasing the use of HVFA concrete will help to improve the sustainability of the concrete industry.

The main problem with using HVFA concrete in construction is the increased setting time. Retarded set time delays form removal, which increases time of construction (Marotta et al., 2011). Since labor is the primary cost contributing factor in construction, the setting time of high-volume fly ash concrete must be accelerated. Previous research has proven that the addition of chemical admixtures or activators, such as calcium hydroxide and gypsum, assist in initiating the hydration process allowing for a shorter curing period, while still gaining sufficient strength.

1.2. OBJECTIVE AND SCOPE OF WORK

The main *objective* of this research study was to evaluate the shear behavior and response of HVFA concrete through material, component, and full-scale testing. This objective included a study and evaluation of current analytical models used to predict the shear response of conventional Portland-cement concrete as applied to HVFA concrete, including recommended modifications.

The following *scope of work* was implemented in order to achieve the objective of the research study:

- Perform a literature review;

- Develop a research plan;

- Develop mix designs for both conventional and HVFA concrete;

- Evaluate the fresh and hardened properties of several HVFA concrete and CC mixes;

- Design and construct small and full-scale specimens;

- Test specimens to failure;

- Record and analyze data from tests;

- Compare test results to current guidelines and previous research findings;

- Provide greater insight into the shear resistance mechanisms and quantify their effect;

- Evaluate the applicability of current analytical models to predict the shear behavior and response of HVFA concrete;

- Develop conclusions and recommendations; and

- Prepare this report to document the details, results, findings, conclusions, and recommendations of this study.

1.3. RESEARCH METHODOLOGY

The proposed research methodology included six (6) tasks necessary to successfully complete the study. They are as follows:

Task #1: Perform a literature review. The goal of the literature review was to become familiarized with testing methods and results from previous studies. This knowledge was used for a better understanding of the behavior of the specimens, to avoid mistakes, as well as to provide support for comparisons.

Task #2: Develop HVFA concrete and CC mix designs. The purpose of this task was to develop HVFA concrete mix designs that maximized the percentage of fly ash, but that still fulfilled typical construction needs, such as early strength development. Conventional concrete mix designs served as controls during this study. ACI 211.1-91 formed the basis for developing the mix designs.

Task #3: Perform material and component testing. A number of hardened concrete property tests were completed to evaluate the performance of the HVFA concrete mix and determine the validity of using these tests to predict the performance of concretes containing high volumes of fly ash.

Task #4: Perform full-scale testing. This task was critical as current shear design provisions for reinforced concrete are largely empirical. This task involved the construction and testing of full-scale specimens to confirm the potential of HVFA concrete. The full-scale specimens included beam specimens for shear testing only. These specimens were constructed with materials from the local Ready Mix Concrete plant to validate the ability of transferring the mix designs from the laboratory to the field. In order to compare the shear strength of conventional and HVFA concrete, full-scale beams were tested in a third point loading configuration. These beams were designed to fail in shear by increasing the flexural reinforcement. Different longitudinal reinforcement ratios and stirrup designs were also considered. Strain gauges were applied to the stirrups and to

the flexural reinforcement, and the maximum load applied to the beam was also recorded and used to calculate the strength of the beams and the different shear components.

Task #5: Analyze test data. The material, component, and full-scale test results were analyzed to evaluate the shear behavior and response of HVFA concrete compared to conventional Portland-cement concrete. The test data included: concrete compressive and tensile strength, modulus of elasticity (MOE), modulus of rupture (MOR), shear force-deflection plots, crack formation and propagation, and reinforcement strains.

Task #6: Develop findings, conclusions, and recommendations. This task synthesized the results of the previous tasks into findings, conclusions, and recommendations on the shear behavior and response of HVFA concrete.

1.4. REPORT OUTLINE

This report includes six chapters. This section will discuss the information that will be presented in more detail throughout this document.

Chapter 1 acts as an introduction to the report. This introduction contains a brief background of fly ash as a material, fly ash as a mineral admixture to concrete, and the environmental concerns regarding Portland cement production. It also discusses the research objective, scope of work, and research plan.

Chapter 2 includes information from previous research performed on the characterization of fly ash and its applications as a concrete binder.

Chapter 3 presents information from previous research performed on shear design including the different methods and approaches formulated to address this phenomenon. Four different approaches are presented: truss model, Strut and Tie Model (STM),

Modified Compression Field Theory (MCFT), and fracture mechanics approach. A collection of three design code philosophies that can be found in North America are also presented in this chapter.

    Chapter 4 includes information about the experimental program. The experimental program consisted of 32 tests performed on full-scale reinforced concrete beams as well as material and component testing to determine hardened concrete properties such as compressive strength, splitting tensile strength, flexural strength, and modulus of elasticity. This chapter also describes the fabrication process, test set-up, and instrumentation for the full-scale testing.

    Chapter 5 presents the test results and the different analyses used to investigate the shear resistance mechanisms. The overall behavior of the specimens is described first, with a focus on crack patterns, failure modes, and shear strength.

    Chapter 6 concludes this document, summarizing the findings and conclusions of this study and proposing recommendations and future research.

2. LITERATURE REVIEW ON FLY ASH

2.1. GENERAL

Conventional Portland-cement concrete is produced more than any other material in the world. It is used in every civil engineering field for applications such as pavements, dams, bridges, and buildings because of its versatility, strength, and durability. In this chapter, a brief review is presented of the research performed on concrete mixtures containing high levels of fly ash by weight of the cementitious materials. Mechanisms are discussed by which the incorporation of high volumes of fly ash in concrete reduces the water demand, improves the workability and finishing aspects of the concrete, minimizes cracking due to thermal and drying shrinkage, and enhances durability to reinforcement corrosion, sulfate attack, and alkali-silica expansion.

Fly ash incorporated in concrete has shown results of increased strength and durability of the concrete. Its utilization in the US stretches back to the 1930s when it was first used on construction of the Hoover Dam. Fly ash from coal-burning electric power plants became readily available as early as the 1930s with the first study published by Davis et al. in 1937.

Concrete with high volumes of fly ash can be produced to achieve desired strengths at various ages, with a given water-cementitious ratio, aggregate size, air content, and slump as it is done for conventional concrete. In some instances 100% fly ash (Class C) concrete has been produced and has been found to meet acceptable concrete standards. However, its use has not yet found much acceptance in the construction industry due to its low early strength.

Concrete with fly ash has been widely used in the highway industry. Fly ash has been used in several engineering applications such as structural fill, waste stabilization and solidification, soil stabilization, aggregate and filler material, road sub-base, raw feed for cement clinkers, mine reclamation, grout, and of course, as partial replacement of Portland cement. However, considering that concrete containing fly ash has been acknowledged as a green product, the amount of fly ash produced is still much greater than the amount of fly ash that is put to beneficial use.

A brief description of two of the major cementitious materials used in concrete, Portland cement and fly ash, is given in this chapter as well as a summary of previous studies on the characterization of fly ash and its applications as a concrete binder.

2.2. USE OF FLY ASH AS SUPPLEMENTARY CEMENTITIOUS MATERIAL

2.2.1. Background. The United States consumes over 108 million tons of Portland cement each year, roughly 25% of which is imported (Butalia and Bargaheiser, 2004). The use of Portland cement is expected to continue to grow throughout the world. Unfortunately, the challenge is that for every ton of cement produced, approximately one ton of carbon dioxide (CO_2) is released into the atmosphere, and carbon dioxide is the primary greenhouse gas (GHG) attributed to global warming and climate change. However, concrete, of which Portland cement is the active ingredient, is an extremely versatile construction material and is, in fact, the second most consumed product in the world, just below water. Current U.S. production of Portland cement contributes over 75 million tons of CO_2 to the earth's atmosphere annually. Governmental regulations and growing concerns over GHG emissions are stimulating the cement industry to examine the increased use of supplementary binder materials in order to reduce CO_2 emissions.

The increased interest in sustainable design and construction has created an interest in Coal Combustion Products (CCPs) or Coal Combustion Residuals (CCRs). According to the United States Geological Survey, CCPs rank third as the most abundant non-fuel mineral resource in the U.S., with its annual production just below crushed stone, sand, and gravel. Seventy percent of all energy in the U.S. is produced by approximately 720 coal-fired power plants in 45 states. When burning coal at these power plants, two main types of ash are produced, fly ash and bottom ash. Fly ash is the very fine material carried in the flue gas, typically collected by a baghouse, and stored in silos as shown in **Figure 2.1**. Bottom ash is the larger/heavier particles that fall to the bottom of the boiler after combustion. The 720 coal-fired power plants produce approximately 63 million tons of fly ash annually. About 31 million tons are disposed of in landfills. Only approximately 12 million tons are recycled and put to beneficial reuse in the concrete industry. The remaining 20 million tons are used for a range of other applications including soil stabilization, roller compacted concrete, road base stabilization, etc.

Figure 2.1- Fly Ash Production
(**http://www.tradeindia.com/fp426361/Ammonia-Flue-Gas-Conditioning-Systems.html**)

2.2.2. General remarks on Portland cement. The manufacture of Portland cement requires raw materials that contain lime, silica, alumina, and iron. After the materials are acquired, the limestone is reduced to an approximately 5 in. size in the primary crusher and further reduced to ¾ in. in the secondary crusher. For a better understanding, **Figure 2.2** presents a flow chart of the manufacture of Portland cement. All raw materials are stored in the bins and proportioned prior to delivery to the grinding mill. There are two processes, the wet process that results in a slurry, which is mixed and pumped to storage bins, and the dry process that produces a fine ground powder which is also stored in bins (Marotta et al., 2011). Both processes feed the rotary kilns where the chemical changes take place. Once the raw feed has been ground and blended, it is fed into the kiln, and as the kiln rotates, the material passes slowly from the upper to the lower end at a rate controlled by the slope and speed of rotation of the kiln. Four distinct processes take place in the kiln: evaporation, calcination, clinkering, and cooling (Mindess et al., 2002). In the evaporation zone, the feed is heated to calcination temperatures to remove free water. In the calcination zone, the feed is transformed into a reactive mixture of oxides that can enter into new chemical combinations. As the material passes through the kiln, its temperature is raised to the point of clinkering. In the clinkering zone, the final chemical combination occurs to form the calcium silicates. Depending on the raw material, this temperature varies between 2400°F and 2700°F. Finally, as the material moves past the flame, it rapidly drops off in temperature in the cooling zone. Here the liquid phase solidifies to produce the hard nodules called clinker. Clinker is the final state of the material as it emerges from the kiln. The clinker produced is black or greenish black in color and rough in texture. The material is then transported

to final grinding where gypsum is added to control the setting time of the Portland

cement when it is mixed with water. If gypsum is not added, flash setting of the clinker

could occur.
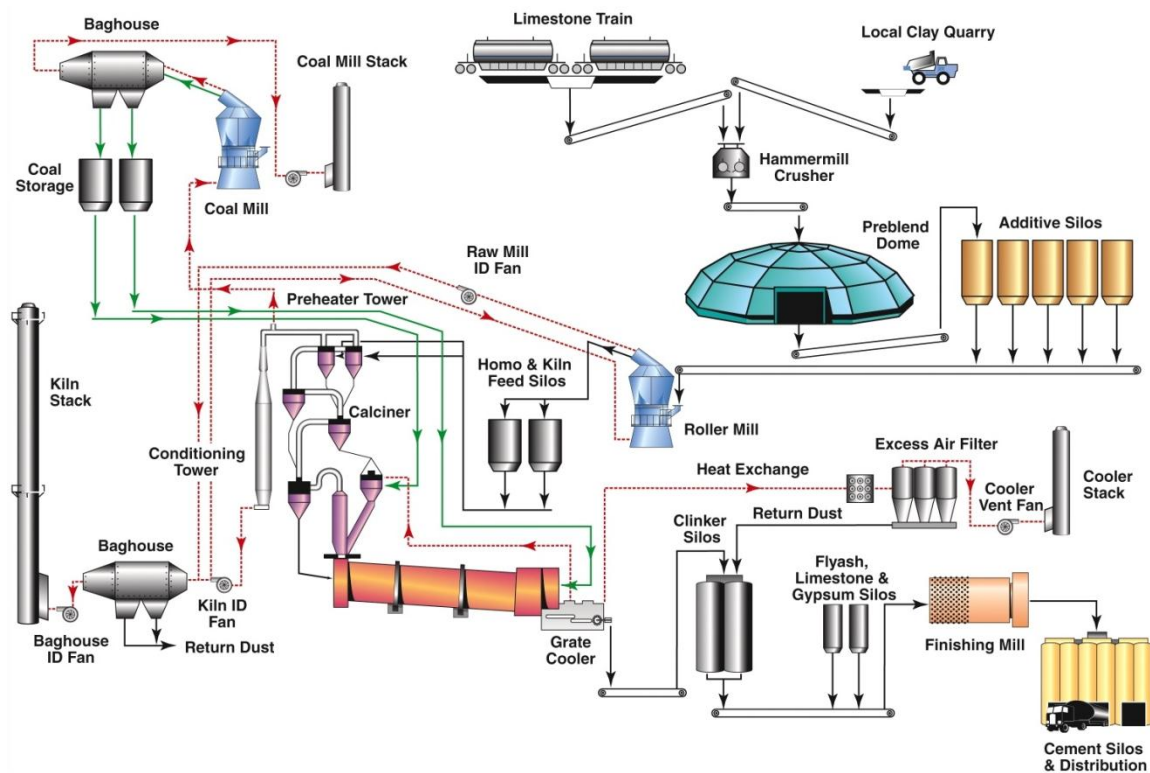
Figure 2.2- Flow Chart of Manufacture of Portland Cement
(http://www.4us2be.com/technology/cement-manufacturing-process/)

Portland cements are typically composed of four basic chemical compounds

summarized in **Table 2.1** with their names, chemical formulas and abbreviations, and

approximate weight percent for an ordinary Portland cement. Each of these compounds

exhibits a particular behavior. The tricalcium silicate hardens rapidly and is largely

responsible for initial set and early strength. The dicalcium silicate hardens slowly and its

effect on strength increases occurs at ages beyond one week. The tricalcium aluminate

contributes to strength development in the first few days because it is the first compound

to hydrate. However, the tricalcium aluminate is the least desirable compound due to its

high heat generation and reactiveness with soils and water with moderate-to-high sulfate

concentration. The tetracalcium aluminoferrite aids in the manufacture of Portland

cement by allowing lower clinkering temperature. The presence of gypsum slows the

early rate of hydration of the tricalcium aluminate.

Table 2.1- Typical Composition of an Ordinary Portland Cement (Mindess et al., 2002)

Chemical name	Chemical formula	Abbreviation	Weight (%)
Tricalcium silicate	$3CaO \cdot SiO_2$	C_3S	55
Dicalcium silicate	$2CaO \cdot SiO_2$	C_2S	18
Tricalcium aluminate	$3CaO \cdot Al_2O_3$	C_3A	10
Tetracalcium aluminoferrite	$3CaO \cdot Al_2O_3 \cdot Fe_2O_3$	C_4AF	8
Calcium sulfate dihydrate (gypsum)	$CaSO_4 \cdot 2H_2O$	$C\bar{S}H_2$	6

Hydration is the chemical reaction that takes place when Portland cement and

water are mixed together. The hydration reaction is considered complete at 28 days. The

process when cement is mixed with water to form a paste is called setting. Most Portland

cements exhibit initial set in about 3 hours and final set in about 7 hours (Marotta et al.,

2011). The hydration reaction of Portland cement is exothermic. Thus, the concrete is

being continually warmed by internal heat during the hardening process.

There are two possible problems of early stiffening on cement paste. The first one

is termed false set, which refers to the rapid development of rigidity in cement paste with

little evidence of significant heat generation. The plasticity can be regained by further

mixing with no addition of water. And the second one is termed flash set, which refers to

the rapid development of rigidity in cement paste with the release of considerable heat. This phenomenon cannot be overcome and the plasticity cannot be regained.

2.2.3. General remarks on fly ash. Fly ash is a coal ash recovered in an electrostatic precipitator (ESP) at coal-fired thermal power plants and contains small amounts of iron, magnesium, and calcium as well as the main elements of silica and aluminum. Most thermal power plants use furnaces fired with pulverized coal. As the coal travels through the high-temperature zone in the furnace, the volatile matter and carbon are burnt off whereas most of the mineral impurities are carried away by the flue gas in the form of ash (Malhotra and Mehta, 2008). These ash particles become fused in the combustion zone of the furnace but once they leave the combustion zone, the molten ash is cooled rapidly and solidifies as spherical, glassy particles.

The ASTM C618 [2008] "Standard Specification for Coal Fly Ash and Raw or Calcined Natural Pozzolan for Use in Concrete" uses the bulk chemical composition to subdivide fly ashes into two classes, C and F, which reflect the composition of the inorganic fractions. However, this standard does not address the nature or reactivity of the particles. Class F fly ashes are produced from either anthracite bituminous or sub-bituminous coals. Class C fly ashes derive from sub-bituminous or lignitic coals. In other words, the two classes of fly ash are distinguished by the silica oxide content of the type of coal burned. Fly ash can be cementitious or pozzolanic, or both. Class F fly ash is pozzolanic while Class C fly ash is cementitious and pozzolanic. Cementitious fly ash hardens when wetted while pozzolanic fly ash requires a reaction with lime before hardening. This is why Class C fly ash has a higher potential for use in high-volume fly ash (HVFA) concrete. **Table 2.2** summarizes the average bulk composition of both class

C and F fly ashes based on 97 and 45 analyses, respectively, developed by Scheetz et al. (1997).

Fly ash consists of heterogeneous combinations of amorphous (glassy) and crystalline phases (ACI 232.2R, 2003). The largest fraction of fly ash consists of glassy spheres of two types, solid and hollow, that usually represent 60 to 90% of the total mass of the fly ash, with the remaining fraction made up of a variety of crystalline phases. This union of phases makes fly ash a complex material to classify and characterize in specific terms.

Low calcium fly ashes (Class F) contain chemically inactive crystalline phases: quartz, mullite, ferrite spinel, and hematite class. High calcium fly ashes (Class C) contain the previously mentioned phases but may also contain additional crystalline phases such as anhydrite, alkali sulfate, dicalcium silicate, tricalcium aluminate, lime, melilite, merwinite, periclase, and sodalite (ACI 232.2R, 2003). These additional phases found in the Class C fly ash are reactive, and this is why Class C fly ash exhibits both cementitious and pozzolanic properties.

Fly ash looks very similar to cement in appearance. However, when magnified, fly ash will appear as spherical particles, similar to ball bearings, whereas cement appears angular, more like crushed rock as shown in **Figure 2.3**. The small size of the fly ash particles is the key to producing smooth cement paste, allowing better bonding between aggregate and cement, and resulting in a more durable concrete. The round shape of the particles increases the concrete workability without adding extra water.

The use of fly ash (Class C and Class F) in concrete offers several significant advantages such as:

- Improved freeze-thaw durability.

- Improved long-term strength of the concrete.

- Increased workability (plasticity) of the concrete.

- Increased flexural and compressive strength of the concrete.

- Increased pumpability.

- Reduced permeability.

- Reduced water-to-cementitious materials ratio ($^w/_{cm}$).

- Reduced concrete segregation.

- Reduced heat of hydration.

- Reduced bleeding of the concrete.

- Reduced corrosion damage.

- Reduced cost of the concrete.

- Reduced volume changes (dry shrinkage).

However, the use of fly ash requires some considerations. Although certain fly ashes exhibit some cementitious properties, the main contribution to the hardened concrete properties results from the pozzolanic reaction of the fly ash with the calcium hydroxide ($Ca(OH)_2$) released by the Portland cement during hydration. The pozzolanic reaction typically occurs more slowly than cement hydration reactions and consequently concrete containing fly ash requires more curing during early ages. **Figure 2.4** presents a graphic description of the pozzolanic reaction (Headwaters Resources Tech Bulletin, 2008).

Table 2.2- Average Bulk Composition of Class C and F Fly Ashes

Oxide	Weight % / STD	
	Class C	Class F
SiO_2	36.9 ± 4.7	52.5 ± 9.6
Al_2O_3	17.6 ± 2.7	22.8 ± 5.4
Fe_2O_3	6.2 ± 1.1	7.5 ± 4.3
CaO	25.2 ± 2.8	4.9 ± 2.9
MgO	5.1 ± 1.0	1.3 ± 0.7
Na_2O	1.7 ± 1.2	1.0 ± 1.0
K_2O	0.6 ± 0.6	1.3 ± 0.8
SO_3	2.9 ± 1.8	0.6 ± 0.5
$Moisture$	0.06 ± 0.06	0.11 ± 0.14
LOI	0.33 ± 0.35	2.6 ± 2.4
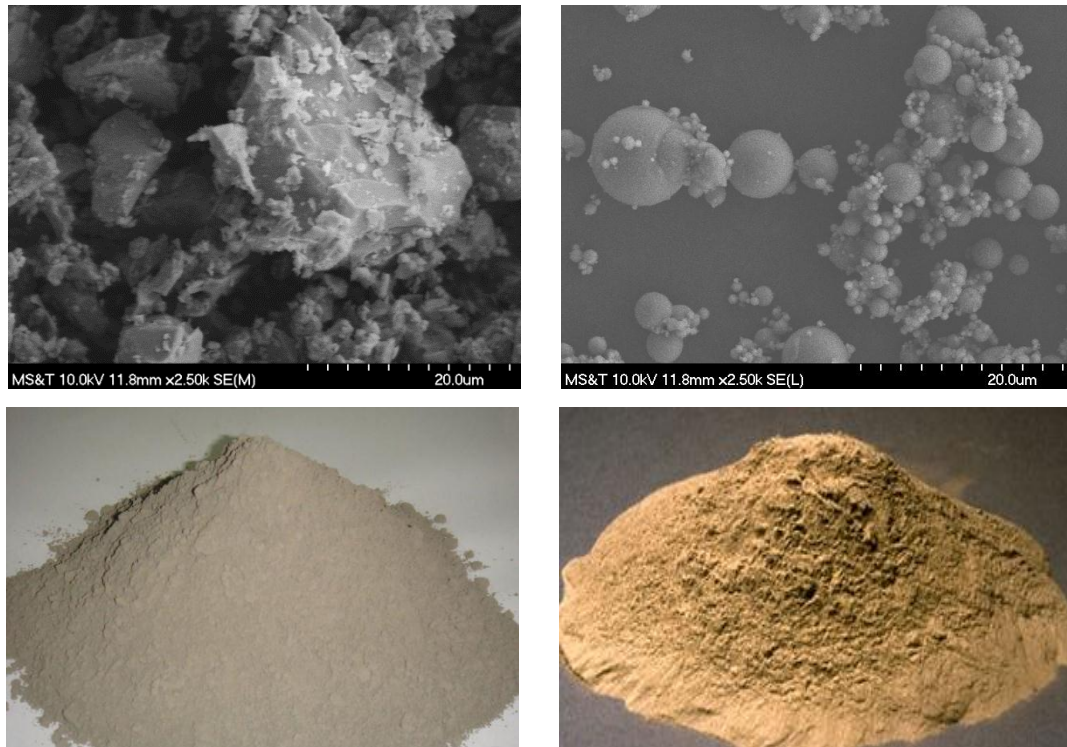
Figure 2.3- Comparison Between Portland Cement (left) and Fly Ash (right) Shapes
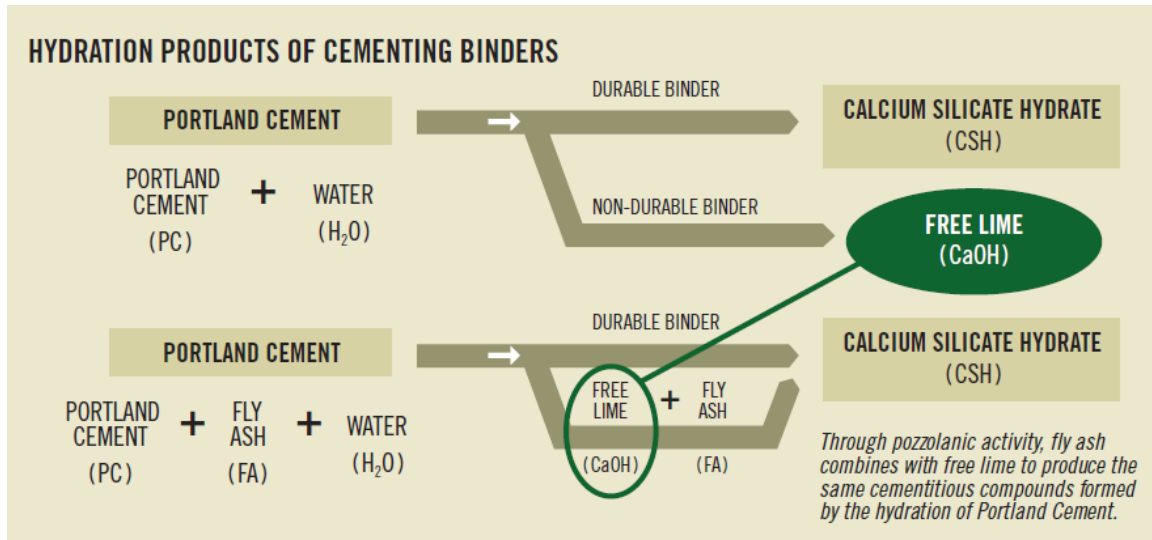
Figure 2.4- Pozzolanic Reaction

2.3. HIGH-VOLUME FLY ASH (HVFA) CONCRETE

Currently in the U.S., traditional specifications limit the amount of fly ash to 25 to 35% replacement by weight of the Portland cement in the concrete. Recent studies have shown that higher cement replacement percentages (up to 70%) can result in excellent concrete in terms of both strength and durability. Referred to as high-volume fly ash (HVFA) concrete, this type of concrete offers a viable alternative to traditional Portland-cement concrete (referred to as conventional concrete) and is significantly more sustainable. HVFA concrete is typically defined as concrete having a fly ash content of 50% or greater by weight of cementitious materials. As sustainability concerns continue to increase in both the construction industry and society as a whole, greater emphasis is being placed on producing concrete mixtures with increased volume fractions of supplementary cementitious materials, such as fly ash.

However, HVFA concrete can be susceptible to long delays in finishing and may sometimes lack necessary early age strength development. At all replacement rates, fly

ash generally slows down the setting time and hardening rates of concrete at early ages. Powder additions examined in previous research (Bentz, 2010) showed that the addition of 5% calcium hydroxide by mass of the total solids provides a significant reduction in the retardation measured in mixtures based on either class of fly ash.

2.4. PREVIOUS STUDIES RELATED TO HVFA CONCRETE

In 1937, Davis et al. conducted a study to determine the effect of using fly ash as a replacement for Portland cement upon the properties of mortars and concretes. This study included fly ashes from 15 different sources and Portland cements of seven compositions. In this study, fly ashes in percentages up to 50% were blended with the Portland cements. The properties investigated included strength, elasticity, volume change, plastic flow, heat of hydration, and durability as indicated by resistance to freezing and thawing, and by resistance to the action of sodium sulfate. The authors concluded that fly ashes of moderately low carbon content and moderately high fineness exhibit a high degree of pozzolanic activity as compared with most natural pozzolans. They reported that when such fly ashes are used in moderate percentages (between 30% and 50%) as replacement of Portland cement, it is possible to produce concretes with the same quality and sometimes superior than those concretes made of Portland cement only. In fact, Davis et al. reported that concrete mixes containing fly ash had lower compressive strengths at early ages but substantially higher compressive strengths at later ages, as well as lower heat of hydration and greater resistance to sulfate attack.

In 1985, the Canada Center for Mineral and Energy Technology (CANMET) developed HVFA concrete incorporating high volumes of low-calcium fly ash (Class F).

Numerous investigations performed at CANMET showed that HVFA concrete has excellent mechanical properties and durability characteristics.

In 1989, Langley et al. investigated concrete incorporating high volumes of Class F fly ash. These concrete mixtures contained 56% replacement of fly ash by weight of the total cementitious materials. The concretes investigated presented several different water-to-cementitious materials ratios. Because of the very low water contents used in this study, a high-range water reducer (HRWR) admixture was used to achieve high slumps. The authors concluded that the use of high volumes of Class F fly ash in concrete provide an economical material for strengths on the order of 9,000 psi at 120 days. They also reported that the extensive laboratory data showed that the optimum percentage of fly ash should be in the range of 55% to 60% of the total cementitious materials content. In terms of significant conclusions, they reported that the test data on strength properties, modulus of elasticity, drying shrinkage, creep, and freeze-thaw durability showed that concrete incorporating low Portland cement contents and high volumes of fly ash compared favorably to conventional Portland-cement concrete.

In 1990, CANMET carried out a project to develop an engineering data base on HVFA concrete incorporating selected fly ashes and cements from the U.S. This investigation was performed by the Electric Power Research Institute (EPRI) in Palo Alto, CA. Eight fly ashes, covering a wide range of mineralogical and chemical compositions, and two ASTM Type I Portland cements from two different sources were used in this study. A total of 16 air-entrained concrete mixtures were considered. The water-to-cementitious materials ratio was maintained at a constant value of 0.33 for all mixtures. The proportion of fly ash in the total cementitious materials content was 58%

by weight. Bilodeau et al. (1994) concluded that regardless of the type of fly ash and the

ASTM Type I brand of cement used, all air-entrained, HVFA concretes exhibited

excellent durability characteristics to freezing and thawing cycling, resistance to chloride-

ion penetration, and water permeability tests. However, they reported that the

performance of HVFA concrete in deicing salt-scaling tests was unsatisfactory.

In 1993, Carette et al. studied the properties of fresh and hardened HVFA

concretes. The properties of fresh concrete investigated included workability, bleeding,

setting time, and autogenous temperature rise. The properties of hardened concrete

investigated were compressive, flexural, and splitting-tensile strengths, modulus of

elasticity, creep, and drying shrinkage. The authors concluded that a high-performance,

air-entrained HVFA concrete can be produced with the eight fly ashes (produced in the

U.S.) and two Portland cements used in this study. The HVFA concrete produced

presented low bleeding, satisfactory slump and setting characteristics, and low

autogenous temperature rise. The authors also reported that these concretes also presented

excellent mechanical properties with compressive strengths reaching as high as 7,000 psi

and modulus of elasticity of 6,000 ksi at 91 days. In terms of significant findings, they

reported that using Portland cement with a high C_3A alkali content resulted in

considerably higher strength values at early ages than those obtained with the use of a

Portland cement with low C_3A alkali content.

In 1994, Berry et al. examined the hydration chemistry and microstructure of a

paste prepared incorporating 58% of a typical Class F fly ash and a Portland cement from

U.S. sources, and a paste with Portland cement only. The authors performed thermal

analysis, x-ray diffraction, pore fluid extraction, and scanning electron microscopy to

study cement and cement-fly ash pastes cured up to 180 days. They observed extensive participation by the fly ash in hydration and cementation reactions. They concluded that cement pastes in which 58% of the mass of Portland cement was replaced by fly ash appeared to hydrate and gain strength by the following mechanisms: (a) the hydration of Portland cement by normal chemical reaction, (b) the improved densification through particle packing, aided by the use of superplasticizers and the spherical shape of the fly ash, (c) the reactions of fly ash particles that produced insoluble silicate and aluminate hydrates at particle boundary regions at late ages, and (d) the hydration of individual fly ash particles that remained physically intact and largely unchanged in morphology, capable of filling in void space (paste densification).

In 1995, Galeota et al. studied the mechanical and durability properties of HVFA concretes for structural applications. They used four different concrete mixtures with fly ash from an Italian source, varying from 0% to 50% replacement by weight of the total cementitious materials. They evaluated the compressive, flexural and splitting-tensile strength, modulus of elasticity, fracture parameters, concrete-steel bond properties, drying shrinkage, and durability properties. The authors reported that concretes containing 30% and 40% replacement of Portland cement with fly ash showed adequate early age compressive strength at 3 days for structural applications (approximately 3,500 psi). They also found that the modulus of elasticity in all the HVFA concretes of this study was a little lower (approximately 10% lower) than that of the conventional mix; however, it was still considered adequate for structural applications. One of the most significant findings the authors reported was that after 28 days there was a high bond

strength gain (up to 60%) between the HVFA concrete and steel as compared to the conventional concrete.

In 1998, Swamy and Hung developed a high performance, HVFA concrete incorporating a small amount of silica fume (SF) and partial replacement of both Portland cement and fine aggregate with fly ash. They studied the engineering properties such as strength, modulus of elasticity, and drying shrinkage of this HVFA concrete. The mixtures were designed to give 4,000 to 6,000 psi cube strengths at 28 days. In each mixture, a 60% replacement of Portland cement with fly ash was considered. Some mixtures contained a 6% replacement of cementitious materials with silica fume and some others a 25% replacement of fine aggregate with fly ash. The authors concluded that the total binder content had little effect on the strength and drying shrinkage, but had a significant effect on the modulus of elasticity, implying a clear densification of the microstructure by the fly ash and silica fume. They also found that 7 days of curing were not enough to reach the full strength potential of the HVFA concrete. In terms of significant findings, the authors reported that a HVFA concrete with replacement of Portland cement and fine aggregate with both silica fume and fly ash showed the best overall performance based on the tests carried out in this study. They recommend HVFA concrete for use in structural and mass concrete applications because the engineering properties found in this study showed good potential and were comparable to those of a conventional Portland-cement concrete.

In 1999, Cabrera and Atis developed a new method for the determination of the optimum water-to-cementitious materials ratio for maximum compaction of no slump concrete made with high volumes of fly ash. This research explored the effect of the fly

ash fineness and, in particular, the carbon content on the compressive strength of the mixtures made with 50% and 70% replacement or Portland cement with fly ash. The authors concluded that the compactability of no slump HFVA concrete can be effectively controlled using the vibrating slump test. Based on this test, the optimum water-to-cementitious materials ratio for maximum compaction can be determined. They also concluded that the compressive strength of HVFA concrete with or without the superplasticizer places these mixtures in the class of high-strength concrete (HSC). Finally, they reported that the fatigue resistance of the HVFA concrete presented better performance results than those of the conventional mix.

In 1999, Jiang et al. tested different pastes made with different fly ash contents, water-to-cementitious materials ratios, and admixtures, such as high-range water reducers (HRWR), for a period up to 90 days. They studied the hydration progress, the hydration product, and the microstructure of the pastes employing strength development tests, thermal analysis, silicate polymerization analysis, pore structure analysis, x-ray diffraction analysis, and scanning electron microscopy. The authors concluded that the HRWR affects the progress of hydration, and activator admixtures accelerate the hydration of HVFA concrete binders. They also observed that the total porosity increases with the increment of the fly ash content, and decreases with time. Other significant findings reported by the authors were that the presence of fly ash can improve the pore size distribution and that the fly ash in HVFA systems cannot be fully hydrated. They recommended that the fly ash content in HVFA concrete should be lower than 70%.

In 2004, Li performed a laboratory study on the properties of high-volume fly ash, high-strength concrete incorporating nano-SiO_2 (SHFAC). The author compared the

results with those of regular Portland-cement concrete and high-volume fly ash, high-strength concrete (HFAC). Assessment of these concrete mixes was based on short- and long-term performance. The author evaluated the compressive strength and pore size distribution, reporting strength increments of about 81% at early ages (3 days) in the SHFAC compared to the HFAC. Some improvements in the pore size distribution of SHFAC were also reported. One of the most significant findings was that the addition of fly ash leads to higher porosity at short curing time, while nano-SiO_2 acting as an accelerating additive leads to more compact structures, even at short curing times.

In 2005, Cross et al. investigated a concrete mixture in which the Portland cement was replaced completely by Class C fly ash for the binder. The authors investigated the engineering properties required for structural design and the behavior and performance of beams and columns made of a 100% fly ash admixture. The engineering properties investigated included the modulus of elasticity, the splitting tensile strength, the tensile flexural strength, the shrinkage properties, and the reinforcing bar bond behavior. The authors evaluated the effectiveness of the empirical equations available to estimate some of these properties for conventional Portland-cement concrete concluding that with a few exceptions, the equations available were found to apply to fly ash concrete. The tensile strength was found to be 15% to 30% lower than would be expected based on the compressive strength. With respect to anchorage and development length, the results were inconclusive because at an embedment length of 12 in., bars embedded in fly ash concrete behaved as expected based on equations for conventional concrete, but in shorter lengths, the results were significantly different. Cross et al. also conducted tests on simple beam and column elements to observe the performance of the fly ash concrete.

Three beams singly reinforced in accordance with the ACI code were tested to failure

using a four-point load test setup. The beams were simply supported with a cross section

of 6 in. × 10 in. Shear reinforcement was provided at 4 in. spacing. All beams were

designed to fail in flexure and they performed satisfactorily. There was no evidence of

any anchorage problems with the flexural or shear reinforcement during the tests. The

beam behavior observed during the tests matched the predicted behavior using the same

theoretical approach as that for a conventional concrete RC beam. All of the beams

presented adequate shear resistance. In the column elements, the specimens matched the

same behavior expected of a conventional concrete column. The columns measured 6 in.

in diameter with a length of 18 in. They were tested in uniaxial compression to failure. As

a final conclusion, the authors reported that existing flexural design procedures can be

employed on fly ash concrete elements with the exception of the embedment length

calculations.

In 2007, Bouzoubaâ et al. investigated HVFA concrete using fly ash with ordinary

Portland cement and Portland-pozzola cement. A total of 7 mixtures with three different

target compressive strengths (3,000, 6,000, and 9,000 psi) were used. For the ordinary

Portland cement, four mixes including a control mix were used incorporating 30%, 40%,

and 50% replacement of Portland cement with fly ash. For the Portland-pozzola cement,

three mixes including a control mix were used incorporating 40% and 50% replacement

of this cement with fly ash. For each concrete mixture, the authors measured the

compressive strength at 1, 3, 7, 28, 56, and 91 days, the splitting-tensile strength, flexural

strength, and resistance to chloride-ion penetration at 28 and 91 days. They concluded

that for similar target compressive strength, slump range, and cementitious materials

content, the water required decreased with the increment of fly ash content. They reported that it was possible to design concrete incorporating up to 50% replacement with fly ash that meets the strength requirements of the target compressive strengths. In terms of significant findings, the HVFA concrete considered in this study was found to develop acceptable early-age strength, higher later-age strength, and lower chloride-ion penetrability when compared to the conventional concrete made with ordinary Portland cement.

In 2008, Koyama et al. investigated the ultimate mechanical behavior and deformability of RC beams containing large quantities of fly ash. Eleven test beams were fabricated and tested under monotonic bending and shear. The experimental variables included the shear span-to-depth ratio, the amount of transverse reinforcement, and the amount of fly ash. The shear span-to-depth ratios studied in this program included values of 1.0, 1.5, and 2.0 that represent specimens with a deep beam behavior. In this study, the amount of Portland cement was held constant as well as the water-to-cementitious materials ratio, and the fly ash was used as a replacement of the fine aggregate. The cross section of the beams measured 9.8 in. × 15.7 in. The authors tested three beams under pure bending while the other eight beams were subjected to monotonic shear. Five of the shear specimens were constructed without shear reinforcement. All of the beams were simply supported using a three-point load test setup. The authors concluded that the specimens constructed using a 50% replacement of the fine aggregate with fly ash presented a higher shear strength and a steeper crack angle. They also concluded that it is possible to change the failure mode of the beams from a shear failure to a flexural failure by incorporating large quantities of fly ash in the mix.

In 2009, Namagga and Atadero studied the benefits of using high lime fly ash in concrete as a replacement for large proportions of cement. They focused on testing the compressive strength, durability, and bond strength properties of concrete. They varied the amounts of fly ash as partial replacements of the Portland cement and fine aggregate. The authors compared the results with conventional concrete to indicate whether the use of fly ash can improve strength so that fly ash can be accepted as a cost effective solution. Their findings included that the replacement of high lime fly ash in concrete generally increases the ultimate strength. They also reported that a 25% to 35% fly ash replacement provides the most optimal strength results, because beyond 35% fly ash replacement, the rate of gain of compressive strength decreases but still maintains a strength value above the desired strength.

In 2010, Bentz conducted isothermal calorimetry studies to examine excessive retardation in HVFA mixtures based on both Class C and Class F fly ashes. In order to quantify the retardation, the author used the calorimetric curves to evaluate the performance of mitigation strategies based on various powder additions. He examined powder additions including aluminum trihydroxide, calcium hydroxide, cement kiln dust, condensed silica fume, limestone, and rapid-set cement. He reported that using an addition of either 5% calcium hydroxide or 10% rapid-set cement by mass of total cementitious materials provides a significant reduction in the retardation measured in mixtures based on either class of fly ash for the material combinations examined in his study. Bentz concluded that these two powder additions provide viable solutions to mitigate excessive retardation, extending the use of HVFA mixtures in practice.

In 2011, Mohan Rao et al. conducted a study on the shear resistance of RC beams without web reinforcement using a high volume fly ash concrete mix with a 50% replacement by mass of the Portland cement. The authors used a water-to-cementitious material ratio of 0.32. The shear specimens presented a constant shear span-to-depth ratio of 2.50. The beams were simply supported with a cross section of 3.9 in. $\times$ 7.9 in. Various longitudinal reinforcement ratios were considered such as 0.58%, 1.0%, 2.0%, and 2.95%. Mechanical properties including compressive strength and split tensile strength were also studied. All the beams were loaded symmetrically under a four point load test setup. The authors compared the results of the HVFA specimens with others obtained from a conventional mix. Comparison with codes of practice and other empirical models was also carried out. As remarkable finding, the authors reported that the experimental results were very close to the theoretical values obtained using the CEB-FIP model code.

The ACI 232.2R (2003) document on fly ash mentions the wide range of applications of fly ash materials in the concrete industry. Fly ash can be used in ready-mixed concrete, concrete pavements, mass concrete, roller-compacted concrete (RCC), self-consolidated concrete (SCC), high-volume fly ash (HVFA) concrete, high-performance concrete (HSC), concrete masonry units, concrete pipes, precast/prestressed products, no-slump extruded hollow-core slabs, grouts and mortars, controlled low-strength materials, soil cements, sulfur concrete, cellular concrete, shotcrete, blended cements, oil-well cementing, and finally as a filler.

Table 2.3 summarizes all the variables addressed in previous research such as the percentage replacements of Portland cement with fly ash, the properties investigated, and the presence of full-scale testing.

Table 2.3- Summary of Studies in HVFA Concrete

Researcher (s)	Year	Fly ash addition			Properties investigated								Full-scale testing
		50%-59%	60% -69%	70% - 100%	Strength	Modulus of elasticity	Bond properties	Durability	Heat of hydration	Plastic flow	Dry shrinkage	Creep	
Davis et al.	1937	X			X	X		X	X	X			
Langley et al.	1989				X			X			X	X	
Carette et al.	1993		X		X			X				X	
Berry et al.	1994	X							X				
Bilodeau et al.	1994	X						X					
Galeota et al.	1995	X			X	X		X			X		
Swamy and Hung	1998		X		X	X					X		
Cabrera and Atis	1999	X	X		X					X			
Jiang et al.	1999		X						X				
Li	2004	X			X				X				
Cross et al.	2005			X	X	X		X			X		X
Bouzoubaâ et al.	2007	X			X			X					
Koyama et al.	2008	X			X								X
Namagga and Atadero	2009				X			X	X				
Bentz	2010	X			X				X				
Mohan Rao et al.	2011	X			X								X

2.5. CONCLUDING REMARKS

The literature review reported that incorporating fly ash in concrete reduces the compressive strength at early ages but there is a valuable increase in the compressive strength at later ages. It was found that the early age strength is reduced further if the percentage of replacement is increased. However, on the other hand, when the percentage of replacement is increased, the water-to-cementitious materials ratio can be reduced,

therefore increasing the later age compressive strength. Properly cured HVFA concrete products are very homogenous in microstructure and highly durable. Several studies showed that HVFA concrete presents lower heat of hydration and higher resistance to chloride-ion penetration. Several researchers recommended that the fly ash content in HVFA concrete should be lower than 70%. In conclusion, HVFA concrete could offer a solution to the problem of meeting the increasing demands for concrete in the future in a sustainable manner and at reduced or no additional cost, and at the same time reducing the environmental impact of two industries that are essential to economic development, the Portland cement industry and the coal-fired power industry. The use of high volumes of fly ash in concrete generates a direct link between durability and resource productivity, thus increasing the use of HVFA concrete will help to improve the sustainability of the concrete industry.

3. LITERATURE REVIEW ON SHEAR

3.1. GENERAL

The main subject of this document is the shear behavior of reinforced concrete (RC) beams composed of high-volume fly ash (HVFA) concrete. The current shear design methods and guidelines are presented in this chapter. Four different approaches are presented: truss model, Strut and Tie Model (STM), Modified Compression Field Theory (MCFT), and fracture mechanics approach. A collection of three design code philosophies that can be found in North America will also be used in the evaluation of the shear strength. Some of these guidelines rely on empirical formulas, such as the ACI 318-08, while others, such as the AASHTO LRFD and CSA A23.3-04, rely more on concrete models such as the MCFT.

3.2. FACTORS AFFECTING SHEAR BEHAVIOR

Shear strength is controlled by the presence of web reinforcement, longitudinal reinforcement, coarse aggregate size, presence of axial loads, depth of the member, tensile strength of the concrete, and shear span to depth ratio (a/d). Some of these parameters are included in design equations and others are not.

Web reinforcement, typically called stirrups, is used to increase the shear strength of concrete beams and to ensure flexural failure. This is necessary due to the explosive and sudden nature of shear failures, compared with flexural failures which tend to be more ductile. Web reinforcement is normally provided as vertical stirrups and is spaced at varying intervals along a beam depending on the shear requirements. Alternatively, this reinforcement may be provided as inclined longitudinal bars. In general, small sized bars

such as #3 and #4 are used in a U-shaped configuration that may be open or closed, or used as multiple legs.

Shear reinforcement has very little effect prior to the formation of diagonal cracks. However after cracking, the web reinforcement enhances the beam in the following ways (Nilson et al., 2004):

- The stirrups crossing the crack help in resisting the shear force.

- The stirrups restrict the growth of the cracks and reduce their penetration further into the compression zone.

- The stirrups oppose widening of the cracks, which helps to maintain aggregate interlock within the concrete.

- The presence of stirrups provides extra restraint against the splitting of concrete along the longitudinal bars due to their confinement effect.

The longitudinal reinforcement ratio (ρ_L) affects the extent and the width of the flexural cracks. If this ratio is small, the flexural cracks extend higher into the beam and open wider. When the crack width increases, the components of shear decrease, because they are transferred either by dowel action or by shear stresses on the crack surfaces.

The coarse aggregate type and size noticeably affect the shear capacity, especially for beams without stirrups. Lightweight aggregate has a lower tensile strength than normal aggregate. The shear capacity of a concrete beam with no stirrups is directly related to the tensile strength, therefore, the failure due to mortar cracking, which is more desirable, could be preceded by aggregate failure instead. The aggregate size also affects the amount of shear stresses transferred across the cracks. Large diameter aggregate

increases the roughness of the crack surfaces, allowing higher shear stresses to be transferred (Wight and MacGregor, 2009).

Researchers have concluded that axial compression serves to increase the shear capacity of a beam while axial tension greatly decreases the strength. As the axial compressive force is increased, the onset of flexural cracking is delayed, and the flexural cracks do not penetrate as far as into the beam (Wight and MacGregor, 2009).

The size of the beam affects the shear capacity at failure. If the overall depth of a beam is increased, it could result in a smaller shear force at failure. The reasoning is that when the overall depth of a beam increases, so do the crack width and crack spacing, causing loss of aggregate interlock. This condition is known as a size effect.

The tensile strength of the concrete (f_{ct}) also affects the shear strength. Because of the low tensile strength of the concrete, diagonal cracking develops along planes perpendicular to the planes of principal tensile stress. The shear strength of an RC beam increases as the concrete material strength increases. The tensile strength of the concrete is known to have a great influence on the shear strength, but the concrete compressive strength (f'_c) is used instead in most shear strength formulas. This approach is used because tensile tests are more difficult to conduct and usually show greater scatter than compression tests.

The shear span to depth ratio (a/d) does not considerably affect the diagonal cracking for values larger than 2.5. The shear capacity increases as the shear span to depth ratio decreases. This phenomenon is quite significant in deep beams ($a/d \leq 2.5$) because a portion of shear is transmitted directly to the support by an inclined strut or

arch action. For deep beams, the initial diagonal cracking develops suddenly along almost the entire length of the test region (Wight and MacGregor, 2009).

3.3. BASIC SHEAR TRANSFER MECHANISMS

The 1973 ASCE-ACI Committee 426 Report concluded that shear is transferred by the following four mechanisms: shear stress in the uncracked concrete, interface shear transfer, dowel action, and arch action. In a RC beam, after the development of flexural cracks, a certain amount of shear is carried by the concrete in the compression zone. The shear force carried by the uncracked concrete in the compression zone can be represented by the compressive strength of concrete and the longitudinal reinforcement ratio. Shear may continue to be transferred across a crack in the concrete by interface shear transfer, also known as aggregate interlock. Since the flexural crack width is approximately proportional to the strain of the tension reinforcement, the crack width at failure becomes smaller as the longitudinal reinforcement ratio is increased. It is also expected that the interlocking force will be increased when the compressive strength of the concrete is high. If longitudinal reinforcing bars cross a crack, dowel forces in the bars will resist shear displacement. The dowel force induces tension in the surrounding concrete that may produce splitting cracks along the longitudinal reinforcement. Although there is some contribution in dowel action by the number and arrangement of longitudinal bars, spacing of flexural cracks, and the concrete cover, the main factors influencing this mechanism are the flexural rigidity of the longitudinal bars and the strength of the surrounding concrete. Arch action occurs where shear flow cannot be transmitted. Arch action is dominant in deep beams. For this mechanism to be developed, a tie is required

to restrain the thrust developed as a result of the arch. For deep beams, failure is often due to anchorage failure of the bars restraining this thrust.

Shear can be carried through beam action, arch action or any combination of the two. When shear is carried through beam action, the tensile force in the reinforcement varies through bond stresses and plane sections remain plane. These are the normal assumptions of elastic beam theory.

The 1998 ASCE-ACI Committee 445 Report highlights a new mechanism, residual tensile stresses, which are transmitted directly across cracks. The basic explanation of residual tensile stresses is that when concrete first cracks, small pieces of concrete bridge the crack and continue to transmit tensile force as long as cracks do not exceed 0.00197-0.0059 in. in width. The application of fracture mechanics to shear design is based on the premise that residual tensile stress is the primary mechanism of shear transfer.

3.4. SHEAR DESIGN PRINCIPLES

3.4.1. Truss model. The truss method of analysis has for some time been accepted as an appropriate method for the design of structural concrete members comprising both reinforced and prestressed concrete elements, and now forms the basis of many design standard recommendations. The truss model was presented by the Swiss engineer Ritter (1899) to explain the flow of forces in cracked reinforced concrete. The principle of the truss model is based on the following assumptions: (1) the longitudinal tension reinforcement acts as a tension chord of the truss while the flexural compressive zone of the beam acts as the compression chord, and (2) the diagonal compressive

stresses (green lines in **Figure 3.1**) act as diagonal members, and the stirrups (blue lines in **Figure 3.1**) are considered as vertical tension members.

Mörsch (1902), a German engineer, pointed out that the compression diagonals do not need to extend from the top of one stirrup to the bottom of the next stirrup, and that the stirrups represent a continuous field of stresses rather than discrete diagonal compressive struts. Mörsch and Ritter neglected the tensile stress in cracked concrete assuming that only after cracking the diagonal compression stresses would remain at 45 degrees. Mörsch also proposed truss models to explain the behavior of beams detailed with bent-up longitudinal reinforcing bars. He also used the principal stress trajectories as an indication of how tensile reinforcement should be proportioned and detailed in a region where the internal stress flow is complex. **Figure 3.2** presents the model proposed by Mörsch.
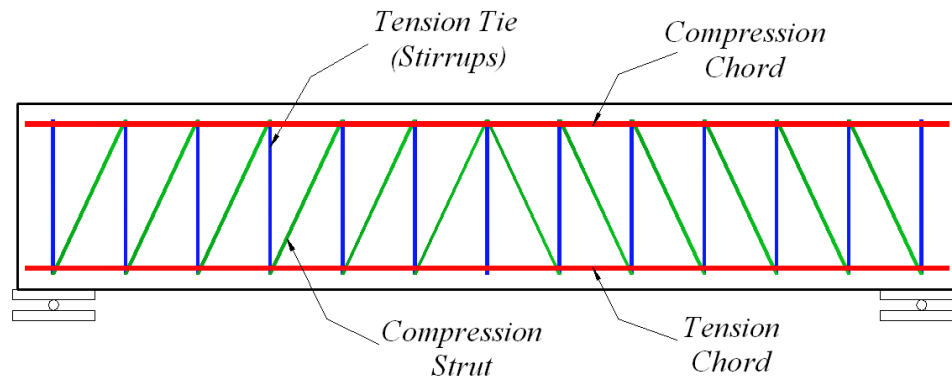

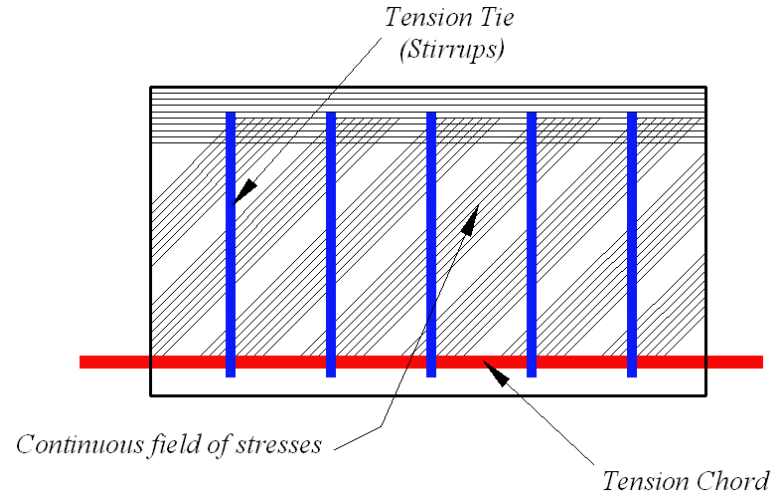**Figure 3.1- Ritter's Truss Analogy for Shear**

Tension Tie
(Stirrups)

Continuous field of stresses

Tension Chord

Figure 3.2- Truss Model for Beams Postulated by Mörsch

The truss model is derived using the equilibrium condition between the external and internal forces as presented in **Figure 3.3**. The shear stresses are assumed to be uniformly distributed over an effective shear area b_w wide and d deep. Between the external shear force V, and the total diagonal compressive force, **Equation 3-1** can be written, from which the principal compressive stress (f_2) can be determined assuming a crack angle of 45 degrees.

The longitudinal component of the diagonal compressive force is considered equal to the external shear force. The tensile stress in stirrups is determined considering **Equation 3-2**. Allowing only the use of the 45 degrees crack angle the method is robust and gives conservative results, and it is widely used by designers because of its simplicity.
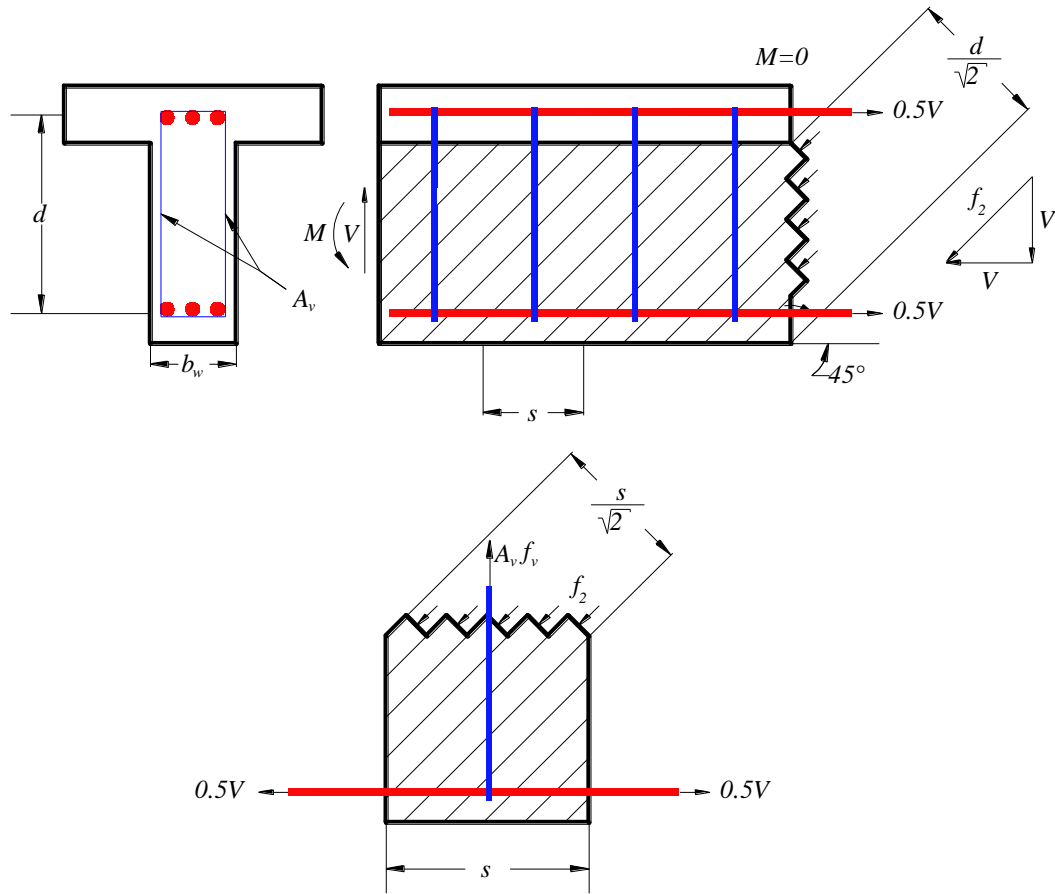
Figure 3.3- Equilibrium Conditions for the Truss Model (Collins and Mitchell, 1991)

$$\frac{f_2 b_w d}{\sqrt{2}} = \sqrt{2}V \qquad (3\text{-}1)$$

$$\frac{A_v f_v}{s} = \frac{V}{d} \qquad (3\text{-}2)$$

The variable-angle truss model is derived from the Mörsch truss model. This model adds a concrete contribution to shear strength to compensate for the conservative nature of the model based on a variable angle of the crack (θ). The principle is very similar to the one presented in **Figure 3.3**. In this model, the required magnitude of the principal compressive stress (f_2) is determined from the equality between the resultant of the diagonal stresses and the projection of the shear force, as stated in **Equation 3-3**. The tensile force in the longitudinal reinforcement (N_h) due to shear will be equal to the

horizontal projection of the shear force, as stated in **Equation 3-4**. The tensile stress in the stirrups is multiplied by the factor $\tan \theta$, as stated in **Equation 3-5**.

$$f_2 = \frac{V}{b_w d}(\tan \theta + \cos \theta) \tag{3-3}$$

$$N_h = V \cos \theta \tag{3-4}$$

$$\frac{A_v f_v}{s} = \frac{V}{d} \tan \theta \tag{3-5}$$

Since there are only three equations of equilibrium (**Equations 3-3**, **3-4**, and **3-5**), and there are four unknowns (f_2, N_h, f_v, and θ), the stresses in a beam caused by a given shear force cannot be explicitly determined. For design considerations, the shear force can be predicted assuming the crack angle at 45 degrees and the tensile stress in the stirrups as the tensile strength of steel (f_y). Another approach could be assuming the compressive stress in the concrete to determine the crack angle (**Equation 3-3**) and the shear force (**Equation 3-5**). Other approaches to solving the variable angle truss model have been developed based on subsequent test data. For instance, it has been suggested that the effective compressive strength should be taken as $0.6 f'_c$, and that the factor $\tan \theta$ should be less than 0.5 (Collins and Mitchell, 1991).

Proportioning and detailing of the transverse reinforcement in members with a complex flow of internal stresses was a main aspect of structural concrete research in central Europe during the 1960s and 1970s. Leonhardt, from the University of Stuttgart in Germany, and Thürlimann and Müeller, from the Swiss Federal Institute of Technology in Zürich, were instrumental in the development of analysis and design methods for structural concrete regions with complex internal stress flows. Leonhardt focused mainly

on the analysis and design of deep beams and anchorage end regions in post-tensioned beams. In most of his work, the detailing of the reinforcing steel closely followed the principal tensile stress trajectories found from an elastic analysis of a homogeneous isotropic element. Thürlimann focused mainly on the application of the theory of plasticity in reinforced and prestressed concrete, with practical applications to the design for shear and torsion.

In the mid-1970s, Park and Paulay, from the University of Canterbury, extended many of the analytical and design concepts developed by Leonhardt to include, for the first time, the detailing of regions having a complex flow of stresses and subjected to cyclic load reversals caused by earthquake excitation (Park and Paulay, 1975). One of these regions is the joint between the beam and column in a moment resisting frame. In the analysis and design of beam-column joints, Park and Paulay deviated from Leonhardt's method by proposing a simple mechanism of shear transfer that did not follow the principal tensile stress trajectories shown by an elastic analysis. This model requires vertical and horizontal reinforcement to sustain the diagonal compressive field introduced into the joint as a result of bond forces from the outermost longitudinal column and beam bars.

The truss model is also the starting point of the shear friction model, also known as Loov's theory (1998), in which the shear forces are carried by stirrups and shear friction across the concrete crack. The method comprises the calculation of the shear capacity from all possible crack angles by identifying the weakest plane of failure. The force that holds the two surfaces together is equal to the yield stress multiplied by the cross-sectional area of any steel crossing the crack for bars perpendicular to the failure

plane. In addition to the friction of the failure plane surface, the model accounts for shearing of the reinforcement and the dowel action that they generate. The main drawback to the use of the shear friction models for beam shear is that the critical failure plane is typically unknown, so an interactive approach must be conducted to find the weakest or most critical failure plane.

3.4.2. Strut and tie model. The Strut and Tie Model (STM) was developed in the late 1980s. It was formalized and popularized by Schlaich et al. in a comprehensive paper published in 1987. Reinforced concrete theory hinges on various assumptions of simple beam theory such as plane sections remaining plane. However, regions near a discontinuity do not satisfy this assumption and are called D-regions, which stands for disturbed regions that do not follow simple beam theory. These regions extend approximately a distance h away from the discontinuity which may include concentrated loads, openings, or changes in the cross section. Entire beams consisting of a D-region are called deep beams. Regions in between these areas are subjected to typical beam behavior and are called B-regions. **Figure 3.4** shows the distribution of D- and B-regions, where D stands for discontinuity or disturbed, and B stands for beam or Bernoulli. The STM was developed based on the truss model to account for these D-regions. They consist of struts, ties, and nodal zones. **Figure 3.5** shows how each are combined within a beam.
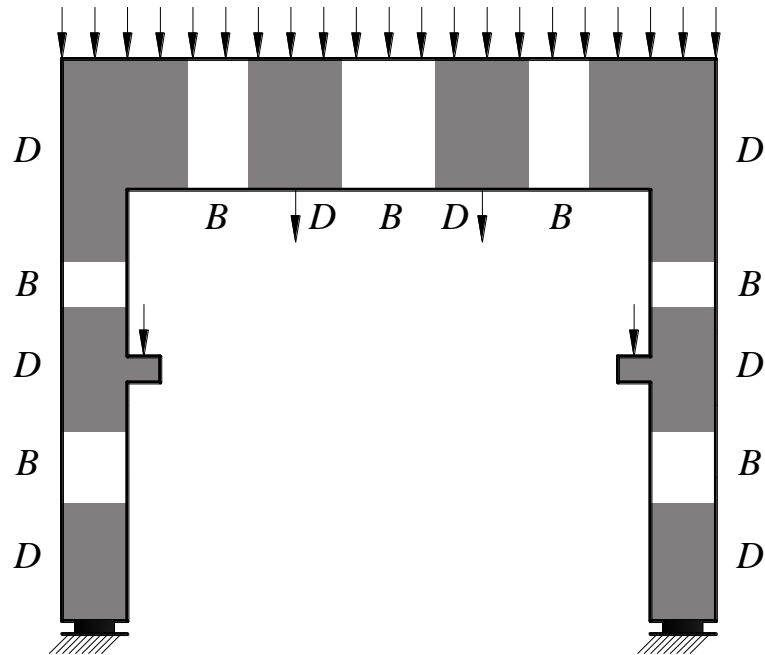
Figure 3.4- B-Regions and D-Regions (Schlaich et al., 1987)

Struts are internal concrete compression members which may be rectangular or bottle-shaped. Bottle-shaped struts swell throughout their depth, and are wider at the center than at the ends. The STM shown in **Figure 3.5** features a rectangular strut, but the bottle-shaped strut is depicted with dashed lines. Ties are tension members within the model and consist of steel reinforcement, plus the portion of concrete surrounding the steel. However, the model assumes that the steel carries all of the tension force. Nodal zones are regions where struts, ties, and concentrated loads meet. Nodes are classified by the types of forces passing into them, which create four types: (a) C-C-C, (b) C-C-T, (c) C-T-T, and (d) T-T-T, where C represents compression and T represents tension. **Figure 3.6** presents each node type.

The following procedure is used to develop a STM:

- Defining of the D-region; borders and forces within these boundaries.

- Drawing a STM based on the assumed node geometry.

- Solving for the truss member forces.

- Calculating the reinforcement layout providing the required tied capacity and enough anchorage length for the bars to ensure the correct behavior at the nodes.

- Dimensioning nodes using truss member forces obtained previously.

- Repeating analysis for the new geometry in order to find a converged solution.

The STM method is not always trouble-free and has many uncertainties. There are four major problems in developing STM, and these are:

- Uncertainties in obtaining dimensions, stiffness, and effective strength of strut, ties, and nodes for the truss models.

- Need to select the optimal STM and iteratively adjust and refine the truss geometry.

- Need to combine different load cases.

- Multiple potential solutions for statically indeterminate models.
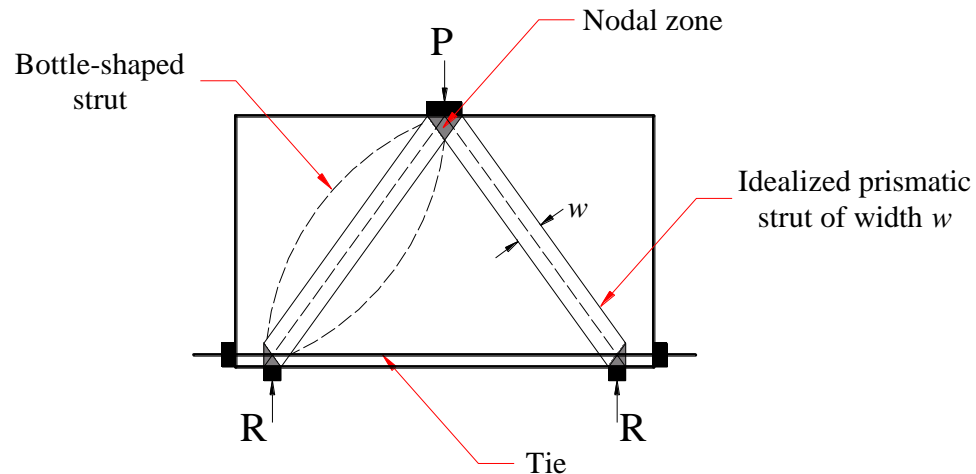
Figure 3.5- Strut and Tie Model (Nilson et al., 2004)

(a) C-C-C   (b) C-C-T   (c) C-T-T   (d) T-T-T
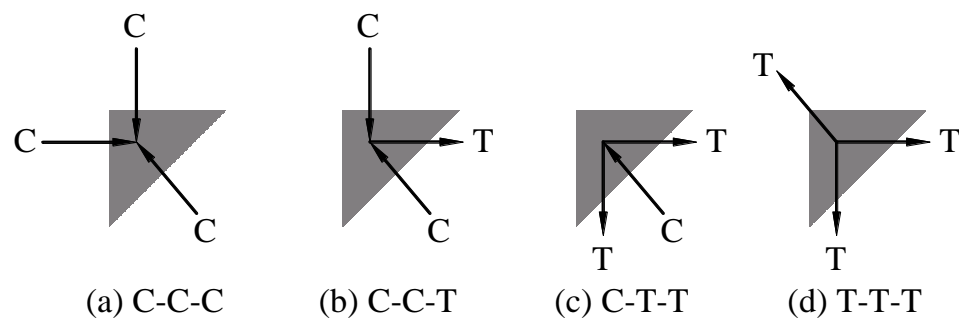
Figure 3.6- Nodal Zones (Nilson et al., 2004)

The creation of the strut and tie model offers no unique solution, and more than one admissible model may be valid for a given problem. The STM must be statically admissible, thus, in equilibrium with the external loads, reactions and nodes. Design takes place by selecting the amount of steel for the tension ties, effective width of the strut, and shape of the nodal zone such that the strength is adequate.

Previous researchers (Kani, 1967) have found that beams with shear span-to-depth ratios greater than 2.5 are governed by conditions away from the disturbed regions adjacent to the support and the loads. In this range, the strength of the beam is not influenced by details such as the size of the bearing plates, and the strength decreases by

only a small amount as the shear span increases. Collins and Mitchell (1997) presented an

example of the use of the strut and tie model illustrated in **Figure 3.7**, which shows how

the shear strength of a simply supported reinforced concrete beam loaded with two point

loads changes as the shear span changes. This study shows that a beam can resist a higher

shear force if the shear is produced by a load that is closer to the support. This series of

beams was tested by Kani (1967), and based on the observation of the results, it was

concluded that the shear strength was reduced by a factor of about 6 as the shear span-to-

depth ratio decreased from 1 to 7 (Collins and Mitchell, 1997). This result can be

explained by the fact that deep beams carry the load by strut-and-tie action, and as the

applied load moves closer to the support, the angle of the compression strut increases,

reducing the force (stress) in the strut, and thus increasing the capacity of a given cross

section. Typical failure mode of these beams involves crushing of the concrete strut.
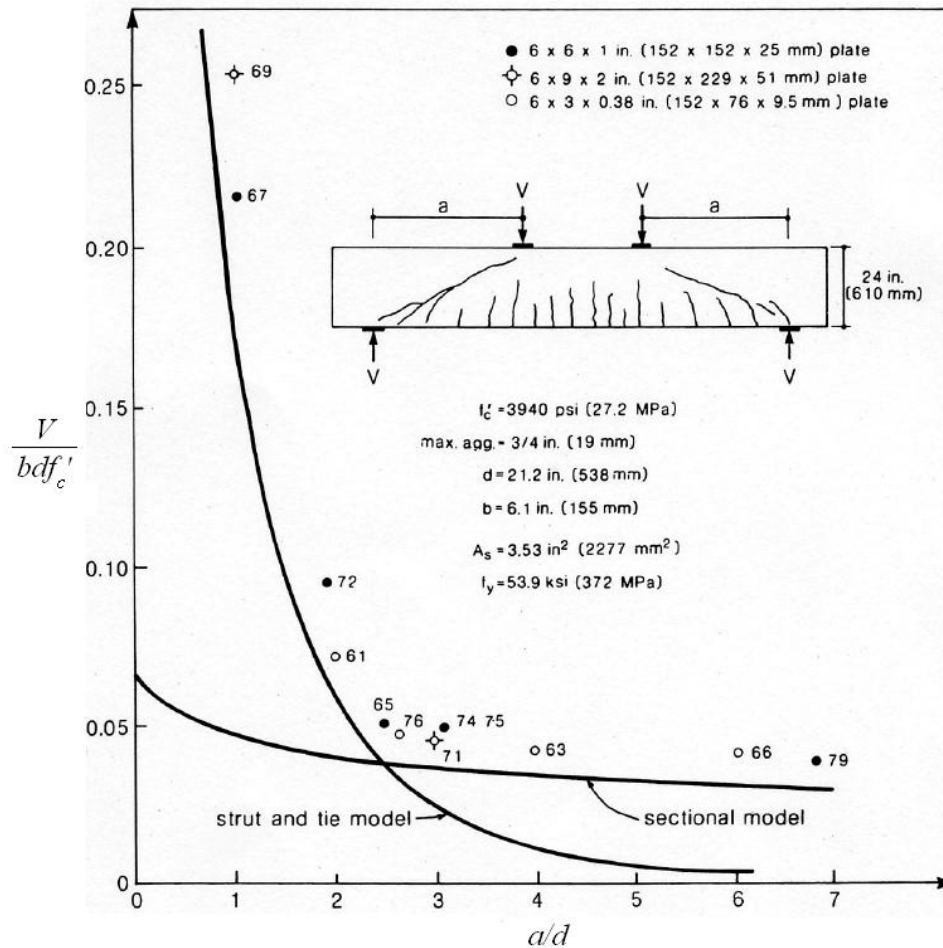
Figure 3.7- Predicted and Observed Strengths of a Series of RC Beams Tested by Kani (Collins and Mitchell, 1997)

The STM approach is rapidly gaining popularity for the analysis and design of

deep beams, and has been adopted in several North American codes, such as the

American Concrete Institute (ACI) Building Code Requirements for Structural Concrete

(ACI 318-08) and the Canadian Standard Association (CSA) Design of Concrete

Structures (CSA A23.3-04). Appendix A of ACI 318-08 provides guidance for sizing

struts, nodes, and ties. The code addresses the performance of highly stressed

compression zones that may be adjacent to or crossed by cracks in a member, the effect

of stresses in nodal zones, and the requirements for bond and anchorage of ties. However,

ACI 318-08 provides no clear guidance to indicate when a strut should be considered as rectangular or bottle-shaped.

Furthermore, as shown in **Figure 3.8**, structural elements may consist of B-regions, D-regions, or a combination of both depending on several factors. ACI 318-08 states that if there is a B-region located between D-regions in a shear span, as shown in **Figure 3.8(b)**, the strength of the shear span is governed by the strength of the B-region if the B- and D-regions have similar geometry and reinforcement. This is because the shear strength of a B-region is less than the shear strength of a comparable D-region. Shear spans containing B-regions are designed for shear using traditional truss model approaches.

Figure 3.9 presents the layout and dimensions of the beam specimens tested in the current study. Based on the previous discussion, the presence of B-regions within the shear span precludes the application of a STM approach in determining the capacity of this section. Instead, these beams are governed by the traditional truss model approach.

3.4.3. Modified compression field theory. The Modified Compression Field Theory (MCFT) was developed by Vecchio and Collins in 1986, and is a further development of the Compression Field Theory (CFT) derived by Collins and Mitchell in 1980. In the CFT it is assumed that the principal tensile stress (f_1) is zero after the concrete has cracked while in the MCFT the effect of the residual stress in the concrete between the cracks is taken into account. Tensile stresses across the diagonal struts increase from zero at the cracks to a maximum in the middle of the strut as shown in **Figure 3.10**.
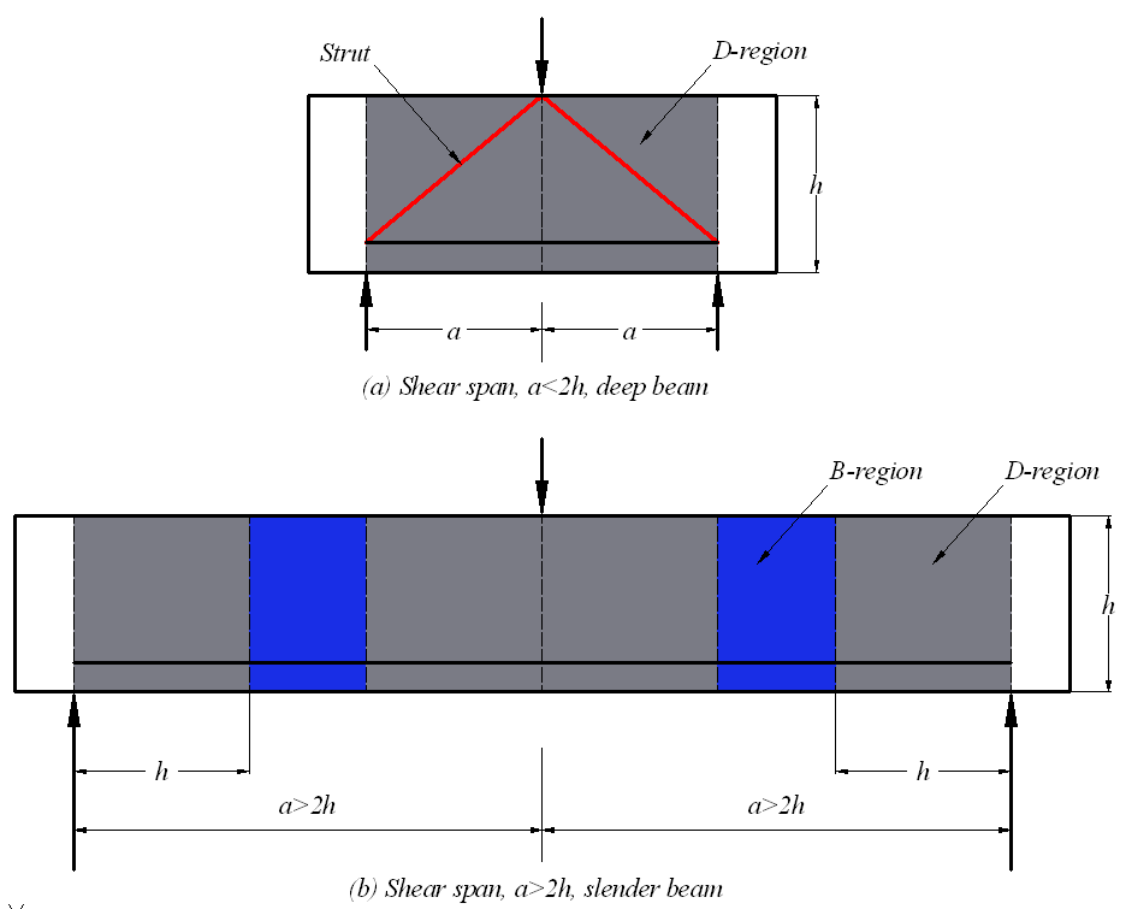
Figure 3.8- Description of Deep and Slender Beams (ACI 318-08)
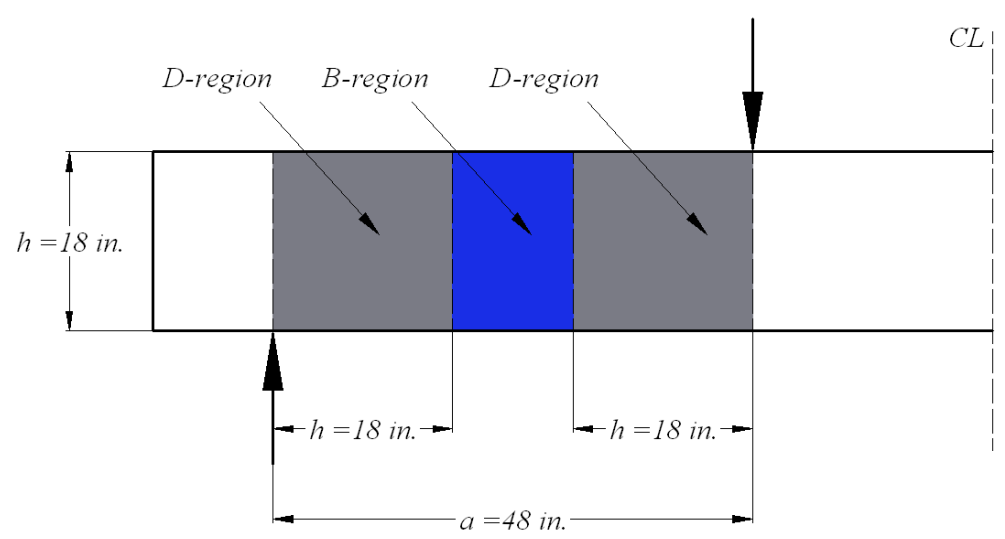
Figure 3.9- Slender Beams Used in This Study

The MCFT model consists of strain compatibility and equilibrium equations which can be used to predict the complete shear deformation response. All the compatibility equations are expressed in terms of average strains measured over base lengths long enough to include several cracks. The compatibility equations for both the CFT and the MCFT are given in **Equations 3-6**, **3-7**, and **3-8**, which are obtained from the Mohr's circle shown in **Figure 3.11**.
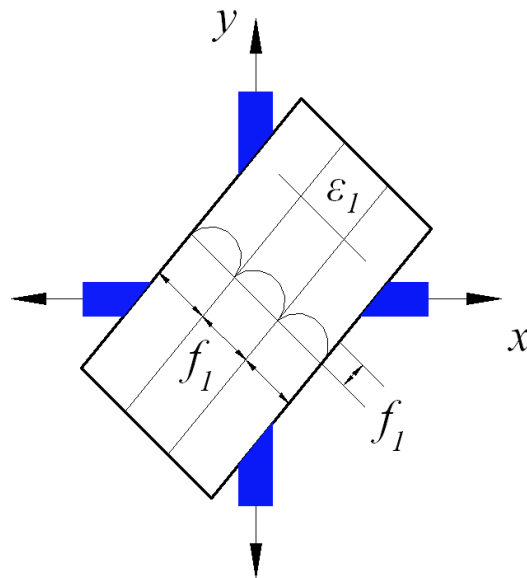
Figure 3.10- Tensile Stress Along a Cracked Strut (Vecchio and Collins, 1986)

$$\gamma_{xy} = \frac{2(\varepsilon_x - \varepsilon_2)}{\tan\theta}$$ (3-6)

$$\varepsilon_1 + \varepsilon_2 = \varepsilon_x + \varepsilon_y$$ (3-7)

$$tan^2\theta = \frac{\varepsilon_x - \varepsilon_2}{\varepsilon_y - \varepsilon_2} = \frac{\varepsilon_1 - \varepsilon_y}{\varepsilon_1 - \varepsilon_x}$$ (3-8)

where γ_{xy} is the shear strain, ε_x is the strain in the x-direction, ε_y is the strain in the y-direction, ε_1 is the principal tensile strain in concrete (positive value), and ε_2 is the principal compressive strain in concrete (negative value).
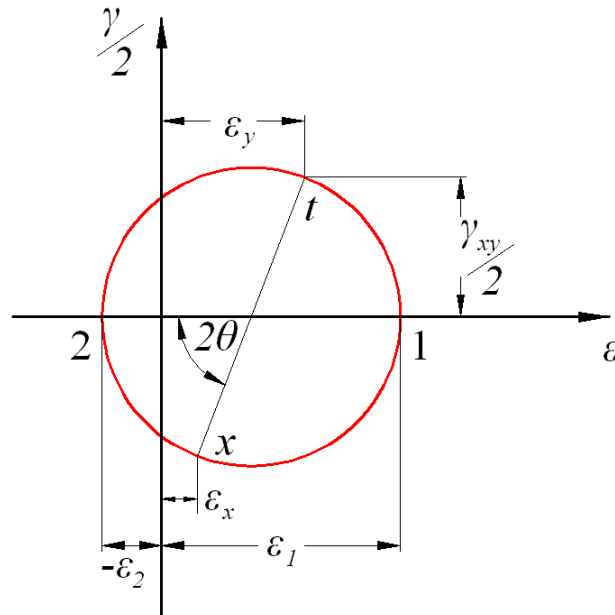
Figure 3.11- Mohr's Circle for Average Strains

The concrete element shown in **Figure 3.12** will resist concrete shear forces (v_{cxy}), horizontal concrete stresses (f_{cx}), and vertical concrete stresses (f_{cy}). All three forces combine to form the principal tensile stress (f_1), and the principal compressive stress (f_2). Converting these stresses into a Mohr's circle of stress, as shown in **Figure 3.13**, the equilibrium **Equations 3-9** and **3-10** can be derived.
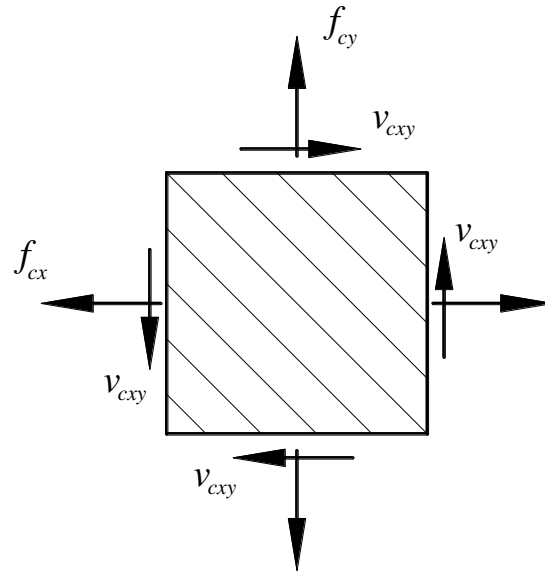
Figure 3.12- Average Concrete Stress in a Cracked Element (Vecchio and Collins, 1986)
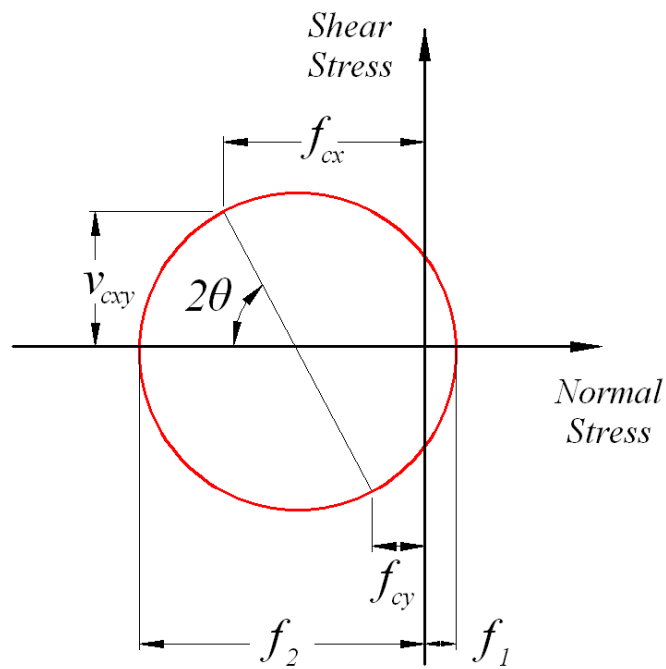
Figure 3.13- Mohr Stress Circle for Average Concrete Stresses

$$f_{cx} = f_1 - \frac{v_{cxy}}{\tan \theta} \qquad\qquad (3\text{-}9)$$

$$f_{cy} = f_1 - v_{cxy} \tan \theta \qquad\qquad (3\text{-}10)$$

The Mohr's circle can also be used to derive an equation for relating the principal compressive stress (f_2) and tensile stresses as shown in **Equation 3-11**.

$$f_2 = (\tan\theta + \cot\theta)v - f_1 \qquad (3\text{-}11)$$

where, $v = \dfrac{V}{b_w jd}$ and jd is the distance between the resultants of the internal compressive and tensile forces on a cross section.

The equilibrium conditions for a symmetrical cross section subjected to pure shear are shown in **Figure 3.14**. These conditions can be expressed as shown in **Equation 3-12**.
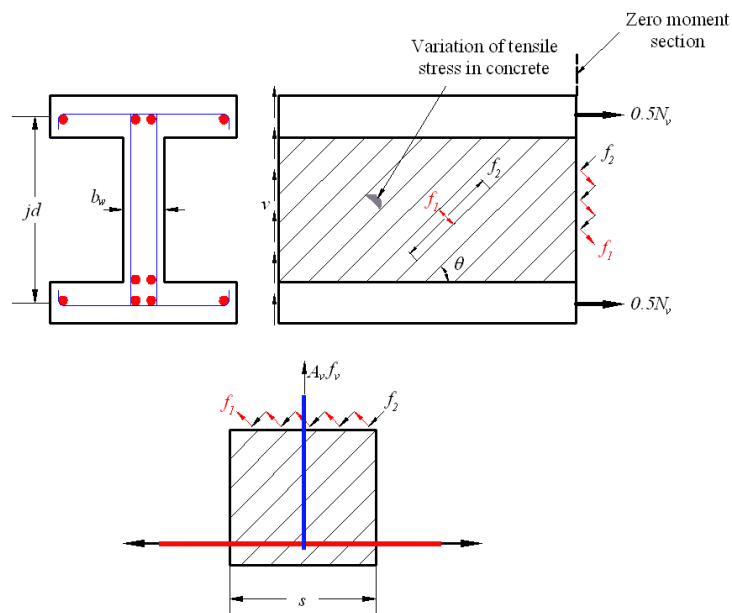
Figure 3.14- Cross Section, Principal Stresses, and Tension in Web Reinforcement (Collins and Mitchell, 1991)

$$A_v f_v = (f_2 sin^2\theta - f_1 cos^2\theta)b_w s \qquad (3\text{-}12)$$

where A_v is the steel vertical reinforcement area and f_v is the stress in the stirrups.

Substituting **Equation 3-11** into **3-12** generates the expression in **Equation 3-13**.

$$V = f_1 b_w jd \cot\theta + \frac{A_v f_v}{s} jd \cot\theta \qquad (3\text{-}13)$$

Collins and Mitchell (1991) noted that **Equation 3-13** expresses shear resistance in terms of the sum of the concrete and steel contributions, as the traditional or classical method. The concrete contribution depends on the average tensile stresses in the concrete, and the steel contribution depends on the tensile stresses in the stirrups. It must be clarified that although the MCFT and the truss model approaches might seem to be similar, the concrete contribution from the concrete suggested by the MCFT is not constant as assumed in the classical truss model. The shear contribution of the concrete (V_c) in the MCFT is not equal to the shear strength of a similar member without shear reinforcement. According to the MCFT, the contribution of the concrete is a function primarily of the crack width. Increasing the number of stirrups reduces the crack spacing, this decreases the crack width and thus increases the concrete contribution (Cladera, 2002).

One of the most important features of the MCFT is the average strain-stress relationships derived from the tests of reinforced panels subjected to pure shear (Vecchio and Collins, 1986). The concrete compressive strength is reduced to take into account softening due to transverse tensile strain (ε_1). Initially, a parabolic relationship for

cracked concrete in compression subjected to high tensile strains in the direction normal to the compression was suggested, as shown in **Equation 3-14**.

$$f_2 = f_{2,max} \left[2 \left(\frac{\varepsilon_2}{\varepsilon'_c} \right) - \left(\frac{\varepsilon_2}{\varepsilon'_c} \right)^2 \right]$$

(3-14)

where ε'_c is the strain in the concrete, and for the MCFT, $\beta = \frac{f_{2,max}}{f'_c} =$

$\frac{1}{0.8 - 0.34 \frac{\varepsilon_1}{\varepsilon'_c}} \leq 1.0$

This relationship for the concrete softening (β) was derived for the MCFT in which the crack slip is not taken into account. According to Vecchio and Collins (1993), concrete strength can also have an influence in concrete softening. Moreover, size effects can also have an effect. For concrete in tension, the curve proposed in Vecchio and Collins (1986) is given by **Equations 3-15** and **3-16**.

$$\text{If } \varepsilon_1 \leq \varepsilon_{cr} \text{ then } f_1 = E_c \varepsilon_1$$

(3-15)

$$\text{If } \varepsilon_1 > \varepsilon_{cr} \text{ then } f_1 = \frac{f_{cr}}{1 + \sqrt{200 \varepsilon_1}}$$

(3-16)

where ε_{cr} is the crack strain, E_c is the modulus of elasticity of the concrete, and f_{cr} is the stress in the concrete at cracking.

Equation 3-16 was updated by Vecchio and Collins (1993) to include two new parameters (α_1 and α_2) to account for the bond characteristics of the reinforcement and the type of loading. The updated equation is presented in **Equation 3-17**.

$$f_1 = \frac{\alpha_1 \alpha_2 f_{cr}}{1+\sqrt{500\varepsilon_1}} \qquad (3\text{-}17)$$

where, $f_{cr} = 0.33\sqrt{f'_c}$

The stress and strain formulations adopted in the MCFT use average values, so local variations are not considered. In this methodology, a check must be done to ensure that the reinforcement can take the increment in tensile stress at the crack. In order to make this check, a value of the stress along the crack must be assumed. The shear transfer at the cracks by aggregate interlock action is estimated using the relationship in **Equation 3-18**. This equation was developed based on Walraven's (1980) experiments.

The MCFT can provide accurate predictions of shear strength and deformation. The first and most important assumption made in the MCFT is that of a rotating crack model in which previous cracks are assumed to be inactive. The MCFT assumes that the angles of the axes for the principal strains and principal stresses coincide (θ). The crack in which all the checks are performed is assumed to be oriented at the same angle, θ, as the compressive stress field.

$$v_{ci} = 0.18v_{ci,max} + 1.64f_{ci} - 0.82\frac{f_{ci}^2}{v_{ci,max}} \quad (3\text{-}18)$$

where, $v_{ci,max} = \frac{\sqrt{f'_c}}{0.31+\frac{24w}{a+16}}$

In the expression above, a is the maximum aggregate size in millimeters, and w is the average crack width over the crack surface which is estimated as the product of the

principal tensile strain (ε_1) and the crack spacing (s_θ). The spacing of shear cracks is

considered to be dependent on the crack spacing in the longitudinal and transverse

reinforcement directions. The crack spacing can be calculated by using **Equation 3-19**. In

this equation s_{mx} is the average spacing of cracks perpendicular to the longitudinal

reinforcement, and s_{mv} is the average spacing of cracks perpendicular to the transverse

reinforcement. Finally, s_{mx} and s_{mv} are estimated using the formulas given by

Equations 3-20 and **3-21**.

$$s_\theta = \frac{1}{\frac{\sin\theta}{s_{mx}} + \frac{\cos\theta}{s_{mv}}} \tag{3-19}$$

$$s_{mx} = 2\left(c_x + \frac{s_x}{10}\right) + 0.25k_1\frac{d_{bx}}{\rho_x} \tag{3-20}$$

$$s_{mv} = 2\left(c_y + \frac{s}{10}\right) + 0.25k_1\frac{d_{bv}}{\rho_v} \tag{3-21}$$

where c_x and c_y are the concrete covers for the longitudinal and transverse

reinforcement respectively; s_x and s are the spacing of the longitudinal and transverse

reinforcement respectively; d_{bx} and d_{bv} are the bar diameters of the longitudinal and

transverse reinforcement respectively; ρ_x and ρ_v are the ratios for the longitudinal and

transverse reinforcement respectively; and k_1 equals 0.4 for deformed bars and 0.8 for

plain bars.

The MCFT has been criticized from a practical perspective since it requires the

use of a computer in order to solve the system of equations. This problem was addressed

by Bentz and Collins by providing two free software packages, called RESPONSE 2000 and MEMBRANE 2000, to solve these equations.

Bentz et al. (2006) developed simplified versions of the MCFT which can be used in order to predict the maximum shear capacity rather than the complete load-deformation response. **Equations 3-22** and **3-23** present these expressions that are also incorporated in the Canadian Code CSA A23.3 (2004).

$$V_r = V_c + V_s \leq 0.25 \emptyset_c f'_c b_w d \qquad (3\text{-}22)$$

$$V_r = \emptyset_c \beta \sqrt{f'_c} b_w d + \emptyset_s \frac{A_{sw}}{s} f_y d \cot \theta \qquad (3\text{-}23)$$

where $\emptyset_c$ and $\emptyset_s$ are the capacity reduction factors, b_w is the width of the web, d is the effective shear depth ($d_v = 0.9d$), A_s is the area of longitudinal reinforcement on the flexural tension side. The parameter β represents the shear retention factor that can be defined as the ability of cracked concrete to transmit shear by means of aggregate interlock, while θ is the angle of inclination of the strut. These two parameters are estimated in terms of the longitudinal strain at the mid-depth of the section using **Equations 3-24** and **3-25**.

$$\beta = \frac{0.40}{1 + 1500\varepsilon_x} \cdot \frac{1300}{1000 + s_{xe}} \qquad (3\text{-}24)$$

$$\theta = 29 + 7000\varepsilon_x \qquad (3\text{-}25)$$

where, $\varepsilon_x = \dfrac{\frac{M_f}{d}+V_f}{2E_sA_{sl}}$

The parameters V_f and M_f are the factored shear force and moment at the section.

The effective crack spacing (s_{xe}) is taken as 11.8 in. for members with at least minimum

stirrups and for members without stirrups, $s_{xe} = \dfrac{35s_x}{15+a_g} \geq 0.85s_x$. The crack spacing

parameter (s_x) is the longitudinal spacing between cracks, measured at mid-depth of the

member. For members without horizontal reinforcement at the web, s_x is usually taken as

d_v.

3.4.4. Fracture mechanics approach. Although fracture mechanics was

developed by Griffith in 1920, for half a century, it was considered inappropriate for

concrete. The reason that it took so long to apply this method to concrete is that the

traditional fracture mechanics approach was developed for homogeneous materials, such

as steel. However, the existence of a size effect observed in experimental results obtained

during previous research (Bazant and Kim, 1984) prompted several researchers to apply

fracture mechanics to shear failures. The use of fracture mechanics in design could

increase the safety and reliability of concrete structures. Numerous analytical and

numerical tools have been developed to simulate the fracture behavior of concrete

structures, and in connection with these developments, researchers are focused on

designing experimental methods to measure the different parameters required for these

models. The ACI 446.1R (1999) document highlights five compelling reasons to use a

fracture mechanics approach. The first one is the energy required for crack formation.

This reason states that the actual formation of cracks requires energy, called fracture

energy, which represents the surface energy of a solid. The second one is the objectivity

of the calculations. Any physical theory must be objective and the result of the

calculations must not depend on subjective aspects such as choice of coordinates, mesh,

etc. Objectivity should come ahead of experimental verification. The third reason is the

lack of yield plateau. Based on load-deflection diagrams, there are two distinguishable

basic types of structural failure, plastic and brittle. Plastic failures typically develop a

single-degree-of-freedom mechanism such that the failure proceeds simultaneously in

various parts of the structure. These failures are characterized by the presence of a long

yield plateau on the load-deflection diagram. If this diagram does not have such a plateau,

the failure is brittle or brittle-ductile. The fourth reason is capability to absorb energy, as

related to ductility. The area under the complete load-deflection diagram represents the

energy which the structure will absorb during failure, and this energy must be supplied by

the loads. The current plastic limit analysis cannot give information on the post-peak

decline of the load and energy dissipated in this process. The fifth and most compelling

reason for using fracture mechanics is the size effect. ACI 446.1R (1999) defines the size

effect through a comparison of geometrically similar structures of different sizes,

characterized in terms of the nominal stress at maximum ultimate load. When this

nominal stress does not change its value for geometrically similar structures of different

sizes, it can be said that there is no size effect.

The study of fracture mechanics of concrete started in 1961 with Kaplan. Later, in

1972, Kesler et al. concluded that the classical linear elastic fracture mechanics (LEFM)

approach with only one fracture parameter, either the fracture energy or the fracture

toughness, was not applicable to concrete. Kesler et al. suggested at least two fracture

parameters.

The simplest model that describes the progressive fracture process is the cohesive crack model (Hillerborg et al., 1976). Hillerborg et al. proposed the cohesive crack model for simulation of plain concrete, in which concrete fracture energy characterized the softening response of a cohesive crack that could develop anywhere in a concrete structure. The softening curve is the main feature of the cohesive crack model. This curve presents an initial portion with a steep descending slope, followed by a smooth drop when the stress reaches a value approximately equal to 1/3 of the nominal tensile strength (f'_t), and a long tail asymptotic to the horizontal axis (crack opening, w) as shown in **Figure 3.15**. Geometrically, the area under the complete curve represents the fracture energy. The fracture energy is defined as the amount of energy necessary to create a crack of unit surface area projected in a plane parallel to the crack direction.

Hillerborg (1985) provided a theoretical basis for a concrete fracture energy testing procedure, often referred to as the work-of-fracture method (WFM), in which the fracture energy per unit area of concrete is computed as the area under the experimental load-deflection response curve for a notched concrete beam subjected to three-point bending, divided by the area of fracture concrete.
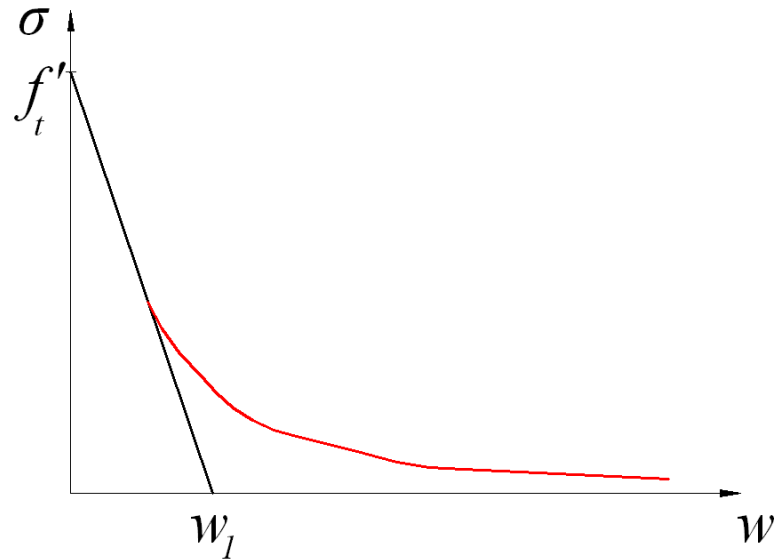
Figure 3.15- Softening Function and Initial Tangent for Cohesive Crack Model (Einsfeld and Velasco, 2006)

For example, when conducting three-point bending tests on notched beams, as the beam splits into two halves, the fracture energy (G_F) can be determined by dividing the total dissipated energy by the total surface area of the crack as shown in **Equation 3-26**.

$$G_F = \frac{W}{b(d-a_0)}$$ (3-26)

where W is the total energy dissipated in the test, and b, d, and a_0 are the thickness, height and notch depth of the beam, respectively.

Several additional test methods have been proposed in recent years to determine concrete fracture properties from which fracture energy may be computed.

In 1987, Bazant and Pfeiffer concluded that the cohesive crack model results in fracture characteristics that are ambiguous and size-dependent. As a consequence, different values for the fracture energy could be obtained for specimens of different sizes.

Bazant and Pfeiffer proposed a method where the fracture energy is calculated based on the size effect law. In this approach, the fracture energy is independent of the size of the specimens. This asymptotic approach is known as the size effect method (SEM). Bazant and Pfeiffer suggested the following relationship shown in **Equation 3-27**.

$$\sigma_N = B(1 + \beta^k)^{\frac{1}{2k}}$$

(3-27)

where σ_N is the nominal stress at failure, B is the coefficient obtained through the linear regression plot of the results, β is the brittleness number, and k is a parameter to reflect the size effect.

The brittleness number indicates whether the behavior of any structure is related to either the limit state analysis or to LEFM analysis. Bazant and Pfeiffer proposed **Equation 3-28** for the brittleness number.

$$\beta = \frac{d}{d_0}$$

(3-28)

where d is the characteristic dimension of the structure (for their study, the specimen height), and d_0 is a coefficient determined experimentally. The coefficients B and d_0 are determined by linear regression. In this approach, specimens of different sizes but geometrically similar can be rearranged in a linear regression plot as shown in **Equation 3-29**. **Equations 3-30** to **3-33** present the different relationships for the parameters contained in **Equation 3-29**.

Rupture of a structure of infinite size follows the LEFM theory, since the plastic region around the concrete fracture zone is relatively small. In this case, the fracture energy can be calculated using **Equation 3-34**.

$$y = Ax + C \qquad (3\text{-}29)$$

$$y = \left(\frac{1}{\sigma_N}\right)^2 \qquad (3\text{-}30)$$

$$x = d \qquad (3\text{-}31)$$

$$d_0 = \frac{C}{A} \qquad (3\text{-}32)$$

$$B = \frac{1}{\sqrt{C}} \qquad (3\text{-}33)$$

$$G_f = \frac{g_f(\alpha_0)}{AE} \qquad (3\text{-}34)$$

where E is the modulus of elasticity of the concrete, A is the angular coefficient of the linear regression plot, $g_f(\alpha_0)$ is the non-dimensional energy release rate calculated according to LEFM, and α_0 is the relative notch length defined in **Equation 3-35**.

$$\alpha_0 = \frac{a_0}{d} \qquad (3\text{-}35)$$

The fracture energy normally associated with WFM is different from the one calculated through SEM. They are usually differentiated as G_F for values calculated with WFM, and G_f for values calculated using SEM. The values obtained with WFM are

sensitive to the specimen size and shape. On the other hand, values obtained with SEM are independent of the structure size as well as geometry (Einsfeld and Velasco, 2006).

While G_F corresponds to the area under the complete softening stress-separation curve of the cohesive crack model, G_f corresponds to the area under the initial tangent of the stress-separation curve as shown in **Figure 3.16**.

Bazant and Kim (1984) and Bazant and Sun (1987) developed a set of equations to describe the dependence of the diagonal shear strength on the size, shape, and longitudinal reinforcement ratio of beams failing in diagonal shear. The shear strength in this model is assumed to result from the combination of the arching action and the composite beam action. The summation of the two components resulted on an expression similar to that of the ACI building code. However, this expression failed to explain the structural behavior.
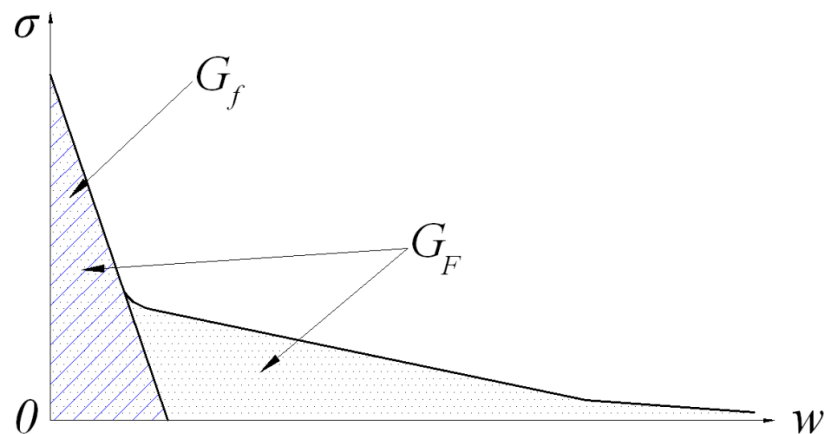

Figure 3.16- Softening Stress-Separation Curve of Cohesive Crack Model (Bazant and Becq-Giraudon, 2002)

Gustafsson and Hillerborg in 1988 investigated the diagonal shear strength of members without stirrups using the cohesive crack concept, with the objective to show that a size effect can be predicted theoretically. This model assumes that a single

polygonal cohesive crack with linear softening is formed, while the bulk of the concrete remains linear elastic. The behavior of the steel is assumed to be linear elastic. The failure criterion adopted is crushing of the concrete. Using this approach Gustafsson and Hillerborg analyzed the influence of the size, longitudinal reinforcement ratio, and the shear span-to-depth ratio.

Jenq and Shah (1989) adopted a more physical approach applying a two-parameter nonlinear fracture mechanics model to the shear failure. In this model, the ultimate shear capacity is assumed to be the summation of the contributions from the reinforcement and the concrete. The concrete contribution is derived using the fracture mechanics model. The steel contribution is estimated by considering the average ultimate bond stress, which is assumed to be proportional to the embedded length.

In 1993, So and Karihaloo criticized Jenq and Shah's approach pointing out that their approach was oversimplified and ignored the influence of the reinforcement on the fracture behavior of the concrete. Large discrepancy between the predicted and measured capacity confirmed their criticism. Khariloo introduced a failure criterion for longitudinal splitting using Van der Veen's model (Van der Veen, 1990) to derive the maximum bond stress. Finally, Karihaloo concluded that the bond-slip relationship, the dowel action, and the aggregate interlock must be taken into account to accurately predict the shear capacity using Jenq and Shah's approach. The only weak point of Karihaloo's model is the significant use of empirical equations.

In 2001, Gastebled and May proposed a fracture mechanics model for the flexural-shear failure of reinforced concrete beams without stirrups. This model was developed assuming that the ultimate shear load is reached when the splitting crack starts

to propagate. The critical load is calculated considering the energy balance of the system during splitting crack propagation. The position of the critical diagonal crack is obtained using Kim and White's semi-empirical formula proposed in 1991. Gastebled and May used the empirical formula for the assessment of the fracture energy proposed by the CEB-FIP Model Code.

The formulation of this model is based on the fundamental relation of LEFM presented in **Equation 3-36**, where G is the fracture energy consumption and W_{ext} is the work of the external force. The external load is produced by the rotation under constant load about the tip of the diagonal crack. In order to calculate the energy release, the rotational stiffness of the beam must be determined. This stiffness depends on the axial and dowel stiffness of the longitudinal reinforcement. The stiffness is calculated based on the free body diagram (FBD) presented in **Figure 3.17**.

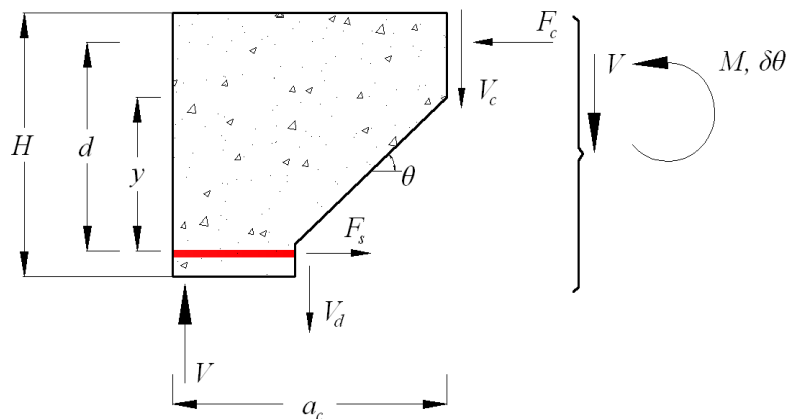$$\delta G = \frac{1}{2} \delta W_{ext} \tag{3-36}$$

Figure 3.17- Free Body Diagram and Notation Definition (Gastebled and May, 2001)

The axial and shear force in the steel bar crossing the diagonal crack were linked to the angle of rotation (θ) using the elastic properties of the bar and the geometry of the deformation mechanism as shown in **Equation 3-37**. The beam bending theory for a circular cross section is also used to derive the dowel force as shown in **Equation 3-38**.

$$F_S = \frac{E_S A_S}{\delta_s} y\theta \tag{3-37}$$

$$V_d = \frac{G_S \Sigma_S}{\delta_s} y\theta = \frac{9}{26} \cdot \frac{E_S A_S}{\delta_s} y\theta \tag{3-38}$$

where F_s is the longitudinal reinforcement force, δ_s is the unbounded length of the reinforcement, y is the diagonal crack extent, θ is the rotation, V_d is the longitudinal reinforcement dowel force, G_s is the shear modulus of steel, and Σ_s is the reduced cross section of the bar (taken as $0.9A_s$).

The equilibrium of the FBD presented in **Figure 3.17** is reached when the following relationships shown in **Equations 3-39** to **3-41** are maintained (horizontal, vertical, and moment equilibrium, respectively). Assuming that the diagonal crack extent and the internal moment arm (jd) are proportional to the height of the beam as shown in **Equations 3-42** and **3-43**, **Equation 3-41** can be rewritten and is presented in **Equation 3-44**. **Equation 3-44** provides the rotational stiffness.

$$F_s = F_c \tag{3-39}$$

$$V_c + V_d = V \tag{3-40}$$

$$F_s jd + V_d y = V a_c \tag{3-41}$$

$$y = \beta H \qquad\qquad (3\text{-}42)$$

$$jd = \gamma H \qquad\qquad (3\text{-}43)$$

$$\beta \left(\frac{9}{26}\beta + \gamma\right) \frac{E_s A_s}{\delta_s} H^2 \theta = V a_c \qquad\qquad (3\text{-}44)$$

After differentiating **Equation 3-44** and using the fundamental relation of fracture mechanics as a criterion for splitting failure as shown in **Equation 3-36**, **Equations 3-45** and **3-46** are derived to obtain the expression for the critical shear load.

$$a_c V_{cr} \delta\theta = 2\Gamma\delta_e \qquad\qquad (3\text{-}45)$$

$$V_{cr} = \sqrt{\frac{9}{13} + 2\frac{\gamma}{\beta}} \cdot \frac{\beta H}{a_c} \cdot \sqrt{\Gamma A_s E_s} \qquad\qquad (3\text{-}46)$$

where δ_e is the variation of the unbonded length, and Γ is the fracture energy necessary to extend the splitting crack by a unit length. For simplicity of calculations and based on experimental observations, γ and β can be taken as 0.9 and 0.8 respectively. The units for this model have been set as follows: V_{cr} in kN, Γ in kN-m/m, A_s in mm^2, and E_s in GPa.

This model uses the equation given by the CEB-FIP Model Code for the assessment of the fracture energy and is presented in **Equation 3-47**. The maximum aggregate size (d_{agg}) is assumed in Gastebled and May's model as 0.75 in. Based on all

the previous assumptions and assuming a dynamic mode of failure, **Equation 3-46** can be simplified and is presented in **Equation 3-48**.

$$G_f = \left(0.0469 d_{agg}^2 - 0.5 d_{agg} + 26\right) \left(\frac{f'_c}{10}\right)^{0.7} \qquad (3\text{-}47)$$

$$V_{cr} = 4.517 \cdot \frac{H}{a_c} \cdot (f'_c)^{0.35} \sqrt{A_s E_s b} \qquad (3\text{-}48)$$

The units for this model have been set as follows: V_{cr} in kN, f'_c in MPa, A_s in m^2, and E_s in GPa, and b in mm.

The only problem in this model is the determination of the location of the critical diagonal crack. Kim and White (1991) postulated the same failure mechanism and adopted a mixed approach, partly physical and partly empirical, to predict the flexural-shear cracking and the position of the critical diagonal crack. **Equation 3-49** presents the model to calculate the location of the critical diagonal crack.

$$a_c = k_3 a_s \left(\frac{\rho_s \left(\frac{d}{a_s}\right)^2}{\left(1 - \sqrt{\rho_s}\right)^2}\right)^{\frac{1}{3}} \qquad (3\text{-}49)$$

where k_3 is an empirical coefficient determined through statistical analysis and has a value of 3.3, a_s is the shear span, ρ_s is the geometrical reinforcement ratio, and d is the effective depth of the beam. Limited experimental data was available to check the position of the critical diagonal crack, however, Kim and White found 14 experimental results to perform the statistical analysis and determine a value for the coefficient k_3. Significant scatter was reported by the authors.

The final expression is obtained by substituting **Equation 3-49** into **Equation 3-48** and is shown in **Equation 3-50**. In this expression, the first term corresponds to the size effect, the second term takes into account the slenderness of the beam, the third and fourth terms reflect the reinforcement ratio influence, and the fifth term corresponds to the influence of the concrete strength.

$$V_{cr} = \frac{1.109}{\sqrt{H}} \cdot \left(\frac{H}{a_s}\right)^{\frac{1}{3}} \cdot \left(1 - \sqrt{\rho_s}\right)^{\frac{2}{3}} \cdot \rho_s^{\frac{1}{6}} \cdot f'^{0.35}_c \cdot \sqrt{E_s} \cdot bH \qquad (3\text{-}50)$$

where H is the height of the beam, a_s is the shear span, ρ_s is the geometrical reinforcement ratio, f'_c is the concrete compressive strength, E_s is the steel modulus of elasticity, and b is the width of the beam.

Bazant and Becq-Giraudon (2002) formulated the empirical expression shown in **Equation 3-51** to compute fracture energy for specimens with rounded aggregate. This equation was calibrated using 161 RILEM work-of-fracture tests whereas the equation proposed by CEB-FIP was calibrated using much less data. Bazant and Becq-Giraudon also reported that G_F data computed from work-of-fracture testing have significantly more scatter than G_f data computed using other test methods and suggested that this scatter was due to errors in measurement of the tail of the load-displacement response curve.

$$G_f = 0.0143\alpha_0 \left(\frac{f'_c}{8.41}\right)^{0.40} \left(1 + \frac{D_{max}}{0.0763}\right)^{0.43} \left(\frac{w}{c}\right)^{-0.18} \qquad (3\text{-}51)$$

where α_0 is an aggregate shape factor ($\alpha_0 = 1$ for rounded aggregate, and $\alpha_0 = 1.12$ for angular aggregate), f'_c is the compressive strength of the concrete, D_{max}

is the maximum aggregate size, and $\frac{w}{c}$ is the water-to-cement ratio of the concrete. The units of this model have been set as follows: f'_c in psi, and D_{max} in inches.

3.4.5. Truss model and modified compression field theory comparison. The MCFT can be explained as a truss model in which the shear strength is the sum of the steel and concrete contributions. The main difference from a classic truss model with concrete contribution is that the concrete contribution in the MCFT is the vertical component of the shear stress transferred across the crack (v_{ci}) and not the diagonal cracking strength.

Cladera (2002) highlighted the main differences between the truss model and the MCFT concrete contributions:

- The truss model concrete contribution is considered equal to the shear strength of a similar beam without shear reinforcement. The MCFT takes into account a concrete contribution based on the actual collapse mechanism of a RC beam.

- The truss model concrete contribution does not vary with the amount of the transverse reinforcement. The MCFT concrete contribution depends on the crack width. The more shear reinforcement, the lesser the crack width, and the greater the concrete contribution.

3.4.6. Summary of shear design. Shear design in structural concrete has been a challenging topic for many years. The truss analogy first proposed by Ritter (1899) and then improved by Mörsch (1902) has been a powerful tool up in understanding the shear transfer mechanism in a RC beam. However, progress has been made since those early truss models. Three different groups of approaches have been developed: (1) 45 degrees

truss model, (2) compression field theories, and (3) fracture mechanics approach. Predictions of the shear provided by these approaches have improved considerably from early formulations, which were based on empirical results. As reported by Collins et al. (2008), early design equations for shear have been proven to be unsafe since the experimental data used in calibrating the models corresponded to rather small specimens. The MCFT offers a rational approach in which the shear transmitted along the crack is limited according to the crack width and aggregate size. The STM which was developed by Schaich et al. (1987) is often claimed as a transparent method for designing and detailing discontinuity regions. It has been highlighted that the method requires several simplifications regarding geometry assumed for the truss elements or the effective strength of the struts. Finally, it is clear that several difficulties can be faced in developing a STM, such as uniqueness of the model, combinations with other load cases or dealing with statically indeterminate systems.

3.5. DESIGN CODES REVIEW

There are a variety of design code philosophies that can be found around the world for shear design. Some of these rely on empirical formulas for estimating the shear strength, such as the ACI 318-08 (2008), while others such as the AASHTO LRFD (2004) rely more on concrete models such as the MCFT. This section will detail three selected design codes.

3.5.1. American Concrete Institute, ACI 318-08. The ACI 318-08 method is most commonly used for shear design in the United States, and is based on a 45 degree truss model. The shear strength is based on an average shear stress distribution across the

entire cross section, and is composed of a concrete component (V_c) and a steel component (V_s). The basic equations for normal-weight, non-prestressed reinforced concrete are listed in **Equations 3-52** to **3-56**.

$$V_u \leq V_n = V_c + V_s \tag{3-52}$$

$$V_c = \left(1.9\sqrt{f'_c} + 2500\rho_w \frac{V_u d}{M_u}\right) b_w d \leq 3.5\sqrt{f'_c} b_w d \tag{3-53}$$

$$\text{Simplified version: } V_c = 2\sqrt{f'_c} b_w d \tag{3-54}$$

$$A_{v,min} = 0.75\sqrt{f'_c} \frac{b_w s}{f_{yt}} \geq 50\frac{b_w s}{f_{yt}} \tag{3-55}$$

$$V_s = \frac{A_v f_{yt} d}{s} \tag{3-56}$$

where, V_u is the factored shear force on the section, $\emptyset$ is the strength reduction factor equal to 0.75 and not shown in **Equation 3-52**, V_n is the nominal shear strength, $\rho_w = \frac{A_s}{b_w d}$, A_s is the area of longitudinal reinforcement, b_w is the width of the web, d is the distance from the extreme compression fiber to the center of gravity of the steel, M_u is the factored moment at the section, f'_c is the concrete compressive strength (psi), f_{yt} is the yield strength of the transverse reinforcement (psi), s is the spacing of the transverse reinforcement, and A_v is the area of shear reinforcement. The following condition must be maintained $\frac{V_u d}{M_u} \leq 1.0$

The ACI 318-08 presents a procedure for calculating the failure shear strength for concrete beams without shear reinforcement. The simplified method is presented in

Equation 3-54. Some research data indicate that **Equation 3-53** overestimates the influence of f'_c and underestimates the influence of ρ_w and $\frac{V_u d}{M_u}$. This is why, for most designs, it is convenient to assume that the second term of this equation equals to $0.1\sqrt{f'_c}$ and use **Equation 3-54** to calculate the shear contribution of the concrete.

      3.5.2. AASHTO LRFD Bridge Design Specifications. The AASHTO LRFD (2007) method is known as the Sectional Design Model, and is based on the MCFT. The nominal shear resistance (V_n) can be computed by **Equations 3-57** to **3-61**.

$$V_n = V_c + V_s + V_p \tag{3-57}$$

$$V_{n,max} = 0.25f'_c b_v d_v + V_p \tag{3-58}$$

$$V_c = 0.0316\beta\sqrt{f'_c}b_v d_v \tag{3-59}$$

$$V_s = \frac{A_v f_y d_v \cot\theta}{s} \tag{3-60}$$

$$A_{v,min} \geq 0.0316\sqrt{f'_c}\frac{b_v s}{f_y} \tag{3-61}$$

      where, V_p is the vertical component of the prestressing force, b_v is the effective width of the web taken as the minimum web width within the depth, d_v is the effective shear depth taken as the greater of $0.9d$ or $0.72h$, β is the factor indicating the ability of diagonal cracked concrete to transmit tension, θ is the angle of inclination of the diagonal compressive struts, f'_c is the concrete compressive strength (ksi), and f_y is the yield strength of the transverse reinforcement (ksi).

For sections containing at least the minimum amount of transverse reinforcement,
the values of β and θ may be found using **Table 3.1**. The designer selects the row
corresponding to the shear design stress ratio $\frac{v}{f'_c} = \frac{V_u}{b_v d_v f'_c}$, and selects the column
corresponding to the longitudinal strain (ε_x) at mid-depth. The longitudinal strain may be
computed using **Equation 3-62**.

Table 3.1- Values of θ and β for Sections With Transverse Reinforcement
(AASHTO LRFD, 2004)

$\frac{V_u}{f'_c}$		$\varepsilon_x \times 1000$									
		$\leq$ -0.20	$\leq$ -0.10	$\leq$ -0.05	≤ 0	≤ 0.125	≤ 0.25	≤ 0.50	≤ 0.75	≤ 1.00	≤ 1.50	≤ 2.00
≤ 0.075	θ	22.3°	20.4°	21.0°	21.8°	24.3°	26.6°	30.5°	33.7°	36.4°	40.8°	43.9°
	β	6.32	4.75	4.10	3.75	3.24	2.94	2.59	2.38	2.23	1.95	1.67
≤ 0.100	θ	18.1°	20.4°	21.4°	22.5°	24.9°	27.1°	30.8°	34.0°	36.7°	40.8°	43.1°
	β	3.79	3.38	3.24	3.14	2.91	2.75	2.50	2.32	2.18	1.93	1.69
≤ 0.125	θ	19.9°	21.9°	22.8°	23.7°	25.9°	27.9°	31.4°	34.4°	37.0°	41.0°	43.2°
	β	3.18	2.99	2.94	2.87	2.74	2.62	2.42	2.26	2.13	1.90	1.67
≤ 0.150	θ	21.6°	23.3°	24.2°	25.0°	26.9°	28.8°	32.1°	34.9°	37.3°	40.5°	42.8°
	β	2.88	2.79	2.78	2.72	2.60	2.52	2.36	2.21	2.08	1.82	1.61
≤ 0.175	θ	23.2°	24.7°	25.5°	26.2°	28.0°	29.7°	32.7°	35.2°	36.8°	39.7°	42.2°
	β	2.73	2.66	2.65	2.60	2.52	2.44	2.28	2.14	1.96	1.71	1.54
≤ 0.200	θ	24.7°	26.1°	26.7°	27.4°	29.0°	30.6°	32.8°	34.5°	36.1°	39.2°	41.7°
	β	2.63	2.59	2.52	2.51	2.43	2.37	2.14	1.94	1.79	1.61	1.47
≤ 0.225	θ	26.1°	27.3°	27.9°	28.5°	30.0°	30.8°	32.3°	34.0°	35.7°	38.8°	41.4°
	β	2.53	2.45	2.42	2.40	2.34	2.14	1.86	1.73	1.64	1.51	1.39
≤ 0.250	θ	27.5°	28.6°	29.1°	29.7°	30.6°	31.3°	32.8°	34.3°	35.8°	38.6°	41.2°
	β	2.39	2.39	2.33	2.33	2.12	1.93	1.70	1.58	1.50	1.38	1.29

$$\varepsilon_x = \frac{\frac{M_u}{d_v} + 0.5 N_u + 0.5 (V_u - V_p) \cot \theta - A_{ps} f_{po}}{2(E_s A_s + E_p A_p)} \qquad (3\text{-}62)$$

For sections containing less than the minimum amount of transverse
reinforcement, the values of β and θ may be found using **Table 3.2**. The designer selects
the row corresponding to an equivalent spacing parameter (s_{xe}), and selects the column

corresponding to the longitudinal strain at mid-depth. The equivalent spacing may be computed using **Equation 3-63**. The longitudinal strain for this case may be computed using **Equation 3-64**.

Table 3.2- Values of θ and β for Sections With Less Than Minimum Transverse Reinforcement (AASHTO LRFD, 2004)

s_{xe} (in.)		$\varepsilon_x \times 1000$										
		$\leq$ -0.20	$\leq$ -0.10	$\leq$ -0.05	≤ 0	≤ 0.125	≤ 0.25	≤ 0.50	≤ 0.75	≤ 1.00	≤ 1.50	≤ 2.00
≤ 5	θ	25.4°	25.5°	25.9°	26.4°	27.7°	28.9°	30.9°	32.4°	33.7°	35.6°	37.2°
	β	6.36	6.06	5.56	5.15	4.41	3.91	3.26	2.86	2.58	2.21	1.96
$\leq$ 10	θ	27.6°	27.6°	28.3°	29.3°	31.6°	33.5°	36.3°	38.4°	40.1°	42.7°	44.7°
	β	5.78	5.78	5.38	4.89	4.05	3.52	2.88	2.50	2.23	1.88	1.65
$\leq$ 15	θ	29.5°	29.5°	29.7°	31.1°	34.1°	36.5°	39.9°	42.4°	44.4°	47.4°	49.7°
	β	5.34	5.34	5.27	4.73	3.82	3.28	2.64	2.26	2.01	1.68	1.46
$\leq$ 20	θ	31.2°	31.2°	31.2°	32.3°	36.0°	38.8°	42.7°	45.5°	47.6°	50.9°	53.4°
	β	4.99	4.99	4.99	4.61	3.65	3.09	2.46	2.09	1.85	1.52	1.31
$\leq$ 30	θ	34.1°	34.1°	34.1°	34.2°	38.9°	42.3°	46.9°	50.1°	52.6°	56.3°	59.0°
	β	4.46	4.46	4.46	4.43	3.39	2.82	2.19	1.84	1.60	1.30	1.10
$\leq$ 40	θ	36.6°	36.6°	36.6°	36.6°	41.2°	45.0°	50.2°	53.7°	56.3°	60.2°	63.0°
	β	4.06	4.06	4.06	4.06	3.20	2.62	2.00	1.66	1.43	1.14	0.95
$\leq$ 60	θ	40.8°	40.8°	40.8°	40.8°	44.5°	49.2°	55.1°	58.9°	61.8°	65.8°	68.6°
	β	3.50	3.50	3.50	3.50	2.92	2.32	1.72	1.40	1.18	0.92	0.75
$\leq$ 80	θ	44.3°	44.3°	44.3°	44.3°	47.1°	52.3°	58.7°	62.8°	65.7°	69.7°	72.4°
	β	3.10	3.10	3.10	3.10	2.71	2.11	1.52	1.21	1.01	0.76	0.62

$$S_{xe} = \frac{1.38 s_x}{a_g + 0.63} \tag{3-63}$$

$$\varepsilon_x = \frac{\frac{M_u}{d_v} + 0.5 N_u + 0.5 (V_u - V_p) \cot \theta - A_{ps} f_{po}}{E_s A_s + E_p A_p} \tag{3-64}$$

If either value computed for ε_x is negative, the user should use **Equation 3-65** to compute the longitudinal steel strain instead.

$$\varepsilon_x = \frac{\frac{M_u}{d_v}+0.5N_u+0.5\left(V_u-V_p\right)\cot\theta-A_{ps}f_{po}}{2\left(E_cA_c+E_sA_s+E_pA_p\right)} \qquad (3\text{-}65)$$

where, A_c is the area of concrete on the flexural tension side, A_p is the area of

prestressing steel on the flexural tension side, A_s is the area of non-prestressed steel on

the flexural tension side, f_{po} is computed by the modulus of elasticity of the prestressing

tendons (E_p) times the locked difference in strain at ultimate load between the

prestressing tendons and the surrounding concrete, N_u is the factored axial force, s_x is the

crack spacing parameter, and a_g is the maximum aggregate size in inches.

A simplified procedure is presented in the AASHTO LRFD (2007) where the

values of β and θ can be calculated using the following expressions shown in **Equations**

3-66 and **3.67**. The parameter s_{xe} can be calculated using **Equation 3-63**.

$$\beta = \frac{4.8}{1+750\varepsilon_x}\cdot\frac{51}{39+s_{xe}} \qquad (3\text{-}66)$$

$$\theta = 29 + 3500\varepsilon_x \qquad (3\text{-}67)$$

3.5.3. Canadian Standards Association, CSA A23.3-04. The Canadian

Standards Association method, also based on MCFT, gives the following **Equations 3-68**

to **3-76** to calculate the shear strength of a section using their general method. Note that

the equations are given in psi and in. units, with the same notation defined in previous

sections.

$$V_n = V_c + V_s + V_p \qquad (3\text{-}68)$$

$$V_{n,max} = 0.25f'_cb_vd_v + V_p \qquad (3\text{-}69)$$

$$V_c = \beta \sqrt{f'_c} b_v d_v \tag{3-70}$$

$$\beta = \frac{0.40}{1+1500\varepsilon_x} \cdot \frac{1300}{1000+s_{ze}} \tag{3-71}$$

$$s_{ze} = \frac{35s_z}{15+a_g} \tag{3-72}$$

The term a_g should be taken as zero if f'_c exceeds 10,150 psi. The crack spacing

parameter s_z can be taken as d_v or as the maximum distance between layers of

distributed longitudinal reinforcement, whichever is less. Each layer of reinforcement

must have an area at least equal to $0.003b_v s_z$. However, $s_{ze} \geq 0.85s_z$.

$$\varepsilon_x = \frac{\frac{M_u}{d_v}+0.5N_u+V_u-V_p-A_{ps}f_{po}}{2(E_s A_s + E_p A_p)} \tag{3-73}$$

$$V_s = \frac{A_v f_y d_v \cot\theta}{s} \tag{3-74}$$

$$\theta = 29 + 7000\varepsilon_x \tag{3-75}$$

$$A_{v,min} \geq 0.06\sqrt{f'_c}\frac{b_v s}{f_y} \tag{3-76}$$

4. EXPERIMENTAL PROGRAM

4.1. GENERAL

The objective of this study was to investigate the shear performance of reinforced concrete (RC) beams composed of high-volume fly ash (HVFA) concrete. The experimental program consisted of 32 tests performed on full-scale RC beams. The principal parameters investigated were:

(1) concrete type – HVFA concrete or conventional concrete (CC),

(2) total amount of cementitious material – with one mix having a relatively high total cementitious content and the other mix having a relatively low total cementitious content,

(3) amount of longitudinal reinforcement, and

(4) amount of shear reinforcement.

Also, as part of this study, small scale testing was performed to determine hardened concrete properties such as compressive strength, flexural strength, splitting tensile strength, and modulus of elasticity.

4.2. TEST BEAMS

The reinforcement for the beams was designed in accordance with the AASHTO LRFD Bridge Design Specifications (AASHTO LRFD, 2007). Each beam measured 14 ft. in length with a cross section of 12 in. x 18 in. The cross section was selected to maintain a slender beam with a shear span-to-depth ratio larger than 3.0, thus avoiding any deep beam effects. The longitudinal reinforcement was selected to ensure a shear failure prior to a flexural failure yet still remain below the maximum amount allowed by

code. Each beam had two test regions, with each region measuring approximately 4 ft. in length. All of the specimens had #3 stirrups spaced at 2 in. within the bearing area to prevent premature failure as well as #3 stirrups spaced at 7 in. within the middle region to support the reinforcing cage and prevent any premature failure outside of the shear test regions. For the shear specimens with transverse reinforcement, the shear reinforcing consisted of #3 stirrups spaced at 7 in.

Table 4.1 summarizes the test matrix used in this study. The beam designation included a combination of letters and numbers: NS and S stand for no stirrups and stirrups, respectively, within the test region. The numbers 4, 5, 6, and 8 indicate the number of #7 longitudinal reinforcement bars within the tension area of the beam section. For example, NS-6 indicates a beam with no stirrups and 6 #7 bars within the bottom of the beam. Two beams were constructed and tested for each combination of variables shown in Table 4.1. The cross sections for these specimens are shown in Figure 4.1. Figure 4.2 shows the load pattern and location of strain gauges on the test beams.

Table 4.1- Shear Beam Test Matrix

Cementitious Content	Section	Bottom reinforcement	Top reinforcement	ρ	Stirrups
High	NS-5	5#7	4#4	0.0159	-
	NS-6	6#7	4#4	0.0203	-
	NS-8	8#7	4#4	0.0271	-
	S-8	8#7	4#4	0.0271	#3@7 in.
Low	NS-4	4#7	2#4	0.0127	-
	NS-6	6#7	2#4	0.0203	-
	NS-8	8#7	2#7	0.0271	-
	S-8	8#7	2#7	0.0271	#3@7 in.

4#4   4#4   4#4

5#7   6#7   8#7

NS-5   NS-6   NS-8 & S-8
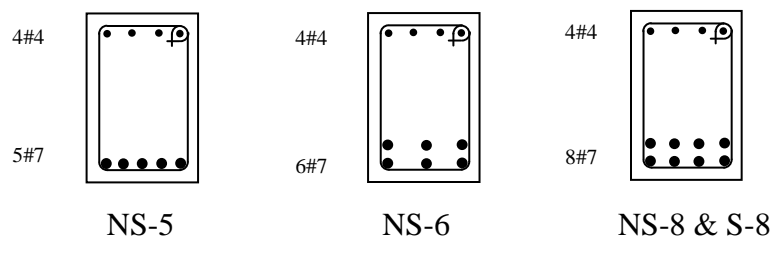
a) Sections used for High Cementitious Content Mix

2#4   2#4   2#4

4#7   6#7   8#7

-8
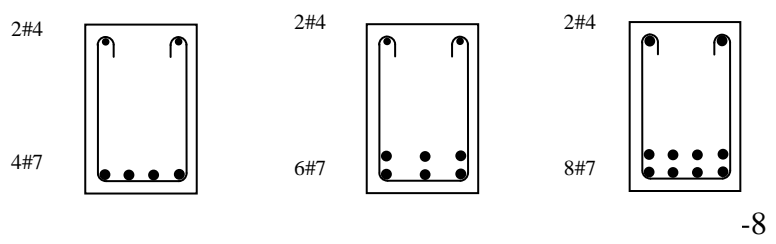
b) Sections used for Low Cementitious Content Mix

Figure 4.1- Cross Sections and Reinforcement Layout of the Beams

a) Without stirrups in test region

b) With stirrups in test region
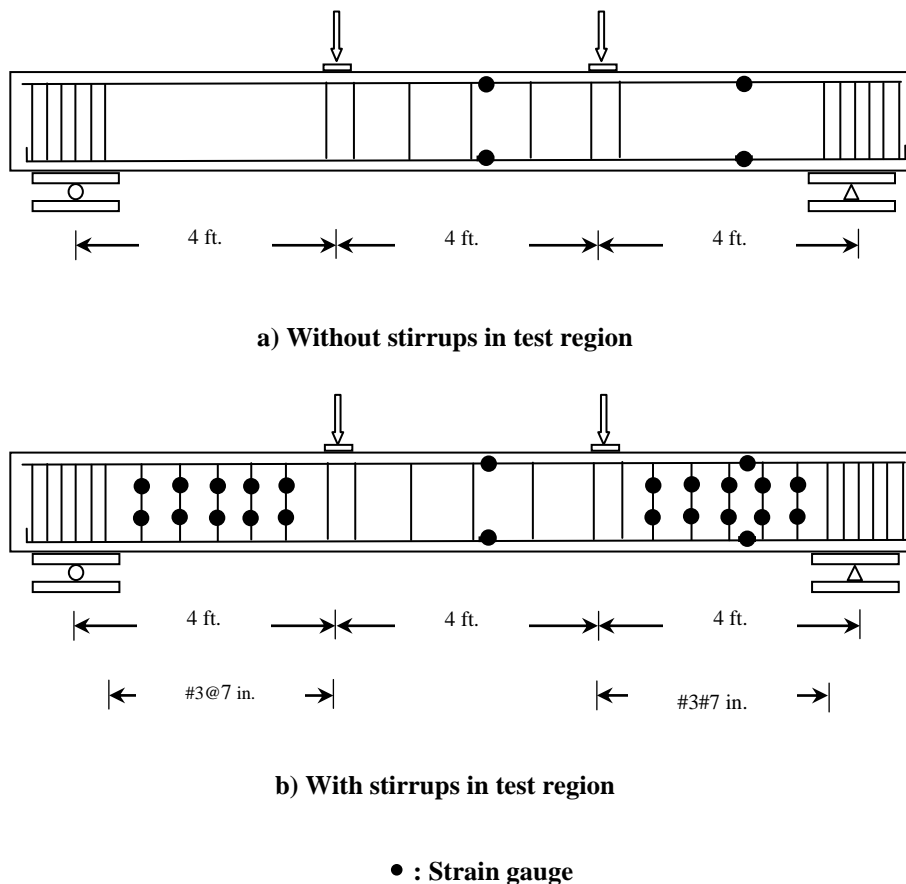
● **: Strain gauge**

Figure 4.2 – Load Pattern and Location of Strain Gauges on the Test Beams

4.3. MATERIALS

4.3.1. Concrete. The concrete mixtures with a target compressive strength of 4000 psi were delivered by a local ready-mix concrete supplier (Rolla, MO). The purpose of using the ready-mix supplier was to validate the HVFA concrete concept in actual production runs. The mixture proportions are given in **Table 4.2**. The design of the mixes was based on significant input from MoDOT as well as results of previous research conducted at Missouri S&T. The HVFA concrete mixes used a 70% replacement of cement with fly ash – with one mix containing a relatively high total cementitious content

(756 lb/yd^3) and the other mix containing a relatively low total cementitious content (564

lb/yd^3). In addition to the HVFA concrete mix designs, two conventional concrete (CC)

mix designs were used for comparison, which were identical to the HVFA concrete mixes

except they used 100% Portland cement for the binder. The notation for the mix designs

consisted of CC-H and HVFA-70H for the high cementitious content conventional and

HVFA concrete mixes, respectively, and CC-L and HVFA-70L for the low cementitious

content conventional and HVFA concrete mixes, respectively.

Table 4.2- Mix Designs per Cubic Yard

	CC-H	HVFA-70H	CC-L	HVFA-70L
Cement (Type I) (lb)	756	219	564	155
Fly Ash (lb)	0	511	0	360
w/cm	0.45	0.40	0.40	0.40
Coarse Aggregate (lb)	1750	1754	1860	1860
Fine Aggregate (lb)	1110	1080	1240	1240
HRWR (fl. oz)	0	0	16.9	15.5
CaOH (lb)	0	51	0	39
Gypsum (lb)	0	21	0	16

For the HVFA concrete mixes, the gypsum was used to maintain the initial

hydration stage by preventing sulfate depletion, while the calcium hydroxide ensured a

more complete hydration of the fly ash with the low content of Portland cement in the

mix. The drums were charged at the ready-mix facility with the required amounts of

cement, fly ash, sand, coarse aggregate, and water, while the powder activators (gypsum

and lime) were added when the truck arrived at the lab, approximately 5 minutes later, as

shown in **Figure 4.3**. After the gypsum and lime were added, the HVFA concrete was

mixed at high speed for 10 minutes. For the CC mixes, all of the constituents were added

at the ready-mix facility. **Table 4.3** presents representative fresh and hardened strength

properties of the CC and HVFA concrete mixes.

Table 4.3- Typical Fresh and Hardened Concrete Properties for CC and HVFA Concrete Mixes

Property	CC-H	HVFA-70H	CC-L	HVFA-70L
Slump (in.)	4.5	5	4.5	5.5
Air content (%)	1.5	1.5	2.5	2.5
Unit weight (lb/ft^3)	149	146	144	147
Split cylinder strength (psi)	480	380	420	410
Compressive strength (psi)	5010	3540	4200	4450

(a) Adding gypsum

(b) Adding calcium hydroxide

(c) Concrete placement

Figure 4.3- HVFA Concrete Mixing Procedures

4.3.2. Steel reinforcement. Shear reinforcement for the test specimens consisted of A615, Grade 60 #3 reinforcing bars. Longitudinal reinforcement for the test specimens consisted of A615, Grade 60 #4 and #7reinforcing bars. All the steel reinforcement was tested in accordance with ASTM A370 (2011) "Standard Test Methods and Definitions for Mechanical Testing of Steel Products" to obtain the mechanical properties, which are summarized in **Table 4.4**. These results are the average of three replicate specimens.

4.4. BEAM FABRICATION

All the test beams were fabricated in the Structural Engineering High-Bay Research Laboratory (SERL) at Missouri S&T. Steel formwork was used to cast the beams. The steel cage was assembled from reinforcement that was bent in the laboratory to the desired geometry. Due to the dimension of the beams, it was possible to cast three beams at a time. After casting, the top surface of the beams was covered with burlap and plastic sheeting, and a wet surface was maintained for three days to retain moisture for proper curing. Cylinders were cured in the same environment as the test beams by placing them next to the beams. The sheeting and burlap were then removed, and the beams were allowed to air cure in the lab environment. Photographs showing the reinforcing cages and the construction process are shown in **Figures 4.4** and **4.5**.

Table 4.4- Mechanical Properties of Steel Reinforcement

Bar size	Yield strength (psi)
#3	67,740
#4	67,970
#7	69,380

(a) Beams with no stirrups in test region

(b) Beams with no stirrups in test region

(c) Beams with stirrups in test region

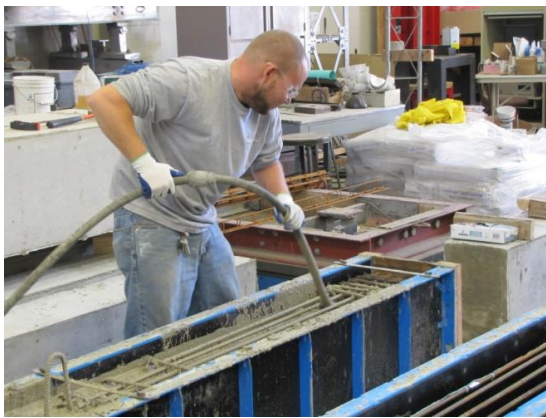(d) Beams with stirrups in test region

Figure 4.4- Reinforcing Cage Assembly

(a) Formwork	(b) Concrete placement

(c) Concrete consolidation	(d) Concrete finishing

Figure 4.5- Beam Construction Process

4.5. TEST SET-UP

All the specimens were tested as simply supported and subjected to a four-point loading. The maximum compression capacity of the actuators available in SERL, when working individually, were insufficient to cause specimen failure. Therefore, the test set-up required the simultaneous action of two actuators as shown in **Figure 4.6**.
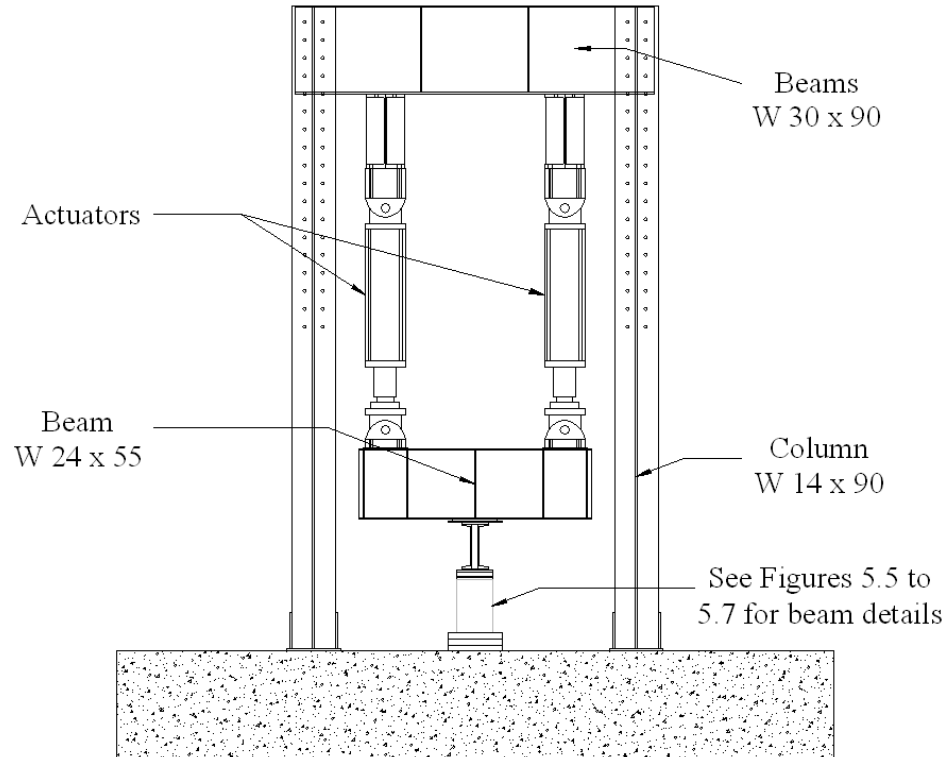
Figure 4.6- Details of Test Set-Up (1)

Two actuators, each with a 140-kip compressive capacity, were used to apply load to the beam specimens, as shown in **Figure 4.7**. The actuators applied load by pushing the steel beam downward to distribute the load onto two points of the test specimen. The loading frame assembly was designed to withstand at least two times the anticipated maximum load applied to fail the beams. Each test was performed under displacement control, and the load was applied in a series of loading steps of 0.05 in., which corresponded to a load of approximately 8 kips, until failure. Electronic measurements of strain and deformation were recorded throughout the entire loading history of the specimens, while hand measurements of strain and crack pattern formations were taken at the end of each load step while the load was paused. Each beam consisted of two test regions. The total beam length was 14 ft, with a simply supported span length of 12 ft.

The load was applied at 4 ft from each support, representing a shear span-to-depth ratio between 3.00 and 3.30 depending on the specimen, as measured from center of support to center of load. **Figure 4.8** shows a photograph of the test set-up.
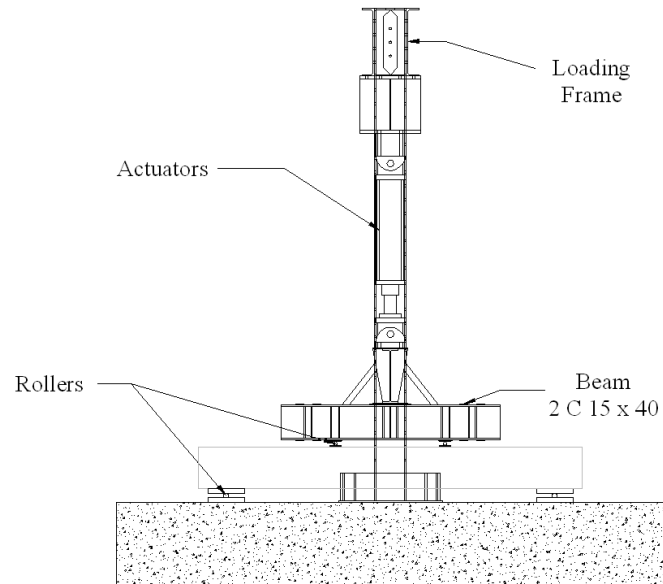
Figure 4.7- Details of Test Set-Up (2)

Figure 4.8- Test Set-Up

4.6. INSTRUMENTATION

The specimens were instrumented with several measurement devices in order to monitor global and local deformations and strains. The load was directly measured from the load cell of the actuators. All devices were connected to a data acquisition system capable of reading up to 120 channels and all the data was recorded as shown in **Figure 4.9.**

Figure 4.9- Data Acquisition System

4.6.1. Local deformations and strains. Electric resistance gauges were used to monitor local strains in the stirrups of the test region. The strain gauges were purchased from Vishay Precision Group. They were made of constantan foil with 120 ohm resistance and had a linear pattern (uniaxial) with a gauge length of ¼ in. Two strain

gauges were installed on each stirrup in the test region as shown in **Figure 4.2.** The strain values obtained from the strain gauges are localized measurements at the point where the gauge is installed. The location of the strain gauges in the transverse reinforcement was chosen to account for the unpredictability of the crack formation. The strain gauge pattern was designed to better capture measurements along the cracks. In addition, strain gauges were placed at various locations along the longitudinal tension and compression reinforcement so that the strain distribution diagrams could be constructed along the height of the cross section at various locations. The first one was located at the midpoint of the shear test region, while the second was located at mid-span.

4.6.2. Global deformations. One Linear Variable Displacement Transducer (LVDT) was used to monitor vertical deflection of the test specimen. The LVDT was located at the midpoint of the test specimen, 3 in. from the top of the beam as shown in **Figures 4.10** and **4.11**.
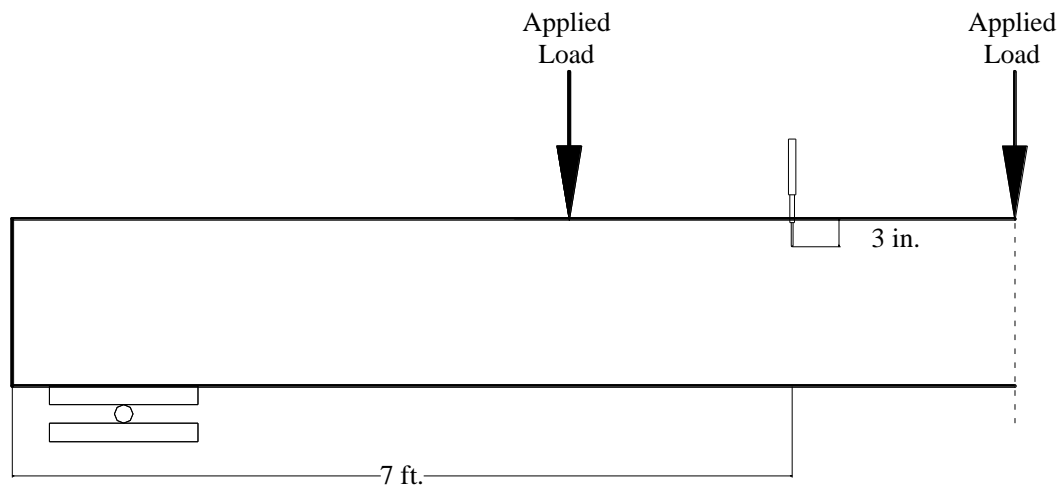
Figure 4.10- Location of LVDT to Measure Deflection

Figure 4.11- Detail of LVDT for Deflection Measurement

5. TEST RESULTS, BEHAVIOR & ANALYSIS

5.1. GENERAL

The purpose of this study was to evaluate the shear behavior of full-scale reinforced concrete (RC) beams constructed from high-volume fly ash (HVFA) concrete, which has not been fully investigated in previous research studies. The objectives of this section are to: (1) discuss the overall behavior of the specimens, (2) discuss the crack morphology and progression, (3) discuss the load-deflection response, (4) evaluate the failure mechanism including critical crack angle and reinforcement strains, (5) compare the test results with predicted capacities based on applicable design standards, (6) compare the HVFA concrete test results with the control specimen results, and (7) compare the test results with a shear test database of conventional concrete specimens.

5.2. TEST RESULTS & BEHAVIOR OF FULL-SCALE SPECIMENS

Table 5.1 summarizes the compressive strength at time of testing, shear force at failure, V_{test}, average shear stress at failure, $V_{test}/b_w d$, ratio of the average shear stress to compressive strength, and ratio of the average shear stress to square root of the compressive strength, $v_{test}/\sqrt{f'c}$. The average shear stress of the CC beams varies from 3.4% to 5.6% of the compressive strength for the low cementitious mix and from 3.4% to 4.8% of the compressive strength for the high cementitious mix. However, for the HVFA concrete beams, the average shear stress increased to 4.4% to 6.8% of the compressive strength for the low cementitious mix and 3.6% to 8.5% of the compressive strength for the high cementitious mix. Another useful comparison is to compare the last column in

Table 5.1 with ACI 318 (2008) Equation 11-3, rewritten in terms of average shear stress for normal weight concrete and shown as **Equation 5-1**. The ratio of experimental shear stress to square root of compressive strength for the beams without stirrups exceeded the ACI coefficient of 2 for all of the beams tested, both CC and HVFA concrete, even at low longitudinal reinforcement ratios.

$$v_c = 2\sqrt{f_c'} \tag{5-1}$$

In addition to studying the behavior of the specimens, the crack patterns experienced by the beams were also evaluated. During testing, cracks within the test region were marked using a permanent marker after each load step. Typical crack pattern progressions are shown in **Figures 5.1** and **5.2** for specimens without and with transverse reinforcement, respectively. Furthermore **Figures 5.3** and **5.4** show the crack pattern for the CC and HVFA concrete beams with different percentages of longitudinal reinforcement, respectively. For both cases, cracks typically began on the tension face of the beam near the loading points. As the loading progressed, the flexural cracks in the shear test region formed inclined flexure-shear cracks. For the specimens with transverse reinforcement, it was observed that at failure, the cracks were typically spaced approximately the same distance as the stirrups, and failure occurred on one side of the beam. For the specimens without transverse reinforcement, the formation of the inclined flexure-shear crack did not result in immediate failure, and additional load was required prior to failure. In general, the failure crack typically extended from the beam support to the loading point on the top side of the beam.

Table 5.1- Test results summary

Mix Design	Section		f'_c	V^*_{test}	$v_{test}=V_{test}/b_w d$	v_{test}/f'_c	$v_{test}/\sqrt{f'_c}$
			psi	kips	psi	%	
CC-H	NS-5	1	5010	31.6	167.8	3.4	2.4
		2	4640	31.0	164.5	3.6	2.4
	NS-6	1	5010	39.1	220.1	4.4	3.1
		2	4640	32.3	182.5	3.9	2.7
	NS-8	1	5010	49.3	278.5	5.6	3.9
		2	4640	33.0	186.4	4.0	2.7
	S-8	1	5020	82.7	467.2	-	-
		2	5020	79.2	447.5	-	-
HVFA-70H	NS-5	1	3190	31.6	167.7	4.8	3.0
		2	3130	25.8	136.9	4.4	2.4
	NS-6	1	3190	29.7	167.8	5.2	3.0
		2	3130	27.3	154.2	4.9	2.8
	NS-8	1	3190	38.4	216.9	6.8	3.8
		2	3130	36.6	206.8	6.6	3.7
	S-8	1	3540	73.9	417.5	-	-
		2	3540	74.8	422.6	-	-
CC-L	NS-4	1	4200	26.9	142.8	3.4	2.2
		2	3840	25.6	135.9	3.5	2.2
	NS-6	1	4200	34.5	194.9	4.6	3.0
		2	3840	32.5	183.6	4.8	3.0
	NS-8	1	4200	33.2	187.5	4.5	2.9
		2	3840	32.3	182.5	4.8	2.9
	S-8	1	4400	67.4	380.8	-	-
		2	4400	71.9	406.2	-	-
HVFA-70L	NS-4	1	4450	30.2	160.3	3.6	2.4
		2	3000	27.6	146.5	4.9	2.7
	NS-6	1	4450	33.8	191.0	4.3	2.9
		2	3000	37.8	213.6	7.1	3.9
	NS-8	1	4450	36.5	206.2	4.6	3.1
		2	3000	45.3	255.9	8.5	4.7
	S-8	1	5030	73.9	417.5	-	-
		2	5030	75.8	428.2	-	-

[*]: Includes part of the load frame not registered by the load cells and also the beam self weight at a distance d from the interior face of the support plate.
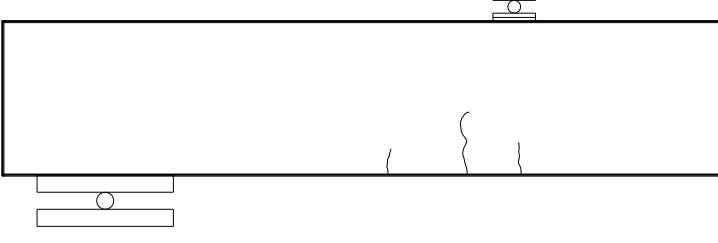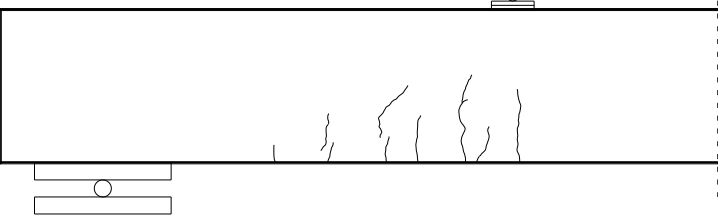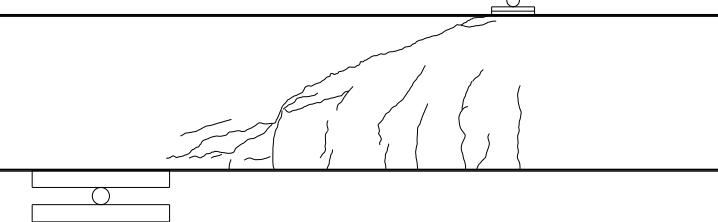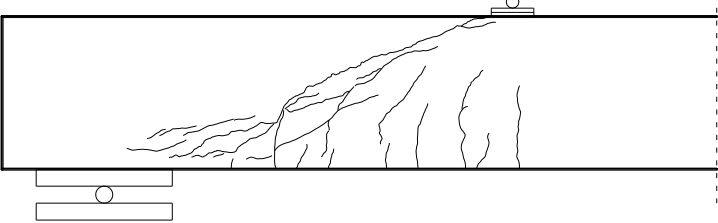
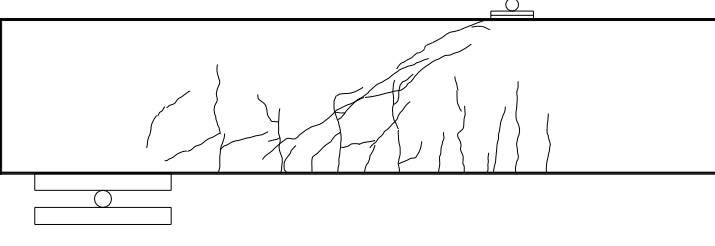| Shear force (kips)	Crack development
15.5	
24.0	
31.0	
36.6 (*Failure*)	

Figure 5.1- Crack progression for HVFA-70H-NS-8-2
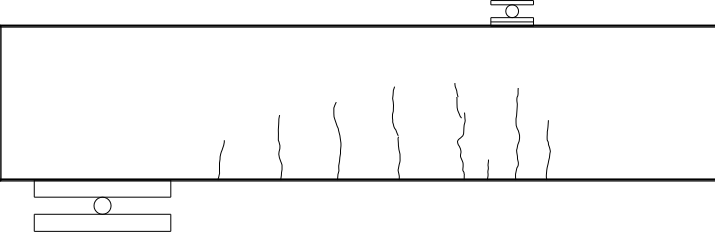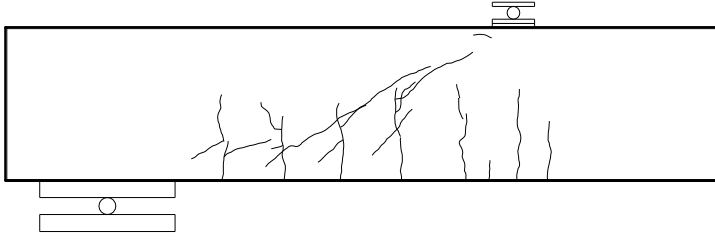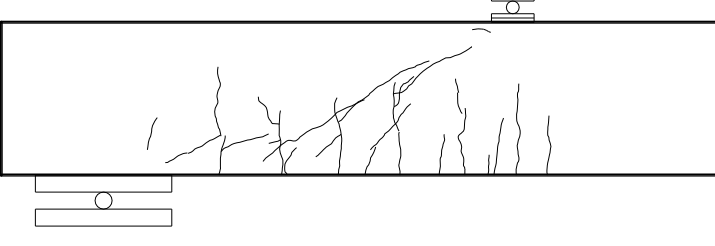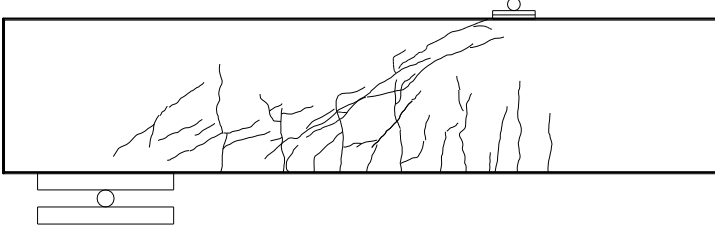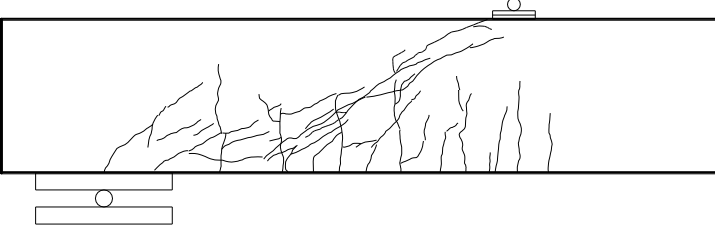
Shear force (kips)	Crack development
26.0	
37.5	
45.5	
53.0	
64.0	
73.9 (*Failure*)	

Figure 5.2- Crack progression for HVFA-70H-S-8-1

CC-H-NS-5

HVFA-70H-NS-5

CC-H-NS-6

HVFA-70H-NS-6
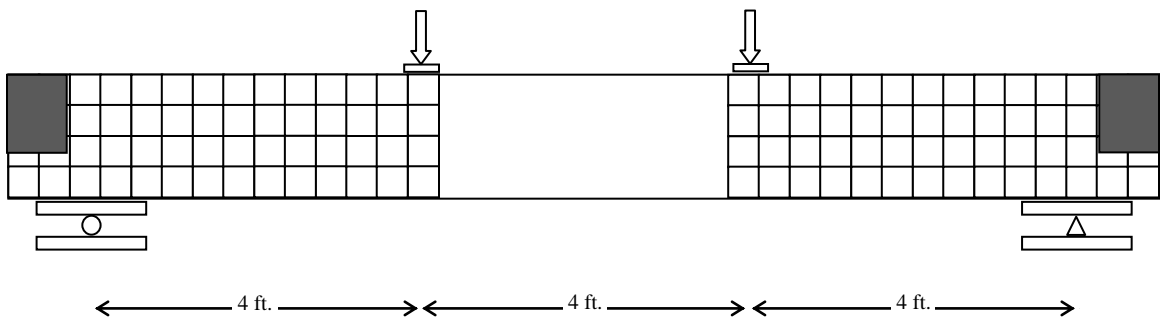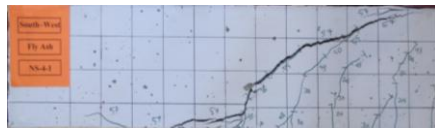
CC-H-NS-8
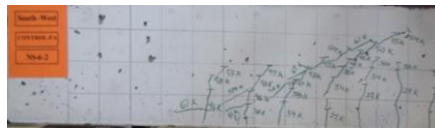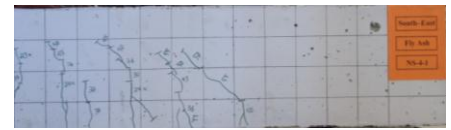
HVFA-70H-NS-8

CC-H-S-8

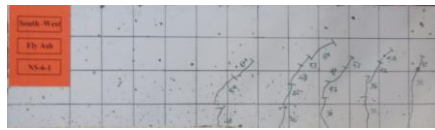HVFA-70H-S-8
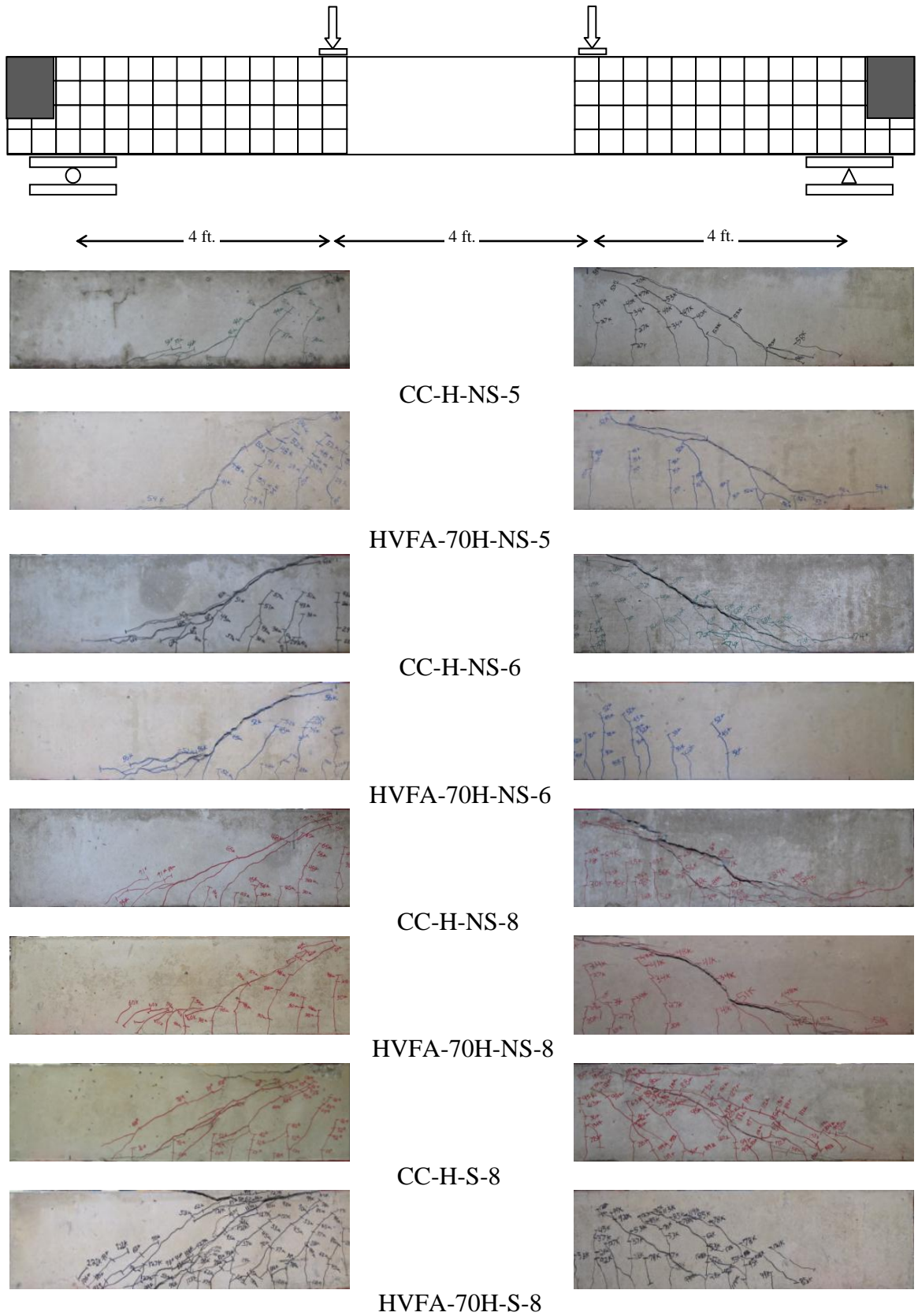
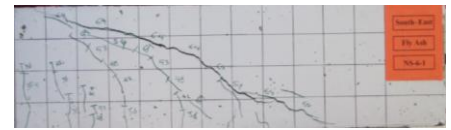**Figure 5.3- Crack Pattern at Failure for CC-H Beams (High cementitious mix)**
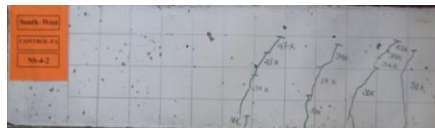
CC-L-NS-4

HVFA-L70-NS-4

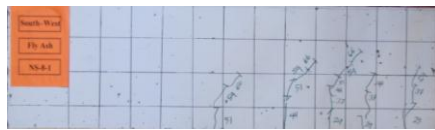CC-L-NS-6

HVFA-L70-NS-6

CC-L-NS-8
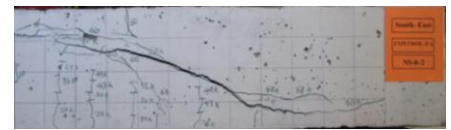
HVFA-L70-NS-8
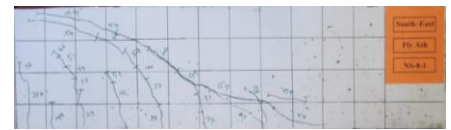
CC-L-S-8
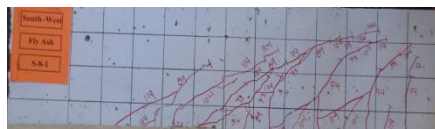
HVFA-L70-S-8

Figure 5.4- Crack pattern of the beams at shear failure (Low cementitious mix)

Figures 5.5 and **5.6** show the load-deflection behavior for the beams with different longitudinal reinforcement ratios (the deflection was measured at midspan) for the high and low cementitious mixes, respectively. Before the first flexural cracks occurred (point A), all of the beams displayed a steep linear elastic behavior. After additional application of load, the beams eventually developed the critical flexure-shear crack, which resulted in a drop in load and redistribution of the internal shear (point B for example). After this redistribution, the beams were able to support additional load until reaching failure. As expected, sections with a higher percentage of longitudinal reinforcement had a higher shear capacity, which can be attributed to a combination of additional dowel action (Taylor 1972, 1974), tighter shear cracks and thus an increase in aggregate interlock, and a larger concrete compression zone due to a downward shift of the neutral axis.
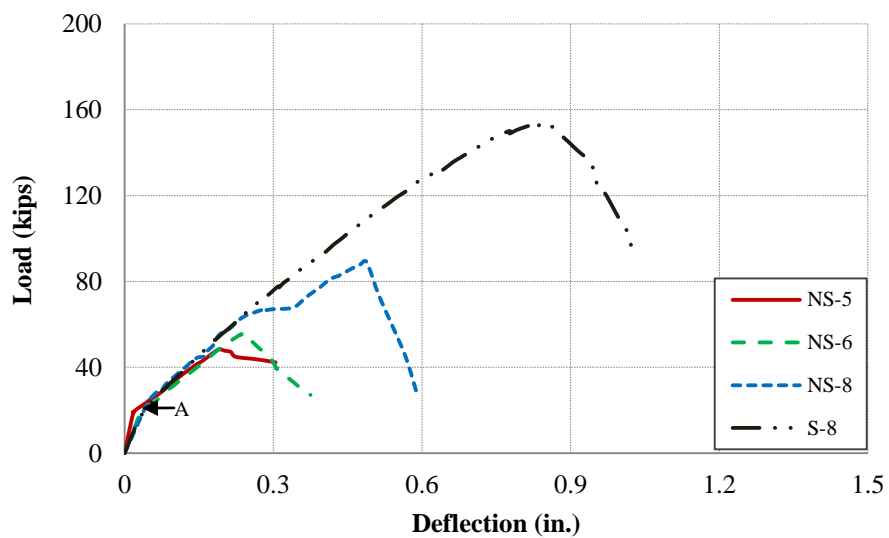
a) CC-H Beams
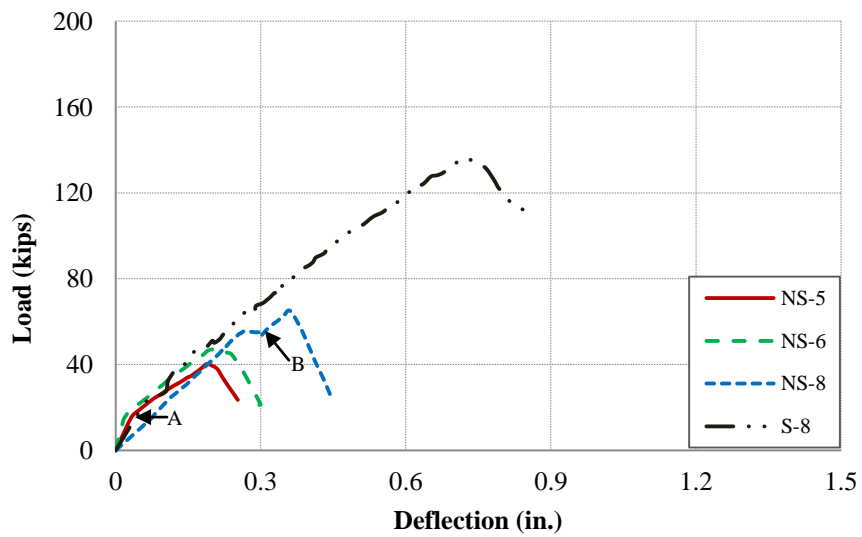
b) HVFA-70H Beams

Figure 5.5- Load-deflection of the Beams (High cementitious content)
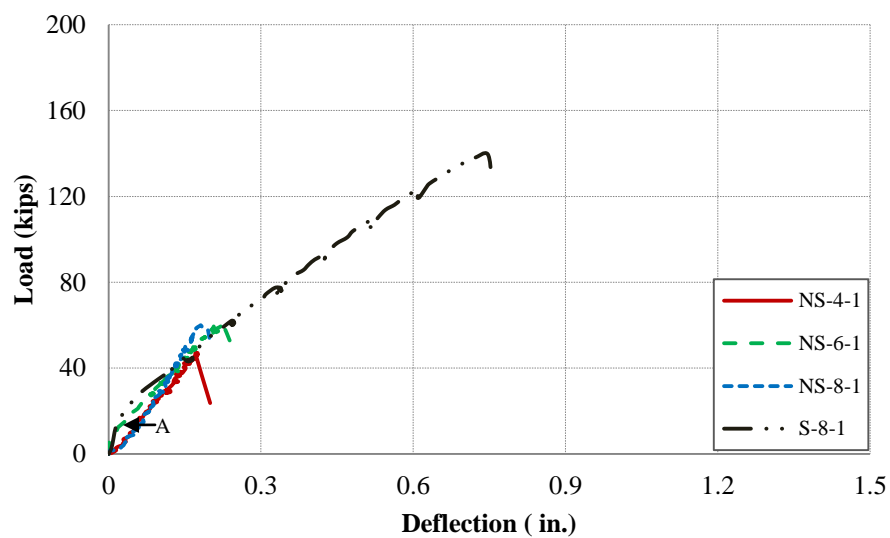
a) CC-L Beams
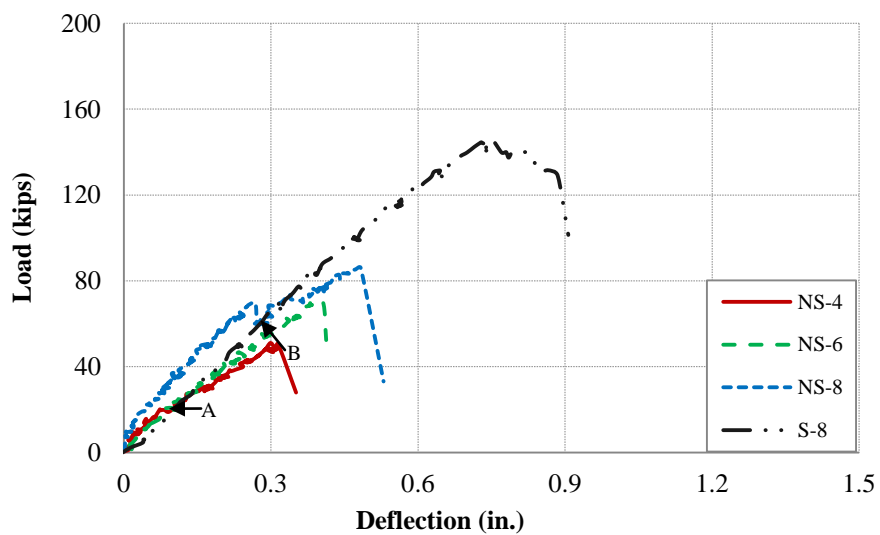
b) HVFA-70L Beams

Figure 5.6- Load-deflection of the Beams (Low cementitious content)

5.3. CRITICAL SHEAR CRACK ANGLE

The angle of the critical shear crack (θ_c) is an important design parameter in the AASHTO LRFD (2007) sectional design method. Although it is difficult to determine precisely as it is open to interpretation, the measurement is valuable in studying the behavior of RC beams subjected to shear failure. The procedure used to determine this angle consisted of measuring the angle of a portion of the critical shear crack between two reference points, with the points corresponding to right after crossing the alignment of the longitudinal reinforcement and before entering the compression zone, as shown in **Figure 5.7.**

Table 5.2 compares measured critical crack angles from test specimens with the calculated angle from the AASHTO LRFD (2007) equation. As it can be seen from **Table 5.2**, the AASHTO LRFD (2007) equation slightly overestimated the critical crack angles for the high cementitious mix, but it very accurately predicted the critical crack angles for the low cementitious mix.
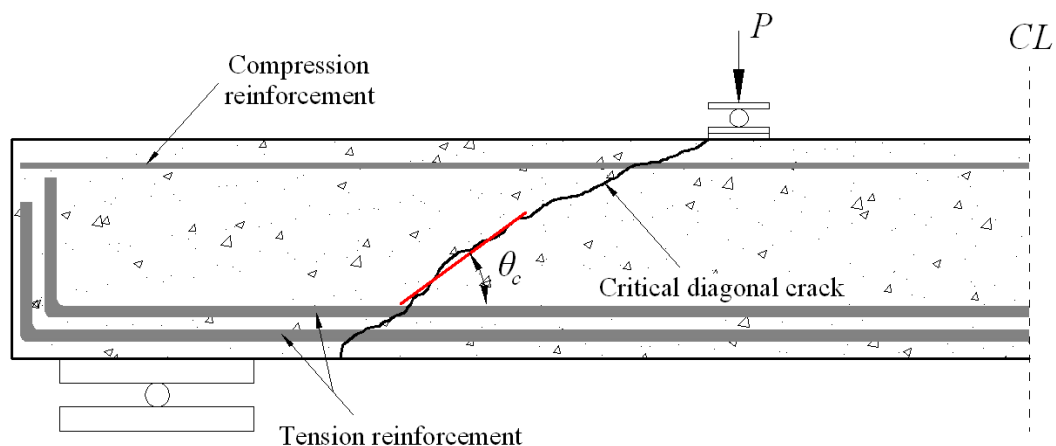
Figure 5.7- Crack angle measurement

Table 5.2- Critical Crack angle

Mix Design	Section		θ_{TEST}	θ_{AASHTO}	$\dfrac{\theta_{AASHTO}}{\theta_{TEST}}$
CC-H	NS-5	1	35	35.7	1.0
		2	29	35.6	1.2
	NS-6	1	26	34.8	1.3
		2	30	33.8	1.1
	NS-8	1	27	34.5	1.3
		2	29	32.7	1.1
	S-8	1	33	38.2	1.2
		2	34	37.8	1.1
Ave.					**1.2**
HVFA-70H	NS-5	1	28	35.1	1.3
		2	34	34.4	1.0
	NS-6	1	29	33.4	1.2
		2	33	33.0	1.0
	NS-8	1	31	33.3	1.1
		2	24	33.1	1.4
	S-8	1	38	37.2	1.0
		2	32	37.3	1.2
Ave.					**1.1**
CC-L	NS-4	1	40	34.7	0.9
		2	34	34.4	1.0
	NS-6	1	41	34.1	0.8
		2	35	33.8	1.0
	NS-8	1	40	32.7	0.8
		2	29	32.6	1.1
	S-8	1	27	36.5	1.4
		2	33	37.0	1.1
Ave.					**1.0**
HVFA-70L	NS-4	1	36	35.4	1.0
		2	45	34.8	0.8
	NS-6	1	35	34.0	1.0
		2	35	34.6	1.0
	NS-8	1	35	33.0	0.9
		2	34	34.0	1.0
	S-8	1	27	37.2	1.4
		2	28	37.4	1.3
Ave.					**1.0**

5.4. COMPARISON OF REINFORCEMENT STRAINS FROM EXPERIMENT AND AASHTO LRFD (2007)

According to the AASHTO LRFD standard (2007), strain in the longitudinal tension reinforcement can be determined by

$$\varepsilon_s = \frac{\left(\dfrac{|M_u|}{d_v} + |V_u|\right)}{E_s A_s} \tag{5-2}$$

Table 5.3 presents the tensile strain in the longitudinal tension reinforcement at the quarter-point of the span (middle of the shear test region) obtained from both the experiments (strain gauges) and the AASHTO LRFD (2007) equation. The AASHTO LRFD equation estimates the strain for both the HVFA concrete and CC beams very well for low and medium reinforcement ratios (NS-4 and NS-6), but it underestimates the strain for the sections with higher reinforcement ratios (NS-8 and S-8). Most importantly, the ratios of analytical-to-experimental strain are relatively consistent between the HVFA concrete and CC specimens.

Table 5.3- Comparison of reinforcement strain from experiment and AASHTO LRFD (2007) equation

Mix	Section		CC			HVFA concrete		
			ε_{s} quarter-point Equation	ε_{s} quarter-point Experiment	$\dfrac{\varepsilon_{s-Eq.}}{\varepsilon_{s-Ex.}}$	ε_{s} quarter-point Equation	ε_{s} quarter-point Experiment	$\dfrac{\varepsilon_{s-Eq.}}{\varepsilon_{s-Ex.}}$
High cementitious	NS-5	1	1179	*		1077	*	
		2	1159	*		962	*	
	NS-6	1	1013	1004	1.01	766	591	1.30
		2	837	692	1.21	706	661	1.07
	NS-8	1	1457	1526	0.95	745	974	0.76
		2	573	641	0.89	709	737	0.96
	S-8	1	1602	2098	0.76	1430	1658	0.86
		2	1536	2038	0.75	1448	1866	0.78
Ave.					0.93			0.96
COV (%)					18.53			21.27
Low cementitious	NS-4	1	1004.0	*		1127.0	1211	0.93
		2	954.0	844	1.13	1029.0	730	1.41
	NS-6	1	892.0	989	0.90	875.0	943	0.93
		2	840.0	906	0.93	977.0	1148	0.85
	NS-8	1	645.0	726	0.89	707.0	780	0.91
		2	626.0	818	0.77	878.0	1483	0.59
	S-8	1	1305.0	1648	0.79	1431.0	1700	0.84
		2	1392.0	1791	0.78	1468.0	1847	0.79
Ave.					0.88			0.91
COV (%)					14.39			25.45

*: No usable data

5.5. STATISTICAL DATA ANALYSIS

Statistical tests were used to evaluate whether there is any statistically significant difference between the normalized shear strength of the HVFA concrete and the CC beams. Both parametric and nonparametric statistical tests were performed.

5.5.1. Parametric Test. The paired t-test is a statistical technique used to compare two population means. This test assumes that the differences between pairs are normally distributed. If this assumption is violated, the paired t-test may not be the most powerful test. The hypothesis for the paired t-test is as follows:

H_o: The means of the normalized shear capacity of the HVFA-70H/70L is higher than the CC-H/L beams.

H_a: Not H_o.

The statistical computer program Minitab 15 was employed to perform these statistical tests. Both Kolmogorov-Smirnov and Anderson-Darling tests showed the data, the differences between the shear capacities of the HVFA concrete and the CC beams, follows a normal distribution. Therefore, the paired t-tests could be performed. The result of the paired t-test showed that the p-values were 0.88 and 0.963 (>0.05) for the high and low cementitious mixes, respectively. This confirms the null hypothesis at the 0.05 significance level. In other words, the means of the normalized shear capacity of the HVFA concrete was statistically higher than the CC beams.

5.5.2. Nonparametric Test. Unlike the parametric tests, nonparametric tests are referred to as distribution-free tests. These tests have the advantage of requiring no assumption of normality, and they usually compare medians rather than means. The Wilcoxon signed-rank test is usually identified as a nonparametric alternative to the paired t-test. The hypothesis for this test is the same as those for the paired t-test. The Wilcoxon signed rank test assumes that the distribution of the difference of pairs is symmetrical. This assumption can be checked; if the distribution is normal, it is also symmetrical. As mentioned earlier, the data follows normal distribution and the

Wilcoxon signed ranks test can be used. The p-values for the Wilcoxon signed rank were

0.78 and 0.995 (>0.05) for the high and low cementitious mixes, respectively. That

confirmed the null hypothesis at the 0.05 significance level. Interestingly, the p-values for

both the paired t-tests (parametric test) and the Wilcoxon signed rank test (nonparametric

test) are very close to each other.

Overall, results of the statistical data analyses showed that the HVFA concrete

beams (both the high and low cementitious) had higher normalized shear capacity than

the CC beams.

5.6. COMPARISON OF TEST RESULTS WITH SHEAR PROVISIONS OF SELECTED STANDARDS

In the following section, the experimental shear strengths of the beams are

compared with the shear provisions of the following standards: AASHTO LRFD (2007),

ACI 318 (2008), and CSA (2004). For this comparison, all of the safety factors of the

standards were set equal to one and all ultimate moments and shear forces were

calculated without load factors.

Table 5.4 presents the ratio of experimental-to-code predicted capacity

(V_{test}/V_{code}) for the selected design standards for all the beams. In comparing the two

mixes, the ratios are very similar, particularly given the wide scatter normally associated

with shear testing of reinforced concrete. Most importantly, the ratio for most of the

beams in all the selected standards is greater than one. This result indicates that existing

code provisions conservatively predict the shear strength of HVFA concrete beams.

For the CC beams without stirrups, the ratios range from 0.96 to 1.48 for the low cementitious mix and 0.91 to 1.41 for the high cementitious mix. For the HVFA concrete beams without stirrups, the ratios range from 1.01 to 1.92 for the low cementitious mix and 1.06 to 1.85 for the high cementitious mix. On average, the ratios for the HVFA concrete beams were higher than those for the CC beams, indicating that the HVFA concrete beams exceeded the code predicted strengths by a larger margin. For the beams with stirrups, the ratios were in much closer agreement between the two concrete types, most likely due to the greater predictability of the stirrup capacity portion of the shear strength, with ratios ranging from 1.16 to 1.60 for the CC and 1.24 to 1.60 for the HVFA concrete. For both mixes and both concrete types, the AASHTO LRFD and CSA offered the closest agreement between experimental and code predicted strengths.

Table 5.4- Comparison of shear strength of experiment and codes

Mix			High Cementitious Mix			Low Cementitious Mix		
Section			AASHTO	ACI	CSA	AASHTO	ACI	CSA
CC	NS-5	1	1.08	1.12	1.09	0.93	1.04	0.94
		2	1.09	1.14	1.10	0.91	1.02	0.91
	NS-6	1	1.31	1.48	1.31	1.19	1.41	1.20
		2	1.04	1.26	1.04	1.15	1.38	1.15
	NS-8	1	1.61	1.86	1.62	1.02	1.33	1.03
		2	0.96	1.26	0.97	1.03	1.34	1.03
	Ave		1.18	1.35	1.19	1.04	1.25	1.04
	COV		20.19	20.57	20.19	10.87	14.02	10.86
	S-8	1	1.55	1.58	1.44	1.20	1.32	1.13
		2	1.46	1.51	1.37	1.31	1.41	1.23
	Ave		1.51	1.54	1.41	1.25	1.36	1.18
	COV		4.22	3.08	3.99	6.30	4.70	6.00
HVFA concrete	NS-5	1	1.18	1.36	1.19	1.07	1.14	1.08
		2	1.01	1.22	1.02	1.14	1.25	1.15
	NS-6	1	1.11	1.48	1.11	1.13	1.34	1.13
		2	1.00	1.38	1.01	1.60	1.82	1.61
	NS-8	1	1.42	1.92	1.43	1.12	1.43	1.13
		2	1.34	1.85	1.35	1.84	2.15	1.85
	Ave		1.18	1.54	1.19	1.32	1.52	1.33
	COV		14.69	18.53	14.65	24.49	25.36	24.42
	S-8	1	1.42	1.58	1.33	1.32	1.40	1.24
		2	1.45	1.60	1.35	1.37	1.44	1.28
	Ave		1.44	1.59	1.34	1.35	1.42	1.26
	COV		1.48	0.89	1.06	2.63	1.99	2.24

5.7. COMPARISON OF TEST RESULTS WITH SHEAR TEST DATABASE

Figure 5.8 presents the normalized shear strength versus longitudinal reinforcement ratio for the beams of this study as well as the wealth of shear test data available in the literature (Reineck 2003). Given the significant scatter of the database of previous shear test results, it is somewhat difficult to draw definitive conclusions on the current test values. Nonetheless, visually, **Figure 5.8** seems to indicate that the CC and HVFA concrete test results fall within the central portion of the data and follow the same general trend of increasing shear strength as a function of the longitudinal reinforcement ratio. Furthermore, statistical analysis of the data indicates that the CC and HVFA concrete test results fall within a 95% confidence interval of a nonlinear regression curve fit of the database. Furthermore, a significant majority of the HVFA concrete test results fall at or above the nonlinear regression curve fit. This result indicates that the test values are very consistent with the wealth of shear test data available in the literature and that, in general, the HVFA concrete test results tend to be greater than CC.

Since span-to-depth ratio plays a significant role in the shear strength of beams (Taylor 1972, 1974), **Figure 5.9** shows the normalized shear strength for the beams of this study with the portion of the database that had similar span-to-depth ratios of the current study (span-to-depth ratio$\pm$ 5% [2.9-3.4]). It can be seen from **Figure 5.9** that the test results of this current study are within a 95% confidence interval of a nonlinear regression curve fit of this subset of the shear database. As a result, it would appear that the shear strength of HVFA concrete is higher than CC for the beams tested in this investigation.
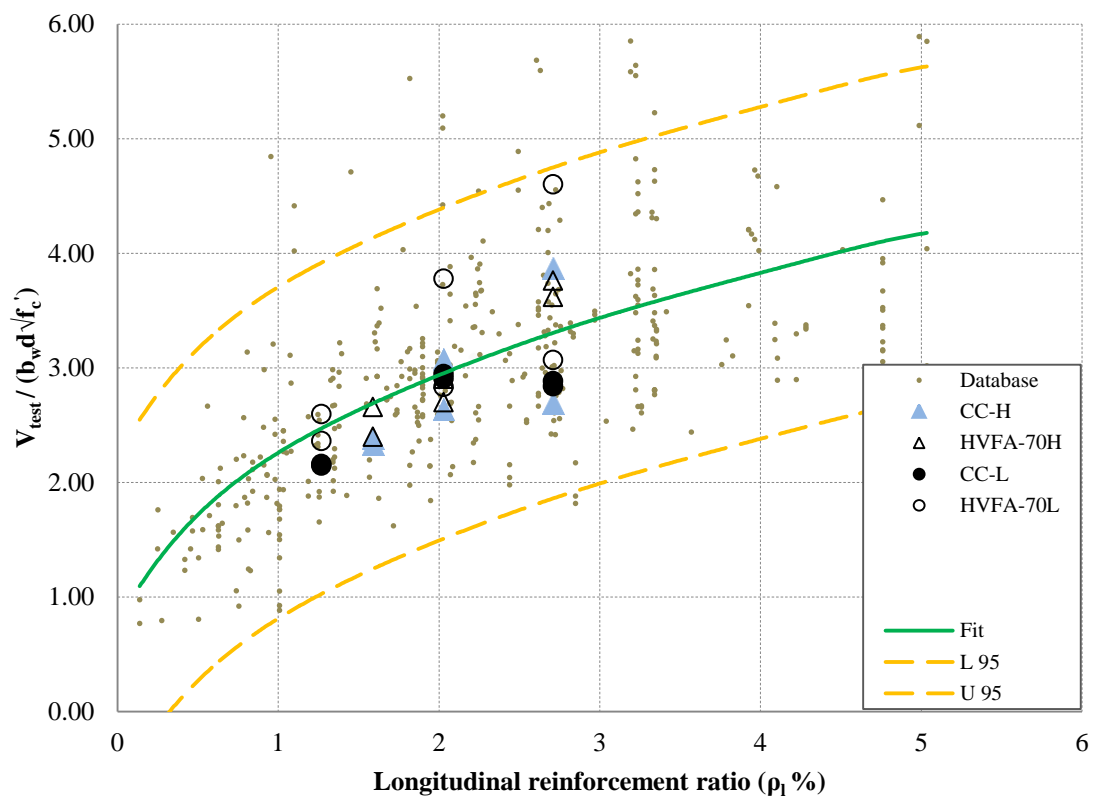
Figure 5.8- Shear strength vs. longitudinal reinforcement ratio; results from Reineck (2003) and test results of this study
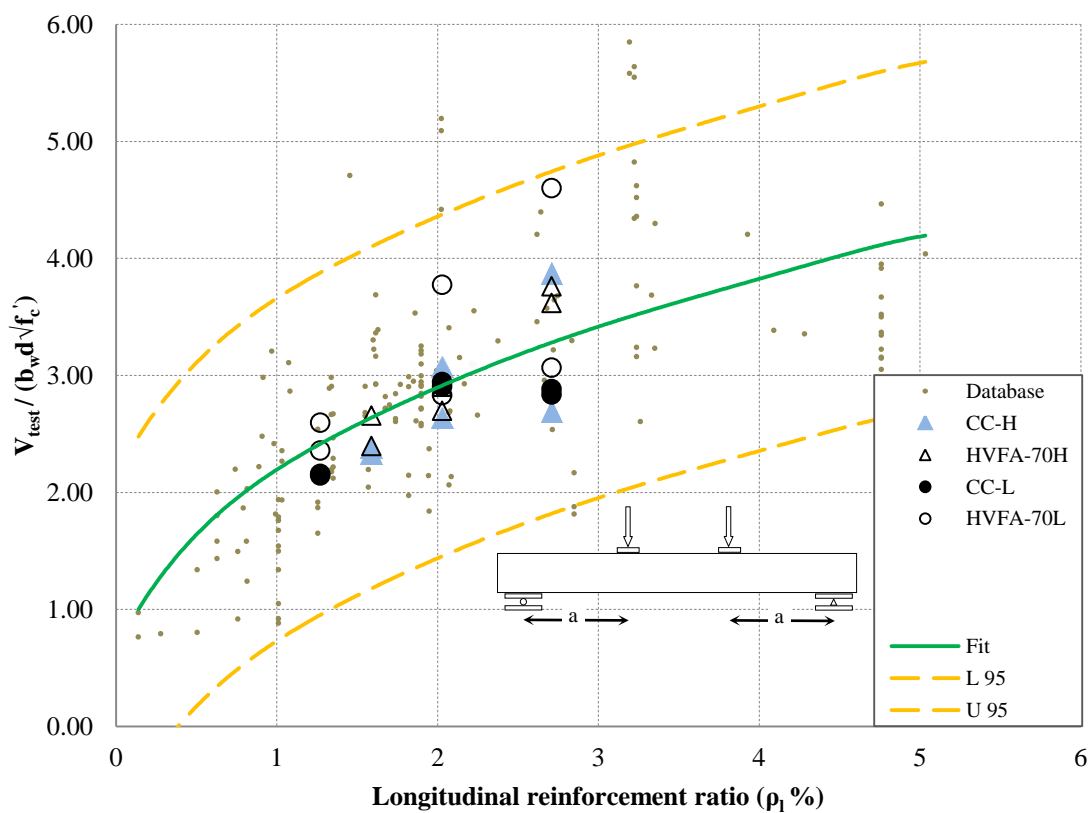
Figure 5.9- Shear strength vs. longitudinal reinforcement ratio; results from (Reineck et al. 2003) ($2.9 \leq \frac{a}{d} \leq 3.4$) and test results of this study

6. FINDINGS, CONCLUSIONS, AND RECOMMENDATIONS

The main objective of this research study was to evaluate the shear behavior and response of high-volume fly ash (HVFA) concrete through material, component, and full-scale testing. The main feature of the experimental program consisted of 32 tests performed on full-scale reinforced concrete beams. The principal parameters investigated were: (1) concrete type – HVFA concrete or conventional concrete (CC), (2) amount of total cementitious material, (3) amount of shear reinforcement, and (4) amount of longitudinal (flexural) reinforcement. The behavior of the HVFA concrete was examined in terms of crack morphology and progression, load-deflection response, failure mechanism including critical crack angle and reinforcement strains, comparison with predicted strengths from design standards, comparison with identical CC test specimens (including statistical analyses), and comparison with a shear test database of CC specimens. This section contains the findings of the test program as well as conclusions and recommendations.

6.1. FINDINGS AND CONCLUSIONS

Based on the results of this research study, the following findings and conclusions are presented:

- In terms of crack morphology, crack progression, and load-deflection response, the behavior of the HVFA concrete and CC beams was virtually identical.

- The AASHTO LRFD equation slightly overestimated the critical crack angles for the high total cementitious content mix but very accurately predicted the

critical crack angles for the low total cementitious content mix. Most importantly, the critical crack angles for the HVFA concrete beams were very consistent with those of the CC beams.

- The AASHTO LRFD equation estimates the reinforcement strain for both the HVFA concrete and CC beams very well for low and medium reinforcement ratios, but it underestimates the strain for sections with higher reinforcement ratios.

- Statistical data analyses – both parametric and nonparametric – showed that the HVFA concrete beams had higher normalized shear capacity than the CC beams.

- Existing design standards (AASHTO, ACI, CSA) conservatively predicted the shear capacity of the HVFA concrete beams.

- In general, the HVFA concrete beams exceeded the code predicted shear strengths by a larger margin than the CC beams.

- The total cementitious content had little effect on the shear behavior of the HVFA concrete beams.

- The HVFA concrete and CC test results fall within a 95% confidence interval of a nonlinear regression curve fit of the CC shear test database.

- A significant majority of the HVFA concrete test results fall at or above the nonlinear regression curve fit of the CC shear test database.

6.2. RECOMMENDATIONS

Based on the findings and conclusions discussed previously, the following recommendations are presented:

- Although the normalized HVFA concrete shear test results exceeded the CC shear test results, due to the inherent scatter associated with shear testing of reinforced concrete, the investigators recommend using existing design equations for HVFA concrete.

- Additional testing is required to determine whether HVFA concrete has increased shear capacity compared to CC. This testing should investigate additional mix design variations, aggregate type and content, cross section aspect ratio, and type of loading. This database will then provide a basis for modifications to existing design standards.

BIBLIOGRAPHY

AASHTO LRFD, (2007). Bridge Design Specifications and Commentary (4th Ed.). American Association of State and Highway Transportation Officials. Washington, DC.

AASHTO T 318 (2002). Water Content of Freshly Mixed Concrete Using Microwave Oven Drying. American Association of State Highway and Transportation Officials, Washington D.C.

American Coal Ash Association (ACAA). (2009). Facts About Coal Ash. Access online at www.coalashfacts.org

ACI Committee 211, (1991). Standard Practice for Selecting Proportions for Normal, Heavyweight, and Mass Concrete (ACI 211.1-91). American Concrete Institute, Farmington Hills, MI.

ACI Committee 232, (2003). Use of Fly Ash in Concrete (ACI 232.2R-03). American Concrete Institute, Farmington Hills, MI.

ACI Committee 318, (2008). Building Code Requirements for Structural Concrete and Commentary (ACI 318-08). American Concrete Institute, Farmington Hills, MI.

ACI Committee 445, (2009). Recent Approaches to Shear Design of Structural Concrete (ACI 445R-99). American Concrete Institute, Farmington Hills, MI.

ACI Committee 446, (1999). Fracture Mechanics of Concrete: Concepts, Models and Determination of Material Properties (ACI 446.1R). American Concrete Institute, Farmington Hills, MI.

ASCE-ACI Task Committee 426, (1973). The Shear Strength of Reinforced Concrete Members. ASCE Journal of the Structural Division, Vol. 99, No. 6, pp. 1091-1187.

ASCE-ACI Task Committee 445, (1998). Recent Approaches to Shear Design of Structural Concrete. ASCE Journal of Structural Engineering, Vol. 124, No. 12, pp. 1375-1417.

ASTM A370, (2011). Standard Test Methods and Definitions for Mechanical Testing of Steel Products. American Society for Testing Materials (ASTM International).

ASTM C109, (2008). Standard Test Method for Compressive Strength of Hydraulic Cement Mortars. American Society for Testing Materials (ASTM International).

ASTM C127, (2007). Standard Test Method for Density, Relative Density (Specific Gravity), and Absorption of Coarse Aggregate. American Society for Testing Materials (ASTM International).

ASTM C128, (2007). Standard Test Method for Density, Relative Density (Specific Gravity), and Absorption of Fine Aggregate. American Society for Testing Materials (ASTM International).

ASTM C138, (2010). Standard Test Method for Density (Unit Weight), Yield, and Air Content (Gravimetric) of Concrete. American Society for Testing Materials (ASTM International).

ASTM C192, (2007). Standard Practice for Making and Curing Concrete Test Specimens in the Laboratory. American Society for Testing Materials (ASTM International).

ASTM C231, (2010). Standard Test Method for Air Content of Freshly Mixed Concrete by the Pressure Method. American Society for Testing Materials (ASTM International).

ASTM C39/C39M, (2011). Standard Test Method for Compressive Strength of Cylindrical Concrete Specimens. American Society for Testing Materials (ASTM International).

ASTM C469, (2002). Standard Test Method for Static Modulus of Elasticity and Poisson's Ratio of Concrete in Compression. American Society for Testing Materials (ASTM International).

ASTM C496, (2004). Standard Test Method for Splitting Tensile Strength of Cylindrical Concrete Specimens. American Society for Testing Materials (ASTM International).

ASTM C566, (1997). Standard Test Method for Total Evaporable Moisture Content of Aggregate by Drying. American Society for Testing Materials (ASTM International).

ASTM C617, (2009). Standard Practice for Capping Cylindrical Concrete Specimens. American Society for Testing Materials (ASTM International).

ASTM C618, (2008). Standard Specification for Coal Fly Ash and Raw or Calcined Natural Pozzolan for Use in Concrete. American Society for Testing Materials (ASTM International).

ASTM C78, (2009). Standard Test Method for Flexural Strength of Concrete (Using Simple Beam with Third-Point Loading). American Society for Testing Materials (ASTM International).

ASTM E178, (2008). Standard Practice for Dealing with Outlying Observations. American Society for Testing Materials (ASTM International).

Bazant, Z.P., and Becq-Giraudon, E., (2002), Statistical prediction of fracture parameters of concrete and implications for choice of testing standards. Cement and Concrete Research Journal, Vol. 32, No. 4, pp. 529-556.

Bazant, Z.P., and Kim, J.K., (1984). Size Effect in Shear Failure of Longitudinally Reinforced Beams. ACI Journal Proceedings, Vol. 81, pp. 456-468.

Bazant, Z.P., and Pfeiffer, P.A., (1987). Determination of Fracture Energy from Size Effect and Brittleness Number. ACI Materials Journal, Vol. 84, No. 6, pp. 463-480.

Bazant, Z.P., and Sun, H.H., (1987). Size Effect in Diagonal Shear Failure: Influence of Aggregate Size and Stirrups. ACI Journal Proceedings, Vol. 84, pp. 259-272.

Bentz, D.P., (2010). Powder Additions to Mitigate Retardation in High-Volume Fly Ash Mixtures. ACI Materials Journal, Vol. 107, No. 5, pp. 508-514.

Bentz, E.C., Vecchio, F.J, and Collins, M.P., (2006). Simplified Modified Compression Field Theory for Calculating Shear Strength of Reinforced Concrete Elements. ACI Structural Journal, Vol. 103, No. 4, pp. 614-624.

Berry, E.E., Hemmings, R.T., Zhang, M., Cornelius, B.J., and Golden, D.M., (1994). Hydration in High-Volume Fly Ash Concrete Binders. ACI Materials Journal, Vol. 91, No. 4, pp. 382-389.

Bilodeau, A., Sivasundaram, V., Painter, K.E., and Malhotra, V.M., (1994). Durability of Concrete Incorporating High Volumes of Fly Ash from Sources in the U.S. ACI Materials Journal, Vol. 91, No. 1, pp. 3-12.

Boresi, A.P., and Schmidt, R.J., (2003). Advanced Mechanics of Materials (6th Ed.). John Wiley & Sons.

Bouzoubaâ, N., Bilodeau, A., Sivasundaram, V., and Chakraborty, A.K., (2007). Mechanical Properties and Durability Characteristics of High-Volume Fly Ash Concrete Made with Ordinary Portland Cement and Blended Portland Fly Ash Cement. ACI Special Publication, Vol. 242, pp. 303-320.

Brooks, J.J., and Sikharulidze, Z.D., (1992). Strength and Fracture Energy of Concrete with and without Fly Ash Cured in Water at Different Constant Temperatures. ACI Special Publication, Vol. 132, pp. 299-317.

Butalia, T.S, and Bargaheiser, K., (2004). Corrosion in Concrete and the Role of Fly Ash in its Mitigation. Energeia, Vol. 15, No. 4, University of Kentucky, Center for Applied Energy Research.

Cabrera, J.G., and Atis, C.D., (1999). Design and Properties of High-Volume Fly Ash High- Performance Concrete. ACI Special Publication, Vol. 186, pp. 21-38.

Carette, G., Bilodeau, A., Chevrier, R.L., and Malhotra, V.M., (1993). Mechanical Properties of Concrete Incorporating High Volumes of Fly Ash from Sources in the U.S. ACI Materials Journal, Vol. 90, No. 6, pp. 535-544.

Cladera, A., (2002). Shear Design of Reinforced High-Strength Concrete Beams. PhD Thesis. Universitat Politécnica de Catalunya. Barcelona, Spain.

Collins, M.P., and Mitchell, D., (1991). Prestressed Concrete Structures. Response Publications.

Collins, M.P., Bentz, E.C., and Sherwood, E.G., (2008). Where is Shear Reinforcement Required? Review of Research Results and Design Procedures. ACI Structural Journal, Vol. 105, No. 5, pp. 590-600.

Collins, M.P., Mitchell, D., and Bentz, E.C., (2008). Shear Design of Concrete Structures. The Structural Engineer, Vol. 86, No. 10, pp. 32-39.

Comite Euro-International du Beton, (1990). CEB-FIP Model Code 1990, Redwood Books, Wiltshire, England.

Coronado, C., (2006). Characterization, Modeling and Size Effect of Concrete-Epoxy Interfaces. PhD Thesis. Pennsylvania State University. United States of America.

Cross, D., Stephens, J., and Vollmer, J., (2005). Structural Applications of 100 Percent Fly Ash Concrete. 2005 World of Coal Ash Conference. Lexington, KY, United States of America.

CSA Committee A23.3, (2004). Design of Concrete Structures (CSA A23.3-04). Canadian Standards Association. Rexdale, ON, Canada.

Dahl, H., and Brincker, R., (1989). Fracture Energy of High-Strength Concrete in Compression. International Conference on Fracture of Concrete and Rock: Cardiff. Elsevier Science, pp. 523-536.

Davis, R.E., Carlson, R.W., Kelly, J.W., and Davis, H.E., (1937). Properties of Cements and Concretes Containing Fly Ash. ACI Journal Proceedings, Vol. 33, No. 5, pp. 577-612.

Duthinh, D., (1999). Sensitivity of Shear Strength of Reinforced Concrete and Prestressed Concrete Beams to Shear Friction and Concrete Softening According to Modified Compression Field Theory. ACI Structural Journal, Vol. 96, No. 4, pp. 495-508.

Einsfeld, R.A., and Velasco, M.S.L., (2006). Measurement of the Ratio G_F/G_f for Numerical Analysis of Concrete Structures. Latin American Journal of Solids and Structures, Vol. 3, pp. 361-376.

Eurocode 2, (2004). Design of Concrete Structures − Part 1.1: General Rules and Rules for Buildings. EN 1992-1-1. Brussels. Belgium.

Galeota, D., Giammatteo, M.M., and Marino, R., (1995). Structural Concrete Incorporating High Volume of Fly Ash. ACI Special Publication, Vol. 153, pp. 25-42.

Gastebled, O.J., and May, I.M., (2001). Fracture Mechanics Model Applied to Shear Failure of Reinforced Concrete Beams without Stirrups. ACI Structural Journal, Vol. 98, No. 2, pp. 184-190.

Ghaemmaghami, A., and Ghaemian, M., (2004). Specific Fracture Energy Approximation of Dam Concrete. 13th World Conference on Earthquake Engineering. Paper No. 69. Vancouver, BC. Canada.

Griffith, A.A., (1920). The Phenomena of Rupture and Flow in Solids. Philosophical Transactions, Series A, Vol. 221, pp. 163-198.

Guinea, G.V., Planas, J., and Elices, M., (1992). Measurement of the Fracture Energy Using Three-Point Bend Tests: Part 1 − Influence of Experimental Procedures. Materials and Structures. Materials and Structures, Vol. 25, pp. 212-218.

Gustafsson, P.J., and Hillerborg, A., (1988). Sensitivity in Shear Strength of Longitudinally Reinforced Concrete Beams to Fracture Energy of Concrete. ACI Journal Proceedings, Vol. 85, pp. 286-294.

Headwaters Resources, (2008). Fly Ash for Concrete. Brochure. http://www.flyash.com/data/upimages/press/fly%20ash%20for%20concrete.pdf

Hillerborg, A., (1985). Theoretical Basis of a Method to Determine the Fracture Energy G_F of Concrete. Materials and Structures, Vol. 18, No. 106, pp. 291-296.

Hillerborg, A., Modeer, M., and Petersson, P.E., (1976). Analysis of Crack Formation and Crack Growth in Concrete by Means of Fracture Mechanics and Finite Elements. Cement and Concrete Research Journal, Vol. 6, pp. 773-782.

Hsu, T.T.C., (1993). Unified Theory of Reinforced Concrete. CRC Press.

Hsu, T.T.C., and Mo, Y.L., (2010). Unified Theory of Concrete Structures. John Wiley & Sons.

http://www.4us2be.com/technology/cement-manufacturing-process/. December, 2011.

http://www.tradeindia.com/fp426361/Ammonia-Flue-Gas-Conditioning-Systems.html. December, 2011.

Irwin, G.R., Kies, J.A., and Smith, H.L., (1958). Fracture Strength Relative to Onset and Arrest of Crack Propagation. Proceedings ASTM, Vol. 58, pp. 640-657.

Jenq, Y.S., and Shah, S.P., (1989). Shear Resistance of Reinforced Concrete Beams − A Fracture Mechanics Approach. ACI Special Publication, Vol. 118, pp. 237-258.

Jiang, L., Lin, B., and Cai, Y., (1999). Studies on Hydration in High-Volume Fly Ash Concrete Binders. ACI Materials Journal, Vol. 96, No. 6, pp. 703-706.

Kaplan, M.F., (1961). Crack Propagation and the Fracture of Concrete. ACI Journal Proceedings, Vol. 58, pp. 591-610.

Kellermann, W.F., (1933). Effect of Size of Specimen, Size of Aggregate and Method of Loading upon the Uniformity of Flexural Strength Results. Public Roads, Vol. 13, No. 11, pp. 177-184.

Kesler, C.E., Naus, D.J., and Lott, J.L., (1972). Fracture Mechanics − Its Applicability to Concrete. Proceedings of the International Conference on the Mechanical Behavior of Materials, Vol. IV, pp. 113-124, Kyoto, Japan.

Kim, J.K., and Park, Y.D., (1996). Prediction of Shear Strength of Reinforced Concrete Beams without Web Reinforcement. ACI Materials Journal, Vol. 93, No. 3, pp. 213-222.

Kim, W., and White, R.N., (1991). Initiation of Shear Cracking in Reinforced Concrete Beams with No Web Reinforcement. ACI Structural Journal, Vol. 88, No. 3, pp. 301-308.

Koyama, T., Sun, Y.P., Fujinaga, T., Koyamada, H., and Ogata, F., (2008). Mechanical Properties of Concrete Beam Made of Large Amount of Fine Fly Ash. The 14th World Conference on Earthquake Engineering. Beijing, China.

Kuchma, D., (2009). Contribution of Stirrups to Shear Resistance. Structures Congress 2009: Don't Mess with Structural Engineers, ASCE, pp. 1587-1594.

Langley, W.S., Carette, G.G., and Malhotra, V.M., (1989). Structural Concrete Incorporating High Volumes of ASTM Class F Fly Ash. ACI Materials Journal, Vol. 86, No. 5, pp. 507-514.

Laskar, A., Hsu, T.T.C., and Mo, Y.L.C., (2010). Shear Strengths of Prestressed Concrete Beams Part 1: Experiments and Shear Design Equations. ACI Structural Journal, Vol. 107, No. 3, pp. 330-339.

Leonhardt, F., and Mönnig, E., (1975). Vorlesungen über Massivbau. Berlin/Heidelberg, Germany.

Li, G., (2004). Properties of High-Volume Fly Ash Concrete Incorporating Nano- SiO_2. Cement and Concrete Research Journal, Vol. 34, pp. 1043-1049.

Loov, R.E., (1998). Review of A23.3-94 Simplified Method of Shear Design and Comparison with Results using Shear Friction. Canadian Journal of Civil Engineering, Vol. 25, No. 3, pp. 437-450.

Malhotra, V.M., and Mehta, P.K., (2008). High-Performance, High-Volume Fly Ash Concrete for Building Sustainable and Durable Structures (3rd Ed.). Supplementary Cementing Materials for Sustainable Development Inc. Ottawa, Canada.

Marotta, T.W., Coffey, J.C., LaFleur, C.B., and LaPlante, C., (2011). Basic Construction Materials (8th Ed.). Pearson-Prentice Hall.

Martin, J., Stanton, J., Mitra, N., and Lowes, L.N., (2007). Experimental Testing to Determine Concrete Fracture Energy Using Simple Laboratory Test Setup. ACI Materials Journal, Vol. 104, No. 6, pp. 575-584.

Mehta, P.K., (2004). High-Performance, High-Volume Fly Ash Concrete for Sustainable Development. Proceedings of the International Workshop on Sustainable Development and Concrete Technology, Center for Transportation Research and Education, Iowa State University. United States of America.

Mindess, S., Young, J.F., and Darwin, D., (2003). Concrete (2nd Ed.). Prentice Hall.

Mohan Rao, R, Mohan, S., and Sekar, S.K., (2011). Shear Resistance of High Volume Fly Ash Reinforced Concrete Beams without Web Reinforcement. International Journal of Civil and Structural Engineering, Vol. 1, No. 4, pp. 986-993.

Mörsch, E., (1902). Der Eisenbetonbau, Seine Theorie und Anwendung. Stuggart, Germany.

Namagga, C., and Atadero, R.A., (2009). Optimization of Fly Ash in Concrete: High Lime Fly Ash as a Replacement for Cement and Filler Material. 2009 World of Coal Ash Conference. Lexington, KY, United States of America.

Neville, A.M., (1997). Properties of Concrete (4th Ed.). John Wiley & Sons.

Nielsen, K.E.C., (1954). Effect of Various Factors on the Flexural Strength of Concrete Tests Beams. Magazine of Concrete Research, No. 15, pp. 105-114.

Nilson, A.H., Darwin, D., and Dolan, C.W., (2004). Design of Concrete Structures (13th Ed.). McGraw Hill.

Padevet, P., and Zobal, O., (2011). Fracture Energy of Cement Paste with Addition of the Fly Ash. 4th International Conference Modelling of Mechanical and Mechatronic Systems 2011, Technical University of Kosice. Kosice. Slovakia.

Park, R., and Paulay, T., (1975). Reinforced Concrete Structures. John Wiley & Sons.

Rangan, B.V., (1991). Web Crushing Strength of Reinforced and Prestressed Concrete Beams. ACI Structural Journal, Vol. 88, No. 1, pp. 12-16.

Reineck, KH, Kuchma, DA, Kim, KS; and Marx, S., (2003). "Shear Database for Reinforced Concrete Members without Shear Reinforcement," ACI Structural Journal, V. 100, No. 2, pp. 240-249.

Raphael, J.M., (1984). Tensile Strength of Concrete. Concrete International, Vol. 81, No. 2, pp. 158-165.

RILEM TC 89-FMT Fracture Mechanics of Concrete-Test Methods, (1990). Determination of Fracture Parameters (K_{IC} and $CTOD_C$) of Plain Concrete Using Three-Point Bend Tests. Materials and Structures, Vol. 23, pp. 457-460.

RILEM TC 89-FMT Fracture Mechanics of Concrete-Test Methods, (1990). Size Effect Method for Determining Fracture Energy and Process Zone Size of Concrete. Materials and Structures, Vol. 23, pp. 461-465.

Ritter, W., (1899). Die Bauweise Hennebique. Schweizerische Bauzeitung. Zurich, Switzerland.

Scheetz, B.E., Menghini, M.J., Hornberger, R.J., Owens, T.D., and Schueck, J., (1997). Beneficial Use of Coal Ash in Anthracite and Bituminous Mine Reclamation and Mine Drainage Pollution Abatement in Pennsylvania. Proceedings of the Air & Waste Management Association. Toronto, ON, Canada.

Schlaich, J., Schäfer, K., and Jennewein, M., (1987). Towards a Consistent Design of Structural Concrete. PCI Journal, Vol. 32, No. 3, pp. 74-150.

Shah, S.G., Bhasya, V., and Chandra Kishen, J.M., (2011). Tension-Softening Properties for Concrete-Concrete Interfaces. ACI Structural Journal, Vol. 108, No. 6, pp. 725-734.

Shah, S.P., and Carpinteri, A., (1991). Fracture Mechanics Test Methods for Concrete: Report of Technical Committee 89-FMT (1st Ed.). Chapman and Hall.

So, K.O., and Karihaloo, B.L., (1993). Shear Capacity of Longitudinally Reinforced Beams – A Fracture Mechanics Approach. ACI Structural Journal, Vol. 90, No. 6, pp. 591-600.

Swamy, R.N., and Hung, H.H., (1998). Engineering Properties of High Volume Fly Ash Concrete. ACI Special Publication, Vol. 178, pp. 331–359.

Taylor, HPJ. (1972). "Shear Strength of Large Beams," Journal of the Structural Division, ASCE, V. 98, No. ST11, Nov., pp. 2473-2489.

Taylor, HPJ. (1974). "The Fundamental Behavior of Reinforced Concrete Beams in Bending and Shear," American Concrete Institute, Shear in Reinforced Concrete, SP-42, pp. 43-77.

Thomas, M., (2007). Optimizing the Use of Fly Ash in Concrete. Portland Cement Association. Skokie, Illinois. United States of America.

Tureyen, A.K., (2001). Influence of Longitudinal Reinforcement Type on the Shear Strength of Reinforced Concrete Beams without Transverse Reinforcement. PhD Thesis. Purdue University. United States of America.

Tureyen, A.K, and Frosch, R.J., (2003). Concrete Shear Strength: Another Perspective. ACI Structural Journal, Vol. 100, No. 5, pp. 609-615.

van der Veen, C., (1990). Cryogenic Bond Stress-Slip Relationship. MS Thesis. Delft University. Delft, Netherlands.

Vecchio, F.J., and Collins, M.P., (1986). The Modified Compression Field Theory for Reinforced Concrete Elements Subjected to Shear. ACI Journal Proceedings, Vol. 83, No. 2, pp. 219-231.

Vecchio, F.J., and Collins, M.P., (1993). Compression Response of Cracked Reinforced Concrete. Journal of Structural Engineering, Vol. 119, No. 12, pp. 3590-3610.

Walraven, J.C., (1980). Aggregate Interlock: a Theoretical and Experimental Analysis. PhD Thesis. Delft University of Technology. Delft, Netherlands.

Whitney, C.S., (1937). Design of Reinforced Concrete Members Under Flexure or Combined Flexure and Direct Compression. ACI Journal Proceedings, Vol. 33, No. 3, pp. 483-498.

Wight, J.K., and MacGregor, J.G., (2009). Reinforced Concrete Mechanics and Design (5th Ed.). Pearson-Prentice Hall.

Wright, P.J.F, (1955). Comments on an Indirect Tensile Test on Concrete Cylinders. Magazine of Concrete Research, Vol. 7, No. 20, pp. 87-96.

Zakaria, M., Ueda, T., Wu, Z., and Meng, L., (2009). Experimental Investigation on Shear Cracking Behavior in Reinforced Concrete Beams with Shear Reinforcement. Journal of Advanced Concrete Technology, Vol. 7, No. 1, pp. 79-96.